# UNMIXING SENSORY CHANNELS ENCODING MECHANICAL AND THERMAL STIMULI: A PROBABILISTIC APPROACH TO STUDY THE SPATIOTEMPORAL DYNAMICS OF NOCICEPTORS

**Inaugural-Dissertation**

**to obtain the academic degree**

**Doctor rerum naturalium (Dr. rer. nat.)**

**submitted to the Department of Biology, Chemistry and Pharmacy**

**of Freie Universität Berlin**

by

**Tara Dezhdar**

**from Teheran**

**2015**

**The research presented in this dissertation was carried out from August 2011 until October 2015 at the Theoretical Neuroscience & Neuroinformatics group, Freie Universitä Berlin, under the supervision of Dr. Michael Schmuker.**

1th Reviewer: Prof. Dr. Martin P. Nawrot - University of Cologne, Cologne.

2th Reviewer: Prof. Dr. Stephan Sigrist- Freie Universität Berlin & NeuroCure, Berlin.

Date of defense: March 02, 2016

## Acknowledgement

I would like to express my special appreciation and thanks to my Ph.D adviser, Michael Schmuker, you have been a tremendous mentor for me. I would like to thank you for giving me the opportunity to dive into the unfamiliar an amazing world of computational neuroscience, for trusting me and for allowing me to explore my way and gain experience. Your outstanding advices on my research and your generous supports, scientifically, morally and otherwise, during the last four years have been invaluable. Thank you so much Michael.

I would like to thank Martin P. Nawrot. He has not only let me to be a part of his group and supported me on my research but he was the initiator of this fascinating journey, as I went to him five years ago and asked him for his advice on how to start.

I thank Rabih A. Moshourab for saving my research with his excellent data and for being a great source of ideas. My great thanks go to Prof. Gary R. Lewin, for supporting my research, giving critical and fruitful feedback and for being an outstanding source of knowledge in field of pain research.

I owe Ingo Fründ my deepest gratitude, your supports and advices helped me to grow as a research scientist. Your fascination for mathematics and statistics encouraged me to learn and explore statistics. Thanks for always being patient and answering my questions at any time, reading my writings, giving me feedback, and motivating me.

I would like to express my deep thanks to Frazad Farkhooi to be a valuable source of hope, help and motivation. I have very much enjoyed our long discussions – both, the scientific ones and the others.

I would specially thank my colleges and friends from the Neuroinformatics group at Freie Universität Berlin, Gundula Meckenhäuser, Joachim Haenicke, Jan Soelter, Evren Pamir, Chris Haeusler, Rinaldo Betkiewicz, and especially Thomas Rost for reading and correcting part of this thesis. I would like to thank Kathrin Brackwehr and Magdalena Nagel for helping with organizational works. Thank you so much.

This journey would not be complete without the supports and love of my friends, Ali for always being there for me, Afagh, Shirin, Hannah, Volker, Pouyan and Marool joonam for her consistently supports and encouragements. My deepest gratitude to Fatima Kamenge, for being the source of love and energy in my life. A big thank to my parents-in-law Brigitte and Heinz-Christian Fründ for their motivating words, and brainstorming discussions.

Words can not say how grateful I am to my mother and father, Zari and Fereydoun, and to Aidin and Shahrzad and to my sweetheart Sophie. Without you there would be nothing.

## This dissertation is based on the following manuscripts:

**A Probabilistic Model for Estimating the Depth and Threshold Temperature of C-fiber Nociceptors.**

*Authors*: Tara Dezhdar[1,2], Rabih A. Moshourab[3], Ingo Fründ,[4], Gary R. Lewin[2,3], Michael Schmuker[1,2,§]

*Author Contributions*: M.S., G.R.L., T.D. and R.M. conceived and designed the study. R.M. performed the experiments. G.R.L. contributed data and materials. I.F. and T.D. developed the probabilistic formulation of the method, I.F. helped design the sampling and numerical integration schemes. T.D. analysed the data and prepared the Figures 1-5. R.M. prepared Fig. 6. T.D., M.S., G.R.L., R.M. and I.F. wrote the paper.

*Manuscript status*: This work is peer-reviewed and has been accepted for publication in the journal *Scientific Reports* (Dezhdar et. al., 2015, in Press)

**Decoding of Polymodal C-fiber Nociceptor Responses with a Generalized Linear Model and L1 norm Regularization.**

*Authors*: Tara Dezhdar[1,2], Ingo Fründ,[4], Rabih A. Moshourab[3], Gary R. Lewin[2,3], Michael Schmuker[1,2,§]

*Author contributions*: R.M. performed the experiments. G.R.L. contributed data and materials. I.F. and T.D. developed the probabilistic formulation of the method.T.D. analysed the data, prepared the Figures wrote the paper. M.S. revised the paper.

*Manuscript status*: A revised version of the current manuscript will be submitted for publication in an international peer reviewed journal.

**Author affiliations:**

[1] Bernstein Center for Computational Neuroscience (BCCN) Berlin, Berlin, Germany

[2] Department of Biology Chemistry Pharmacy, Institute of Biology, Neuroinformatics & Theoretical Neuroscience, Freie Universität Berlin, Berlin, Germany

[3] Department of Neuroscience, Max-Delbrück-Center for Molecular Medicine, Berlin, Germany

[4] Center for Vision Research, York University, Toronto, ON, Canada

[§] Current address: School of Engineering and Informatics, University of Sussex, Brighton, UK

## Zusammenfassung

In dieser Arbeit schlage ich probabilistische und Bayesianische Methoden vor, mit welchen periphere neuronale Schmerzverarbeitung quantitativ untersucht werden kann. Durch Einführung einer detaillierten statistischen Charakterisierung von Nozizeptoren (Schmerzrezeptoren), legt diese Arbeit den Grundstein für ein stärker quantitatives Verständnis der Schmerzverarbeitung in der Peripherie. Ich illustriere meinen Zugang an drei spezifischen Modellen in den Kapiteln 2 bis 4. Jedes der ausgewählten Kapitel lehnt sich dabei an einen der Verarbeitungsschritte peripherer Schmerzverarbeitung an.

In Kapitel 2 entwickle ich Bayesianische Modelle, welche das klassische Verfahren verbessern, mit welchem die Antwortschwelle und die Tiefe von hitzesensitiven Nozizeptoren geschätzt werden. Die vorgeschlagene Bayesianische Methode ist robuster als bisher benutzte, nichtprobabilistische Methoden. Mein neuartiger Zugang ergibt hier bedeutungsvolle und interpretierbare Parameterschätzungen für eine Reihe von Nozizeptoren, bei welchen eine Parameterschätzung mit der klassischen Methode fehlschlägt.

In Kapitel 3 benutze ich "sparsame" (Engl.: "sparse") generalisierte lineare Modelle zur Identifizierung der Reizeigenschaften, welche besonders gut die neuronalen Antworten vorhersagen. Die Likelihoodfunktion dieser Modelle wird durch einen Regularisierungsterm erweitert. Maximierung dieser erweiterten Likelihood führt zu sogenannten sparsamen Modellen, in welchen wenige Reizeigenschaften als Prädiktoren ausgewählt sind (sie haben von Null verschiedene Regressionskoeffizienten), währen die meisten Reizeigenschaften einen verschwindenden Regressionskoeffizienten haben und dadurch nicht in das Modell eingehen. Die ausgewählten Reizeigenschaften sind relativ konsistent über verschiedene Neuronen. Vor allem zeitliche Veränderungen der vertikalen Deformation des Hautgewebes um den Rezeptor scheinen wichtig zu sein, um die neuronalen Antworten auf mechanische Reize zu erklären. Die ausgewählten Reizkomponenten können eventuell Aufschluss über die Aktivierung von Transduktionskanälen geben.

In Kapitel 4 entwickle ich ein parametrisches Modell für die Feuerrate und die Adaptation primärer afferenter Zellen. Die geschätzten Parameter dieser Zellen spannen einen Parameterraum auf, in welchem neuronale Antworten auf ganz verschiedenen Reize einheitlich verglichen und möglicherweise auch unterschieden werden können.

Zum Abschluss diskutiere ich in Kapitel 5 Stärken und Grenzen der präsentierten Modelle. Hier schlage ich einen theoretischen Rahmen vor, in welchem die entwickelten Modelle zu einem generellen Verständnis verbunden werden können. I argumentiere, dass solch ein

vollständig probabilistisches Modell einen vielversprechenden Zugang bildet, um die Informationsverarbeitung in primären afferenten Nozizeptoren zu verstehen.

## Summary

In this work I suggest probabilistic and Bayesian methods to assess the neural processing of noxious (painful) stimulation by primary afferent receptor neurons, called nociceptors. By introducing advanced statistical characterization of nociceptors, this work is leading the way towards a more quantitative understanding of "pain pathways" at the peripheral level. I illustrate these methods through three models in chapters 2 to 4. Each model can be associated with a processing stage of peripheral pain pathway.

In chapter 2, I suggest Bayesian models to improve a classical model for estimating the threshold temperature and depth of heat-sensitive nociceptors. I find that application of this new Bayesian procedure is more robust than previously used, non-probabilistic methods. My novel approach results in meaningful and interpretable parameter estimation for a number of nociceptors for which the classical method failed.

In chapter 3, I use sparse generalized linear models to identify the stimulus features that are most predictive of neural responses. The likelihood of these models is augmented by a regularization term. Maximizing this augmented likelihood results in sparse models in which few stimulus features are selected (i.e. have non-zero coefficients), while most features have a regression coefficient of zero. I find that the selected features are relatively consistent across neurons. The temporary changes of vertical deformation of receptor-embedded tissue seems to be the main feature of spatial deformation caused by mechanical stimuli. The selected features might give insights into the activation of transducer channels.

In chapter 4, I develop a parametric model of firing rate and adaptation of primary afferents. The estimated parameters of these neurons provide a a parametric space to characterize and potentially discriminate the responses of these neurons to different stimulus modalities.

In the end in chapter 5, I discuss strengths and limitations of these models. I suggest a framework to link all developed models towards a general understanding. I postulate that such a fully probabilistic model offers a promising framework to encode the processing carried out by primary afferent nociceptors.

**Keywords:** Nociceptors, C-fibers, pain, Transduction, noise, neural responses, Bayesian inference, GLM, Lasso, sampling, Continuum mechanics, Thermomechanics, Skin tissue

*To Zari and Fereydoun*

# Contents

# Chapter 1

## 1 General Introduction

The sensation of “pain” is a complex experience that is essential to an organism’s survival. It involves the mechanistic aspect of detecting and responding to noxious (painful) stimuli (Woolf & Ma, 2007) (Perl, 2007) (Raja, et al., 1999) but also cognitive and emotional aspects and processing in the brain (Price, 1988) (Apkarian, et al., 2005). Under normal conditions, an organism’s ability to experience pain serves as warning system, marking tissue damage. However, alterations of the pain pathway contravene its usefulness as a warning system, resulting in chronic and debilitating pain experiences. A recent market research report indicates that more than 1.5 billion people worldwide suffer from chronic pain and that approximately 3- 4.5% of the global population suffers from neuropathic pain (Global Industry Analysts, 2011).

Alternations of the pain pathway, often come as a state of peripheral sensitization, in which non-noxious stimuli, such as weak touch or warmth, are perceived as noxious (a condition that is called allodynia) and mildly noxious events are perceived as highly noxious (a condition that is called hyperalgesia). Either conditions elicit different potential therapeutic treatment targets and form broad aspects for the study of pain. Beside the cognitive and emotional aspects of pain, processing of noxious stimuli and perception of pain can be studied at the peripheral level of primary afferent neurons, called nociceptors (Sherrington, 1906), the central level of second order neurons in spinal cord, and at the level of supraspinal pain processing mechanisms (Basbaum, et al., 2009) (Perl, 2011) (Julius & Basbaum, 2001).

The key to understanding pain hypersensitivity or chronic pain is a better understanding of the molecular, cellular and neuronal representation of acute pain at peripheral and/or central loci. In the present work, I studied the neuronal representation of stimuli at the peripheral level by primary afferent neurons responding to noxious stimuli. This work emphasizes the application of probabilistic models to study nociceptors and thus explores the usefulness of advanced methods from computational neuroscience (Pouget, et al., 2013) in the new setting of pain research.

## 1.1 Anatomical Overview

The cell bodies of nociceptors are located in the trigeminal and dorsal root ganglia (DRG) outside the central nervous system (CNS), and generate axonal stalks that split into two sets of fibers. One set reaches the skin and most internal organs such as joints and muscles, where it builds the receptor site, detects noxious (harmful) stimuli and converts them into electrical signals. The other set of fibers runs in the opposite direction and extends toward the dorsal horn of the spinal cord to form synapses with local neurons, which process the sequence of action potentials arriving from the periphery and transmit it to supraspinal sites (see Figure 1).

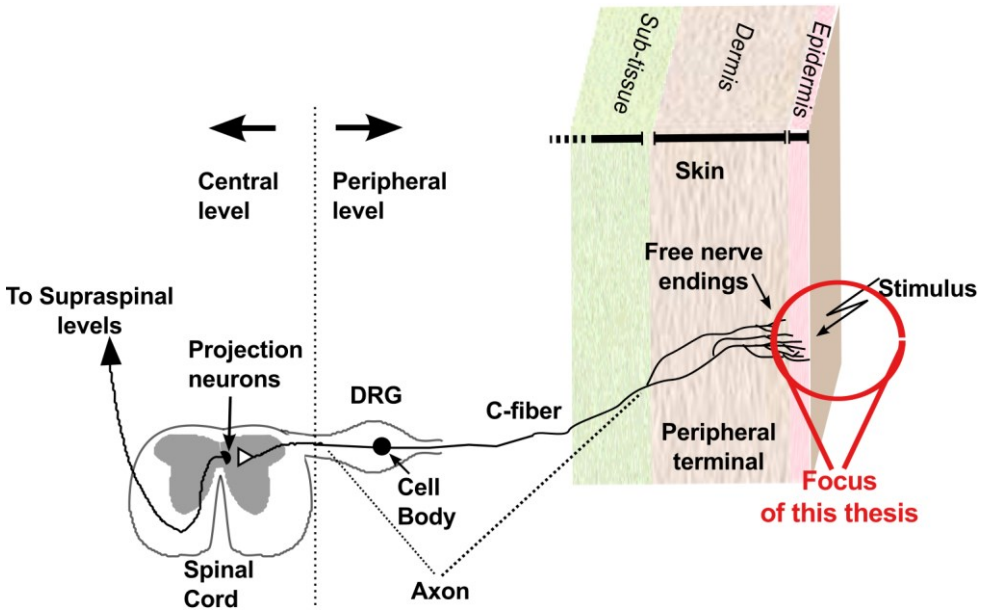


**Figure 1. Schematic of the operational components of a C-fiber nociceptor**. The peripheral terminal of a C-fiber are free nerve endings. They innervate epidermal and dermal layer of skin and transduces noxious stimuli to the receptor potential. The receptor potential triggers generation of action potentials. The axon conducts action potentials from the periphery to the central nervous system. The cell body of a nociceptor is in the dorsal root ganglion (DRG). The central terminal is in dorsal root of spinal cord where information is transferred to second order neurons at central synapses. From there the information is transferred to the suprasipnal levels.

Nociceptors are classified into two broad classes with distinct structure and function. 'C' nociceptors are unmyelinated (i.e. without insulation from a fatty sheath of myelin), hence conduct impulses relatively slowly, at around 0.25-1.25 m/sec, and convey the poorly localized, delayed pain (Julius & Basbaum, 2001). 'A$\delta$' nociceptors are thinly myelinated, conduct impulses fast, at around 5-30 m/sec, and mediate a localized, sharp and fast pain sensation. Additionally, a group of primary sensory neurons, called silent nociceptors, becomes responsive to harmful stimuli only after tissue damage has occurred. Nociceptors

are heterogeneous and exhibit multiple nociceptor subclasses, each expressing a distinctive repertoire of cation channels of the transient receptor signaling proteins (Braz, et al., 2005) (Julius & Basbaum, 2001). After tissue damage, this heterogeneous palette of transduction molecules undergoes profound changes, giving rise to a state of hyperexcitability, called peripheral sensitization.

Electrophysiological recordings of C-fibers show that most (over 70%) nociceptors are polymodal: they can be activated by multiple types of painful stimuli, such as mechanical, thermal, or chemical stimuli (Perl, 1996). Nevertheless, different thermal pain and mechanical pinch thought to be perceived as distinct qualities. This has strengthened the position that the brain's ability to discriminate different noxious stimulus modalities is unlikely to be attributable to modality-specific primary nociceptor subsets. Indeed, one of the central debates in this field has revolved around the question to what extend nociception represents a mechanistically distinct aspect of the different stimulus modalities.

## 1.2 Theories of Pain Processing

Historically, two opposing theories of pain have been put forth to explain how nociceptors encode noxious percepts (Melzack & Wall, 1965) (Melzack & Wall, 1982) (Nathan, 1976). According to the Specificity theory (von Frey, 1894) pain is produced by activation of distinct nociceptor subtypes that are tuned to respond to a specific quality, modality and/or intensity of stimuli. This model supports the idea of a labeled line relationship between the stimulation and neural modules responsible for conscious perception of pain (Bessou & Perl, 1969) (Perl, 2007) and assumed the existence of specialized and functionally distinct subtypes of nociceptors. On the other hand, Pattern theory suggests (Goldscheider, 1894) that pain is produced when a stimulus elicits a pattern of activity across indistinct primary afferent neurons. The resulting pattern is then convoluted within the central nervous system to generate a specific percept representing the noxious mechanical, thermal, or chemical stimulus applied to the peripheral receptive field (Weddell, 1955). This theory recognizes that the spatiotemporal pattern of the impulses from the skin are important. Other theories of pain contain elements of both Specificity theory and Pattern theory. The most studied one is 'gate control' theory of pain suggested by Melzack & Wall (Melzack & Wall, 1965), which extends from the so-called sensory interaction theories. Gate control theory is a pattern-based theory, proposed that low- and high-threshold afferents converge on unspecialized central neurons and that sufficiently strong activation of those central neurons encode pain.

The existence of nociceptor subtypes which preferentially or specifically respond to a certain feature of the stimulus (Basbaum, et al., 2009) rolled out the original form of Pattern theory. On the other hand, the existence of some coding dilemmas such as mismatch between the nature of stimuli and perception of pain (e.g burning cold) (Prescott, et al., 2014) supports the most recent theory of pain. This theory is referred as population coding of somatosensation, or a 'combinatorial' theory (Ma, 2010). Combinatorial coding posits that perception of painful stimuli depends on the combination of nociceptor subtypes, and the proportion to which they are activated. This theory combines the specificity and pattern theory. First, the senses of pain are, at least in part, selectively processed by the subtypes of primary afferent neurons itself and along specific labeled lines (peripheral specificity). Second, an activity pattern of labeled lines in the central nervous system is involved in the emergence of a specific sensation (central pattern). A critical aspect of this hypothesis is that responsiveness of individual nociceptors to a particular stimulus does not need to be directly correlated to the perception of that stimulus (Ma, 2012). This point suggests a key role for polymodal C-fibers, in which the same peripheral neuron conveys the information about different stimulus modalities to the central level of processing. Thus, targeting the mechanism that shapes the discharge responses of C-fibers to different stimulus modalities, or that modulate the communication of these primary afferents with second-order neurons, may provide evidence for each of the hypothesis, may help to formulate these theories more specifically, and may offer therapeutic interventions.

Yet our understanding of the mechanism of how polymodal C-fibers encode pain remains far from complete. An adequate description requires both definitive identification of the constituent transducer channels and their kinetics. Several studies have focused on identification and characterization of ion channels using electrophysiological measuring technics, or genetic- or immunotoxin-based methods combined with behavioral studies (Basbaum, et al., 2009) (Caterina, et al., 1997) (Cho, et al., 2012) (Vriens, et al., 2014). Identification of TRPV1 (Caterina, et al., 1997), has been one of the great success stories of sensory biology and now includes TRP, ASIC, and potassium and ligand-gated ion channels (Basbaum, et al., 2009). While thermal sensitivity in the warm-hot range turns out to be mediated by multiple TRP channels TRPV1, TRPV2, TRPV3, and TRPV4 that all express a particular C-terminal (Dhaka, et al., 2006) (Cho, et al., 2012) (Vriens, et al., 2014). But the extent to which all these TRPs are expressed remains uncertain. There is even more uncertainty about noxious mechanical transduction with several competing candidates (Hu, et al., 2006).

The main reasons hampering identification of transducer channels refer to the technical difficulties to isolate and measure small diameter C-fibers. Free nerve endings of C-fiber

nociceptors are hard to locate in the tissue they innervate, and the small diameter (<0.5 µm) of nerve endings make these neurons inaccessible for standard electrophysiological recordings (Basbaum, et al., 2009). Nevertheless the uncertainty in identification of transducer channels is impeding progress toward the second requirement, namely, identifying the transducer kinetics that might contribute by shaping the firing pattern of C-fibers. With respect to these requirements, chapter 3 of the present work is an abstraction from these specific channel types and a characterization of the features that drive action potential generation by using statistical models.

This study focused on the identification of the temporal features of the neuronal representation that distinguish different stimulus modalities using advanced statistical methods. We used a data set obtained with an *in vitro* skin nerve preparation of mouse saphenous nerve in which noxious mechanical and heat sensation can be reproduced (Milenkovic, et al., 2008). This dataset was designed and recorded in close collaboration with Dr. Rabih A. Moshourab and Prof. Gary R. Lewin in Max Delbrück Institute, Berlin. In chapter 4, I will develop a framework that provides a parametric description of spatiotemporal dynamic of response discharges of single neurons. Such a parametric description allows a quantitative and formally valid characterization of the variability of response properties throughout the population of nociceptors that goes beyond qualitative descriptions such as 'polymodal' or 'unimodal'. The main aim of this study was to provide a probabilistic formulation of the primary afferent neurons' responding properties.

Information about a sensory stimulus is believed to be encoded in a sequence of action potentials. How this happens in detail, is a common problem in system neuroscience. Previous studies gained insight into the computations carried out by neural ensembles using a large array of methods, including mathematical modeling of pain as a complete system (Britton & Skevington, 1989) (Haeri, et al., 2003), biophysically detailed models of ion channel characterization (Tigerholm, et al., 2014), statistical models of cultured DRG neurons (Ratté, et al., 2014) (Rho & Prescott, 2012) , and neuroimaging (Apkarian, et al., 2005) (Cecchi, et al., 2012). Yet, the application of advanced statistical methods to study the responses has proven difficult in the past. On one hand, recordings in C-fibers are challenging, resulting in small data sets, short recording times, and accordingly few repetitions – a situation that calls for an approach using Bayesian inference in a probabilistic model. While classical statistical methods have guaranteed long run performance on large data sets, Bayesian methods perform well on small data sets by gracefully balancing prior knowledge and new evidence (e.g. (Wasserman, 2004)). Bayesian inference requires a probabilistic model of the data generating process. Noise levels in nociceptor responses have typically been assumed to be negligibly small.

Unfortunately, this neglect of nociceptor noise implies that there are hardly any data to characterize the variability in nociceptor responses. This makes it difficult to formulate an accurate probabilistic model for spike responses recorded from nociceptors. In addition, previous studies have often been rather qualitative and did not directly suggest appropriate prior distributions as needed for Bayesian inference. Closing this gap will be one of the main contributions of this thesis.

## 1.3 Receptor Neuron Models

One approach towards descriptive models of response discharge of C-fibers is to construct an accurate model of the mechanisms underlying the spatiotemporal discharge patterns. Which mechanisms affect significantly the initiation and generation of action potentials and to what extend? Addressing this issue was the first step toward developing a receptor model in this study.

Figure 2 illustrates schematically receptor sites of two C-fibers. The main processing steps are indicated by three boxes.

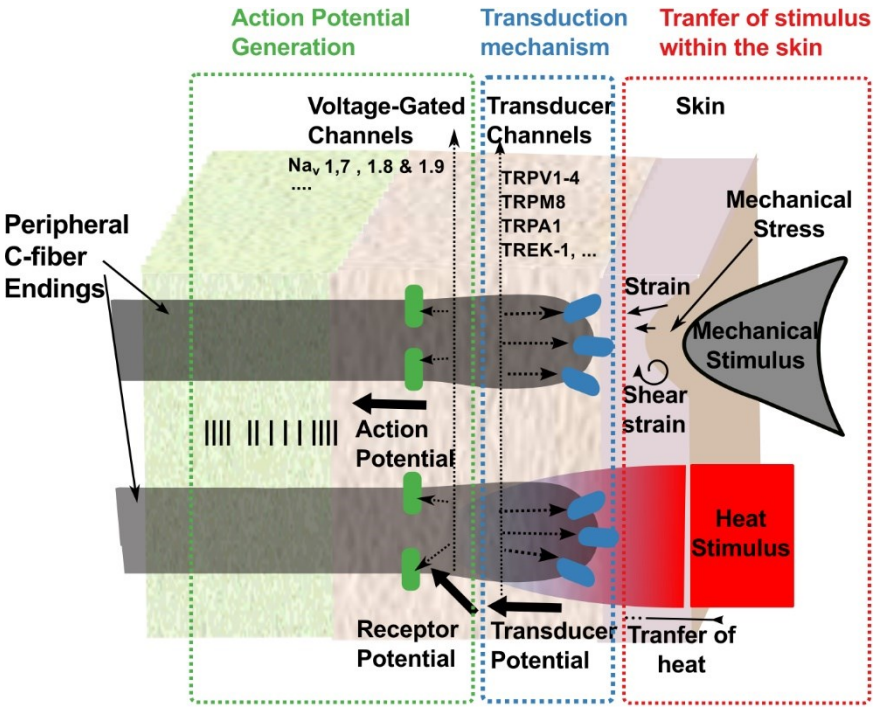


**Figure 2. Schematic of receptor sites of free nerve endings of two C-fibers innervating skin.** Three main processing steps from transferring the stimulus within the skin to transduction of mechanical and thermal stimuli to generation of action potential are shown in individual boxes. Red box: Transfer of stimulus within the skin. A mechanical stimulus applied on the surface of skin causes deformation of skin tissue at receptor site. This deformation is called strain and activates mechano-sensitive transducer channels. A heat stimulus applied on the surface of the skin causes temperature changes at depth of receptor and activated heat-sensitive transducer channels. Blue box: Transduction mechanism. At receptor site activation of mechano-heat-sensitive ion channels triggers a local depolarization of membrane and generation of receptor potential. Green box: Action Potential Generation. Receptor potential triggers action potentials. The temporal dynamics and frequency of action potentials give insight into the main features of original stimulus and dynamics of transducer channels.

The receptor site of the free nerve endings of a C-fiber innervates the epidermal and/or dermal layer of skin. The mechanical or thermal stimuli are often applied to the surface of the skin and are transmitted through the skin tissue to the site of receptor. The first box from the right in Figure 2 ‘Transfer of stimulus within the skin’ shows schematically the transmission of heat and mechanical stimuli to the receptor site(s). Notably, this transmission through the skin is mediated by physical laws from classical mechanics and thermodynamics. At the receptor site, the deformations of skin tissue (strain) caused by mechanical stimuli, or temperature changes caused by thermal stimuli, activate a cascade of chemical processes in transducer channels, (see Figure 2, second box; Transduction mechanism), resulting in ion flow through these channels, which generates a local depolarization (proximal stimulus or receptor potential) that drives the membrane potential towards the threshold. Depolarization of membrane potential generates action potentials, whose temporal dynamic and frequency reflects the main features of the stimulus (see Figure 2, third box; Action Potential Generation).

Hence, an accurate model requires; (1) an understanding of skin mechanics that embeds the nerve terminals and mediates the stimulus to the receptor site. (2) A model to characterize the conversion of local tissue deformation or temperature changes to electrochemical events at receptor site and depolarization of membrane. (3) A model to describe the temporal dynamics of action potentials such as adaptation and refractory periods.

Accordingly, in this study I developed probabilistic models to study each of three steps: (1) Transfer of stimulus within the skin. (2) Combination of different stimulus modalities by peripheral transduction mechanisms. 3) Temporal dynamics of generated action potentials within the fiber.

This work is organized according to three processing steps and as follow.

### 1.3.1 Transfer of stimulus within the skin

In chapter 2, “A Probabilistic Model for Estimating the Depth and Threshold Temperature of C-fiber Nociceptors”, I studied the interaction of thermal stimuli with nociceptor-embedded skin tissue. When the skin comes into the contact with a hot object, the heat conducted from the surface triggers a sequence of events in heat sensitive afferent fibers within the skin. Thereby the original stimulus is encoded in a sequence of action potentials that are relayed to the central nervous system and give rise to the sensation of warmth or heat pain.

Previous studies had shown that the heat threshold of C-fiber mechano-heat sensitive nociceptors (C-MH) primarily depends on the temperature at the depth of receptor (Tillman, et al., 1995) (Stoll & Greene, 1959) and thus for the same stimulus intensity, the pain level could be higher if the nociceptor is closer to the surface. Therefore, the location of receptor terminals and the threshold at this depth have been viewed as important parameters in the modeling of C-MH nociceptors. This hypothesis has provided a classical method of finding the receptor terminal depth and threshold without experimental measurement (Henriques & Moritz, 1947). However, previous studies have shown that certain experimental conditions are required for this method to produce stable results (Tillman, et al., 1995). In this chapter I introduced a probabilistic model which improves the classical method and provides a more reliable estimation of receptor depth and threshold temperature.

### 1.3.2 Transduction mechanism

In chapter 3, “Decoding of polymodal C-fiber nociceptor responses with a generalized linear model and L1 norm regularization”, I investigated within a probabilistic framework the relationship between mechanical and thermal stimuli at receptor site and discharge responses of C-MH nociceptors. This framework comprises an analytical model along with a probabilistic model. The analytical model describes the deformations of skin tissue that can be produced by a mechanical force applied on the surface of skin. The probabilistic model describes the transduction of these deformations at receptor site into neural responses. Within this framework, I ascertained which aspects of the local tissue deformations and thermal stimulus are most predictive of the neural response.

To characterize the deformation in skin tissue at receptor site I used a continuum mechanics model (Phillips & Johnson, 1981b). According to this model a simple mechanical stimulus can induce a complex pattern of spatial deformations at receptor site. But not all aspects of spatial deformation can activate the mechano-sensitive transducer channels. To select the main features of spatial deformation I applied a sparsity based regularization of all candidates (Tibshirani, 1996). The results suggested that among the six deformation candidates that we considered, the derivative of vertical compressive strain, and maximum compressive and tensile strains are most predictive of neural responses. The selected features could be potentially used to characterize individual ion channels rather than complete neurons.

### 1.3.3 Temporal dynamics of generated action potentials within the fibers

In chapter 4, “A Parametric Model of Firing Rates and Adaptation: a Study of Discharge Responses of Primary Afferent Neurons and Nociceptors”, I introduced parametric

dynamical models. These were used to describe the stimulus-driven instantaneous firing rate of response discharges of C-fiber nociceptors to controlled mechanical and heat stimuli. Each model consisted of two coupled ordinary differential equations (ODEs), describing the rate of an inhomogeneous point process and adaptation effects on this rate. I investigated two types of ODEs; one incorporating a linear adaptation process and another incorporating nonlinear, divisive adaptation. I found that these dynamical models provided good characterizations of the recorded spike trains, but observed that more data are needed to conclusively differentiate between different hypothesized dynamics. The estimated parameters of these models offer a potential to provide a parameter space in which to classify the responses of neurons to different modalities of thermal and mechanical stimuli.

# Chapter 2

# 2 A Probabilistic Model for Estimating the Depth and Threshold Temperature of C-fiber Nociceptors

The content of this chapter has been accepted for publication in the journal *Scientific Reports* (Dezhdar, et al., 2015, in press).

The subjective experience of thermal pain follows the detection and encoding of noxious stimuli by primary afferent neurons called nociceptors. However, nociceptor morphology has been hard to access and the mechanisms of signal transduction remain unresolved. In order to understand how heat transducers in nociceptors are activated *in vivo*, it is important to estimate the temperatures that directly activate the skin-embedded nociceptor membrane. Hence, the nociceptor's temperature threshold must be estimated, which in turn will depend on the depth at which transduction happens in the skin. Since the temperature at the receptor cannot be accessed experimentally, such an estimation can currently only be achieved through modeling. However, the current state-of-the-art model to estimate temperature at the receptor suffers from the fact that it cannot account for the natural stochastic variability of neuronal responses. We improve this model using a probabilistic approach which accounts for uncertainties and potential noise in system. Using a data set of 24 C-fibers recorded *in vitro*, we show that, even without detailed knowledge of the bio-thermal properties of the system, the probabilistic model that we propose here is capable of providing estimates of threshold and depth in cases where the classical method fails.

## 2.1 Introduction

For many years, pain has been subject to extensive neurobiological, clinical, and psychophysical studies (Perl, 2007) (Basbaum, et al., 2009) (Perl, 2011). Since the early 20$^{th}$ century when Charles Sherrington conducted neurophysiological experiments that started to define the neural process of detecting and responding to noxious, harmful stimuli as nociception and the responsible afferent neurons as nociceptors (Sherrington, 1906),

different types of nociceptors have been identified (Burgess & Perl, 1967) (Smith & Lewin, 2009). The main group includes polymodal unmyelinated nociceptors (Bessou & Perl, 1969), responding to potentially painful mechanical and heat stimulation, thus defined as mechano-heat sensitive C fibers (C-MH fibers) (Handwerker, et al., 1987) (Kress, et al., 1992) (Fleischer, et al., 1983) (Lewin & Mendell, 1994). Although C-fibers play a pivotal role in perception of noxious heat stimuli, less is known about the underlying mechanisms that transform heat and mechanical stimuli into neural activity (Melzack & Wall, 1962) (Lewin & Moshourab, 2004) (Cavanaugh, et al., 2009).

The pain pathway can be broken down in three major components: (1) transduction of heat or mechanical energy into electrical signals at the receptor site, (2) transmission and modulation of action potentials from peripheral receptor site to the Central Nervous System CNS and higher brain function, and (3) perception of signals as pain (Woolf & Ma, 2007). In recent years mathematical and computational models of the pain pathway have been developed and provided valuable insights into various aspects of pain, like acute pain (Britton, et al., 1995) and neuropathic pain within a dynamical system of neurons (Ratté, et al., 2014) (Rho & Prescott, 2012), relating the input stimulation to the sensation of pain in an artificial neural network (Haeri, et al., 2003) (Minamitani & Hagita, 1981), or the temporal dynamics of pain perception using neuroimaging (Cecchi, et al., 2012). Recently, mathematical modeling of pain at the cellular level drew attention to the plausibility of physiological properties of nociceptors and bio-thermal properties of skin (Xu, et al., 2008) (Tillman, et al., 1995a). In heat sensitive sensory neurons, the threshold temperature was considered as a determinant for activation of heat sensitive ion channels, and to discriminate nociceptors from warm sensitive neurons. Despite the fact that there at least three ion channels activated by noxious heat are expressed in mouse nociceptors (TRPV1, TRPM3 and anoctamin-1) (Vriens, et al., 2011) (Caterina, et al., 1997) (Cho, et al., 2012) (Vriens, et al., 2014) there is still no clear picture of where in the skin (e.g. dermal or epidermal free nerve endings) these physiologically important heat transducing ion channels are located. Thus computational models, based on real experimental data, can potentially provide constraints on the thermal changes that a noxious heat transducer must be able to detect in order to transform thermal energy into a noxious heat code in nociceptors. Measuring the threshold temperature of a nociceptor is complicated by the fact that the temperature at the location of receptor differs from the surface temperature, because the skin is not a perfect heat conductor. In addition, the receptor endings are hard to access, due to the complex and variable histological structure of the skin (i.e. several layers, ridges, hair follicles), branching of the free nerve endings of C-fibers, and small diameters of terminal endings. Even the smallest thermocouples are large with respect to

the epidermal and dermal thickness and as an external object they would change the conditions of heat flows. An infrared camera could detect the flow of heat, but it cannot reveal the position of nerve endings. Therefore, it is currently not possible to measure the temperature at the transduction site(s) in nociceptor endings directly.

To mitigate these shortcomings, mathematical models were used to estimate the threshold temperature as a parameter (Cecchi, et al., 2012) (Hardy & Stolwijk, 1966) (Schepers & Ringkamp, 2009) (Tillman, et al., 1995). *Tillman et al.* (Tillman, et al., 1995) showed that latency of the first action potential fired by a C-MH afferent depends primarily on the temperature at the location of the receptor (its *depth*), and is hence influenced by the heat conductance of the skin. Therefore, to obtain an accurate estimate of threshold temperature of the receptor neurons, the first step has been to model the propagation of the temperature in several layers of the skin from the surface to the receptor depth. Several models have been developed to estimate nociceptor depth and threshold by using neurophysiological recordings of nociceptors or behavioral measurements to parameterize the heat diffusion equation, which describes the ability of the skin to conduct heat energy (Tillman, et al., 1995a) (Stoll & Greene, 1959) (Xu, et al., 2008). In a typical experimental protocol for this purpose, a heat electrode is placed on the skin surface, through which ramped heat stimuli with different rates are applied. The time $\tau$ until the threshold is reached can be the time of reporting the sensation of pain in a behavioral experiment (Stoll & Greene, 1959) (Marchandise, et al., 2014) or the latency of the first action potential in an electrophysiological recording (Tillman, et al., 1995). Assuming that neurons fire at a set temperature, it is possible to estimate the firing threshold temperature and the depth of the receptor from the threshold time $\tau$ by solving the heat diffusivity equation for different ramp stimuli. The estimated threshold temperature reported in previous studies varies in a range from 39-41 °C (Tillman, et al., 1995a) (Tillman, et al., 1995), 43 °C (Patapoutian, et al., 2003), 45 °C (Hardy & Stolwijk, 1966), and 47 °C (Lynn & Carpenter, 1982). However, only in the study by *Tillman et al.* (Tillman, et al., 1995) were threshold temperatures estimated at each neurons' estimated depth, while the other studies obtained threshold temperature at an assumed fixed depth or at the surface of the skin, which may explain the tremendous variability of the estimates in spite of using the same stimulus parameters.

An accurate estimation of the time at which the threshold temperature was reached is essential for the classical approaches. Small inaccuracies in spike time measurement, internal random process which could result in a delay between reaching the threshold and generation of first action potential, and trial-to-trial variability of neural responses, can

result to big inaccuracies in depths, and sometimes even make depth estimation impossible. Additionally, there are many sources of uncertainty in the estimation method. For example, the bio-thermal skin parameters (e.g. thickness, thermal diffusivity) are difficult to estimate accurately, since they vary with the age, gender, recording area and even the hair cycle of the specimen (Wang, et al., 2013). Moreover, repeated recordings from one neuron are often difficult because of the dynamic experimental conditions when recording from C-fibers (Zimmermann, et al., 2009). Therefore, the results of the classical approaches to estimate heat threshold and receptor depth have been disputed (Xu, et al., 2008) and often failed to yield reliable estimates (Tillman, et al., 1995).

In this contribution, we reformulated the established model for temperature propagation in a probabilistic way. We thus open up the way to account for natural variability on receptor response and uncertainties in other model parameters, enabling a statistical approach to the problem of inferring receptor depth from spike times and associated surface temperature. We introduce two modifications to the previous approach. First, we allow for a small, variable delay that can account for the variability of spike latency arising from deterministic properties of the system and/or 'noise', e.g. generated by random processes inside the neuron. Second, we use Monte-Carlo methods to deal with the uncertainty in bio-thermal parameters of skin model. To demonstrate the reliability of the new probabilistic model we applied both the classical approach and the probabilistic approach on a data set of extracellular recordings from 24 C-MH nociceptors. We then estimated the receptor parameters, depth and threshold temperature of all neurons and evaluated the probabilistic model using model evidence tests. The proposed method succeeds in producing realistic estimates of both threshold and depth for all measured neurons, although previous methods failed to provide such estimates for all neurons.

## 2.2 Results

Towards our aim to improve the classical model for depth and threshold estimation we first investigated the factors that rendered previous approaches unstable. We assumed that the instability of the classical model was mainly due to uncertainties of the threshold time and an incomplete skin model. Here, we use the term 'threshold time' to refer to the (not directly measureable) time at which the neuron reaches its firing threshold and action potential initiation. In the classical approach, threshold time is assumed to be equal to the time of the first spike. However, the first spike after stimulation onset may be generated with a small delay (latency noise), or it may be caused by spontaneous sub-threshold activity, especially in cases where the spike latency is very short compared to stimulus

onset. To deal with these uncertainties and variability in spike times we (i) introduce a delay between threshold time and first spike (latency), (ii) allowing for some responses to be outliers that are not driven by the presented stimulus, and (iii) introduce a probabilistic model for the skin.

### 2.2.1 Classical method, directly using the heat transfer model to identify neuron properties

We first assessed the performance of the classical model to estimate receptor depth and threshold, based on the analytical solution of the heat diffusion equation. An attractive feature of the analytical approximation is that the solution at any point in the skin can be obtained independently from the skin model, which is particularly useful when the skin model is not completely determined, or when the skin is stimulated from the corium side to facilitate electrical stimulation and pharmacological manipulation of the primary afferents in *in vitro* skin preparations (Lewin & Moshourab, 2004). Figure 1a depicts a typical skin model in which the heat electrode is applied on the surface of the skin. The heat energy flows from epidermal to dermal and subcutaneous layers and reaches the free nerve endings of C-MH fibers at some point. The ability of each layer to absorb heat energy and attenuate the surface temperature during transfer depends on its thermal diffusivity.

Assuming a fixed temperature threshold of a neuron at a fixed depth, it is possible to infer this depth from the time until this threshold is reached after applying a constant supra-threshold temperature to the surface. Figure 1b depicts the state of the heat gradients within the skin for four different surface temperatures when reaching a threshold of $T$=38.8 °C at a depth of $D$=0.3 mm. Each curve hence refers to a different time point after stimulus onset, i.e. the latency of the first action potential. All curves intersect in a single point: the estimated depth of the receptor.

This idealized example illustrates how the classical approach to depth and threshold estimation depends on reliable spike latency. Neuronal “noise” that causes variability in spike timing unfavorably affects the performance of this method. Real-world measurements affected by noise thus often fail to intersect in a single point, as illustrated in Figure 1c, thereby failing to provide estimates of location and threshold temperature.

We studied the capability of the classical approach to predict receptor threshold and depth in recordings from 24 C-MH neurons. Our experimental protocol consisted of three heat stimuli with three ramp rate durations of long: 16 s, middle: 4 s, and short (see Figure 1d for an example). Each stimulus was applied only once and in the same order. The heat electrode was placed on the corium side of the skin, not on the epidermis (see Figure 1e).

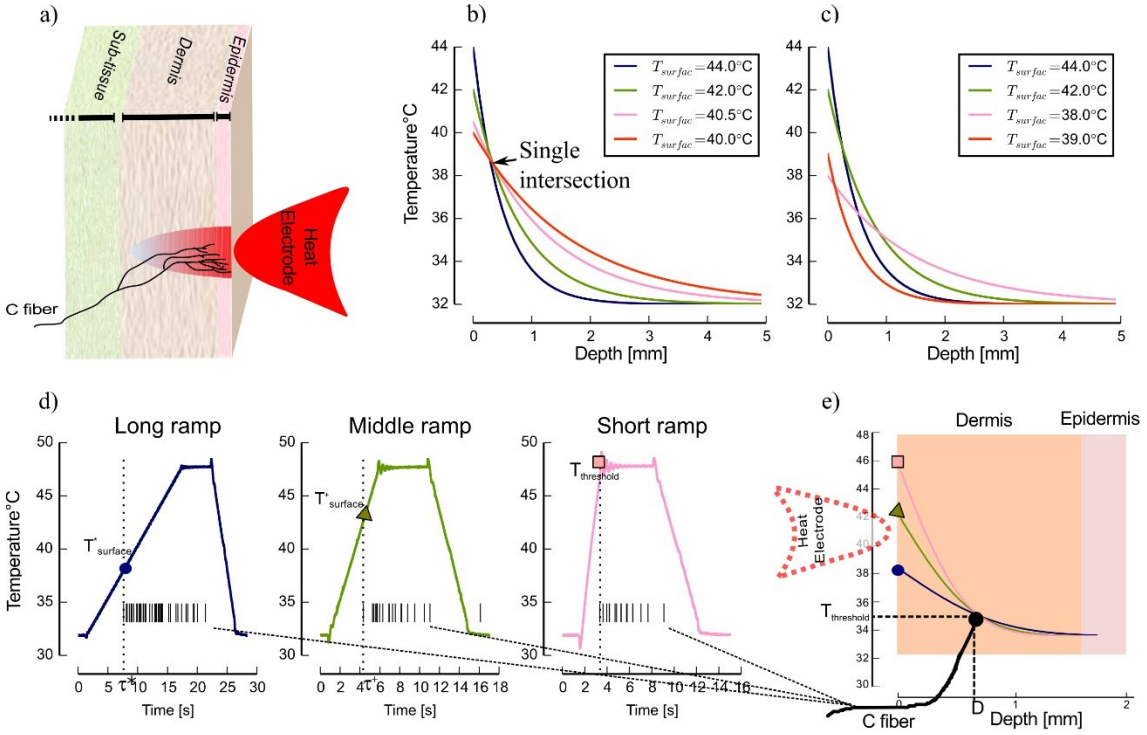


**Figure 1. Experimental conditions and schematic of skin model**. (**a**) Schematic of skin model and a C-fiber. In a typical experimental protocol heat electrode is placed on the surface of the skin. (**b-c**) Drift of different surface temperatures for all locations in the skin up to a depth of D=5 mm as a schematic illustration. Each curve refers to a different surface temperature at different time points after stimulation onset of different experimental conditions. (**b**) All four curves intersect in a single point, which refers to threshold and depth of nerve endings. (**c**) There is no single solution of heat equation that is consistent for all four experimental conditions. (**d**) An example of in this study applied experimental protocol. Three heat ramped stimuli with different ramp durations were applied on the dermal d of the skin while the responses of one C-MH nociceptor to all three stimulus conditions were simultaneously recorded. The surface threshold temperatures $T_{threshold}$ are associated with the first spike times $\tau$ for all three conditions. (**e**) Transfer of initial $T_{threshold}$ of all conditions through the skin layers for the example neuron. The curves intersect at the location of receptor and the same threshold temperature. Note that in our experiments the heat electrode was placed on the inside of the skin.

For a given threshold time $\tau = t^*$ the relation between the surface temperature $T_{surface}(x,t) = T^*(0,t^*)$ at time $t = t^*$ and the attenuated threshold temperature $T_{threshold} = T_{surfance}(x,t^*)$ at the location *x* of the receptor can be entered in the solution of heat equation as formulated by Henriques (Henriques & Moritz, 1947),

$$T_{threshold} = T_{surface} + \left(T_0 - T_{surface}\right)\frac{2}{\sqrt{\pi}}\int_0^{\gamma/\sqrt{\tau}} e^{-x^2}\,dx \qquad (2.1)$$

$$\frac{2}{\sqrt{\pi}}\int_0^{\gamma/\sqrt{\tau}} e^{-x^2}\,dx = \Phi\left[\frac{\gamma}{\sqrt{\tau}}\right].$$

We assume the skin has uniform temperature $T_0$ at stimulation onset. In equation (2.1), we used the short hand notation $\gamma = D/2a$, with $D$ being the receptor depth and $a = \sqrt{\frac{\kappa}{\rho\, c}}$

the thermal diffusivity of skin. In the second equality, $\Phi$ denotes the cumulative distribution function of the standard normal distribution. Then all combinations of receptor depth $D$ and temperature threshold $T_{threshold}$ that are consistent with these experimental conditions lie on a curve in the $D - T_{threshold}$ plane (see Figure 1e). For the same cell under different experimental conditions $t^+, T^+$another curve results (Figure 1d and e). Assuming that the receptor threshold temperature is defined and the same for all three stimulus conditions, then the intersection between these curves corresponds to $D$ and $T_{threshold}$ constellations that are consistent with both measurements.

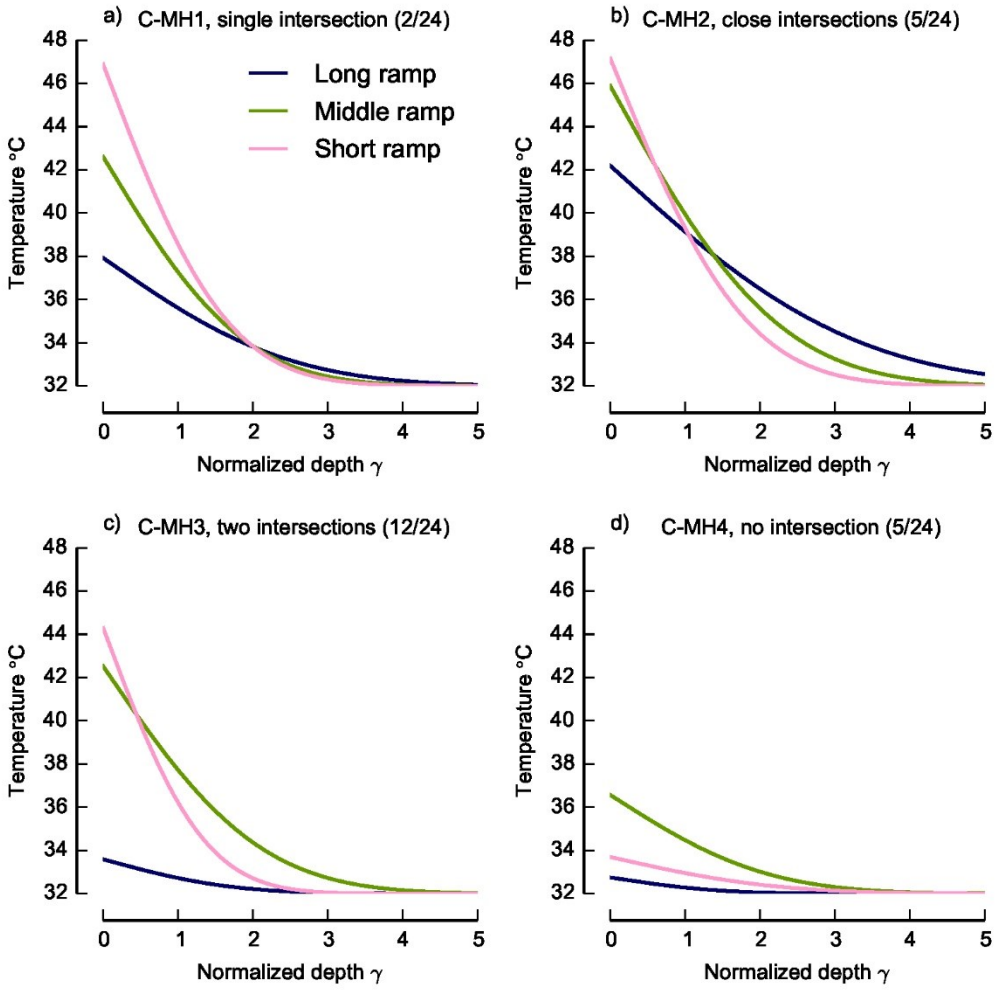


**Figure 2. Transfer curves of surface threshold temperature through the skin in a depth vs receptor threshold plane for three different ramp rates and four neurons.** (**a**) All three curves intersect in a single point, which is the solution of equation (2.1) and refers to threshold and depth of this neuron. (**b**) Three curves intersect in three close points and span a triangle. The resulting threshold and depth was determined as an average over three curves. (**c**) Two curves intersect and the third one start at a very low $T_{surface}$ and remains below the other two. (**d**) The curves start at a very low initial temperature and do not intersect. There is not any single solution for equation (2.1).

To solve the equation (2.1) for three ramped heat stimuli we assumed that the threshold time was equal to the latency of the first spike (i.e. the time from ramp onset to the first spike, corrected by electrical conduction delay) for all three ramped stimuli, and measured the temperature at the surface at that time. Figure 2 shows the solution of the heat function and transfer of three surface temperatures $T_{surface}(t_i)$, ($i = 1,2,3$ number of stimuli) in $D - T_{threshold}$ plane for 4 example C-MH neurons.

Only 2 out of 24 neurons intersected in a single point (Figure 2a shows an example), 5 out of 24 intersected in three close points and spanned a small triangle (e.g. Figure 2b). For 12 out of 24 the temperature curves which correspond to two ramped stimuli intersected in one point but the third curve did not intersect the other two curves (e.g. Figure 2c). For the remaining 5 neurons the curves did not intersect at all (e.g. Figure 2d).

For the 2 neurons with a single intersection point distinct depth and threshold temperature were directly obtained by the intersection. For 5 neurons that the intersections span a small triangle we generated an average over the intersections. For cases where the intersections span wider ranges, generation of an average over stimulations induces a high variance in the estimated depth, leading to an expected large estimation error for threshold and depth.

The mean average receptor threshold temperature for the 2 neurons with a single intersection was 39.44 °C and standard deviation of 5.7 °C, consistent with values found in the literature (Tillman, et al., 1995). Yet, for the majority of neurons (17 out of 24) the classical method could not determine a threshold estimate of all three ramped stimuli, pointing out the potential for improvement of this classical approach toward a better estimation of depth and threshold.

The main limitation of the classical approach lies in its assumption that parameter constellations are either fully consistent with the experimental outcome (i.e. they are on the curve) and can be included in the estimation or they are completely inconsistent with the experimental outcome (not on the curve) and might be discarded. In the following sections we will use equation (2.1) as part of a probabilistic model, which allows us to formulate a continuous measure of consistency with the experimental outcome (a likelihood function). This allows us to identify a unique most likely combination of receptor depth and temperature threshold.

### 2.2.2 Probabilistic method, likelihood function

The classical method for inferring depth and temperature threshold assumes that the latency of the response is exactly equal to the time when the temperature threshold was reached. Here, we weaken this assumption by introducing a delay, Δ between the time to

threshold $t_{threshold}$ and the response latency $t_{lat}$. Thus we now evaluate equation (2.1) at $t_{lat} = t_{threshold} + \Delta$. For $i = 1,2,3$ measured responses to 3 ramped stimuli, we then have,

$$T_{threshold} = T^i_{surface} + \left(T_0 - T^i_{surface}\right)\Phi\left[\gamma/\sqrt{t_{threshold} + \Delta_i}\right] \tag{2.2}$$

In this equation, $T^i_{surface}$ denotes the surface temperature at time $t^i_{threshold} = t^i_{lat} - \Delta_i$ in the $i$-th measurement and $t^i_{lat} = t^i_{threshold} + \Delta_i$ is the latency of the response in the $i$-th measurement. Equation (2.2) is a system of $n = 3$ equations with the same parameter $T_{threshold}$ and $\gamma$ but $n = 3$ different $t^i_{lat}$ and $\Delta_i$ of three conditions. As we have shown in previous section it is not generally possible to determine an intersection point. However, because $t^i_{threshold} \leq \Delta_i \leq t^i_{lat}$, we can postulate that the delays should be (i) positive and (ii) small. We will therefore assume that the $\Delta_i$ are exponentially distributed with a parameter $\lambda$. In our experience the exact value of $\lambda$ did not change the results, so that we fixed $\lambda = 1$ for all of the following. With the given data, we can write $\Delta_i$ as a function of $T_{threshold}$ and $\gamma$, by inverting equation (2.2). This allows us to write the log-likelihood function;

$$\ell(\gamma, T_{threshold}) = -\lambda \sum_{i=1}^{n} \Delta_i(\gamma, T_{threshold}) \tag{2.3}$$

The parameters $\hat{\gamma}$ and $\hat{T}_{threshold}$ that jointly maximize this function are maximum likelihood estimates of the underlying neuron parameters. After finding the estimate for $\hat{\gamma}$, we can derive the depth using the equation $D = \hat{\gamma}.2a$ from it.

We can view the negative of the right side of equation (2.3) as an error function that we attempt to minimize under the constraint that $\Delta_i \geq 0$. The smallest error can be attained if all delays are exactly zero in which case this method agrees with the classical method discussed in the previous section. In cases in which no unique parameters setting exists, the assumption that responses should be instantaneous, is relaxed by letting one or more $\Delta_i$ be larger than zero. Note however that increasing the delays does also increase the error. Thus, the parameter constellation with minimal error will be one that is consistent with the data by assuming only minimal response delays.

Figure 3 shows, for two example neurons C-MH1 (Figure 3a-c, single intersection, in Figure 2a) and C-MH4 (Figure 3d-f, no intersection in Figure 2d) the stimulus traces for three different ramp rates (long-, middle- and short ramps) at the surface together with the attenuated stimulus traces at the classically estimated receptor location $\gamma_{classic}$ and at the probabilistic estimated receptor location $\gamma_{probabilistic}$.

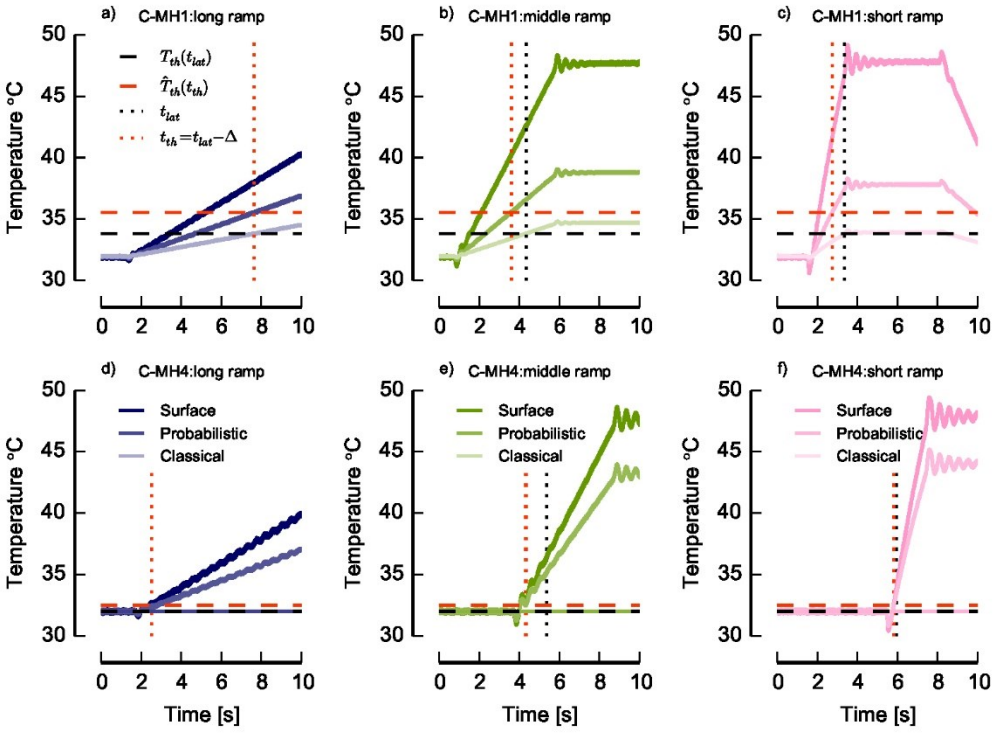


**Figure 3. The measured thermal stimulus traces applied on the surface of the skin with three ramp rates and the estimated stimulus traces within the skin at the estimated depth of neurons' terminals for two example neurons C-MH1 and C-MH4.** The estimation of the depth and $T_{threshold}$ was done according to the classical and probabilistic method. The probabilistic estimated $T_{threshold}$ is the solution of equation (2.3). The classical $T_{threshold}$ is the intersection of $T^{i}_{surface}$ , i = 1,2,3 curves in $D$-$T_{threshold}$ plane for three ramp rates of equation (2.1). (**a-c**) The stimulus traces of neuron C-MH1 for (**a**) long ramp, (**b**) middle ramp, and (**c**) short ramp. Both classical and probabilistic methods successfully estimated the parameters. The classical model approached a single intersection of ramped stimuli and probabilistic method approached small delays. (**d-f**) The stimulus traces of neuron C-MH4 for (**d**) long ramp, (**e**) middle ramp, and (**f**) short ramp. The classical method failed to find an intersection but the probabilistic method resulted successfully to a parameters estimate.

In example neuron C-MH1 the classically estimated normalized depth is $\gamma_{classic} = 2.04$ and probabilistic estimated is $\gamma_{probabilistic} = 1.05$. As Figure 2a shows for C-MH1 the classical model results successfully in a single intersection. The probabilistic estimated location of neuron, however, is closer to the surface compared with the classical estimate. As a result the estimated stimulus at $\gamma_{classic}$ is weaker for all three ramp rates.

Note that in Figure 3a the estimated delay for the longest ramp is close to zero but not for the middle ramp (Figure 3b) and short ramp (Figure 3c).

In the case of neuron C-MH4 the classical method failed to find an intersection of all three ramp stimuli (see Figure 2d) and therefore the stimulus traces could not be tracked at location $\gamma_{classic}$. But the probabilistic method estimated successfully a depth and thus the stimulus traces could be estimated at this location (see Figure 3d-f). Note that neuron C-MH4 shows a small latency for all three ramp stimuli. The first spike in all three conditions occurred immediately after the stimulus onset. This observation may suggest that the first

spike may actually have been caused by sources of activity other than the onset of the heat ramp.

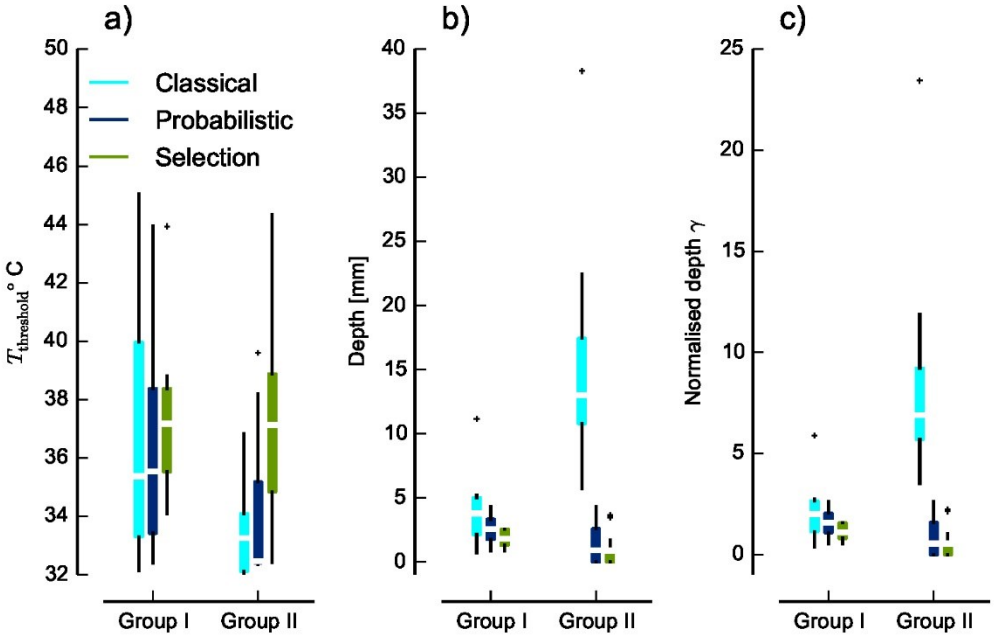


**Figure 4. (a) Estimated threshold temperature $T_{threshold}$, (b) depth $D$, (c) and normalized depth $\gamma$ of 24 C-MH neurons according to three methods: classical model, full probabilistic model and a selection model.** For the selection model, in which the outlier curve was omitted, we chose the model with the highest evidence. Neurons are divided into two groups. In group 'Single intersection' or 'Group I' the classical model was successfully resulted in a single or very close intersection. This group includes 7 neurons. In 'Two/None intersection' or 'Group II' the classical model failed to estimate an intersection. This group includes 17 neurons. The boxes extend from the lower to upper quartile values of the estimated in each group, with a white bar at the median. The whiskers show the range of the estimates. Flier points are those past the end of the whiskers.

Figure 4 summarizes the results of analysis of all neurons for three estimates $T_{threshold}$ depth $D$ and normalized depth $\gamma$. We divided all 24 C-MH neurons into two main groups: The group 'Single intersection' that includes 7 neurons for which the classical model successfully resulted in a single intersection or the intersections span a small triangle like neurons C-MH1 and C-MH2 of Figure 2a-b. We refer to this group as 'Group I'. The group 'Two/None intersections' that includes the remaining 17 neurons for which the classical model failed fully or partly to estimate any intersection like neurons C-MH3 and C-MH4 of Figure 2c-d. We refer to this group as 'Group II'. The estimated parameters in 'Group I' for both classical and probabilistic models compared with the same parameters in 'Group II' reveals that in 'Group I' both approaches were successful. But, the classical model shows very implausible values for the 'Group II': a median threshold temperature of $T_{threshold} = 33.3$ °C and mean depth of $D = 12.5$ mm. Previous studies have shown that the majority

of C-MH fibers display a threshold of 43 °C (Basbaum, et al., 2009) (Patapoutian, et al., 2003), but several studies have reported threshold temperature in a range of 36-47 °C (Hardy & Stolwijk, 1966) (Tillman, et al., 1995) (Bromm, et al., 1984) (Lele, 1954). Given the thickness of the skin <1 mm in our experiments and the reported values of threshold temperature, the classical model failed to estimate the parameters for the 'Group II' with two/none intersections. The full probabilistic model shows for 'Group II' a mean threshold of $T_{threshold} = 32.36$ °C and a mean depth $D = 0.9$ mm. Hence this model likely failed to estimate $T_{threshold}$ (because it is implausibly low), but the estimated depth was consistent with the reported depth from the previous studies in range of 20-570 µm (Tillman, et al., 1995) (Bromm, et al., 1984). Note that in our experimental setup the heat electrode was placed on the inside of the skin, so the depth of the receptor from the epidermis was $D_e = 100$ µm (assuming that the skin is approximately 1 mm thick).

As a brief summary, in this section we showed that using a statistical model to estimate the parameters gives a successful parameter combination of depth for all neurons even when the classical model fails to give any parameter estimate. Yet, in the case of estimated threshold temperatures the values with a median of $T_{threshold} = 32.36$ °C were lower than previously reported thresholds in range of 36-47 °C (Hardy & Stolwijk, 1966) (Tillman, et al., 1995) (Bromm, et al., 1984) (Lele, 1954). We then used the calculated depth to estimate the attenuated stimulus traces at the location of the receptor ending.

The major contribution of the probabilistic model is to incorporate noise by allowing for delay in first spike time. However, we didn't cover the possibility that the first spike recorded after stimulus onset might be an 'outlier' which was not triggered by the stimulus, but rather generated by the (low) resting state activity of the receptor. Next we therefore addressed the question of how our results would change under the assumption that the first spike after stimulus onset may have been triggered by a probabilistic random process.

### 2.2.3 Selection method, discarding outlier responses

Every stimulus that is taken into account for the estimation of depth and threshold adds a certain amount of information and reduces the uncertainty of the estimation. But since there is also a certain probability that the first spike is not a response to the stimulus, every stimulus also adds a certain amount of noise to the estimation. Hence, there exists a potential tradeoff in adding as many recordings as possible to the estimation, or rejecting some of them as outliers. For example in our data for 12 out of 24 neurons in $D - T_{threshold}$ plane, two out of three curves intersect in one point, while the remaining curve either intersects in other points or does not intersect. Essentially, at least two ramp stimuli of different slope are required to observe an intersection of the curves. But, we asked if we

reduce the variability of the estimate in the case of widely spanned ranges of intersections by omitting some curves.

We extended this idea to the maximum likelihood framework described in the previous section. We introduced multiple probabilistic models that could describe the data and then decided which one provides a more concise description.

To discriminate between the models we employed a Bayesian testing procedure (Jeffreys, 1935) and used model comparison based on marginal likelihood (Kass & Raftery, 1995). This approach is usually applied to pairwise comparisons: to compare two models, the marginal likelihood of each model is evaluated. The ratio of the marginal likelihoods from model 1 and model 2 is called the Bayes Factor. If the ratio of marginal likelihoods from model 1 and model 2 is larger than 1, the first model is preferred and vice versa, the second model is preferred.

The main reason for adopting a Bayesian approach for model comparison is that Bayes factors provide a way of including other information as prior knowledge when assessing the evidence for a hypothesis. This is a strong advantage for data with lots of uncertainties, such as a small number of recorded neurons and no repetition of recordings for each stimulus, or an incomplete skin model. We can incorporate histological and bio-thermal information and results reported by other investigators as prior knowledge and use this to improve the estimation of receptor parameters. Furthermore, by integrating over the full parameter space, marginal likelihoods penalize complex models in a very natural way (Kass & Raftery, 1995) (Kass & Wassermann, 1995).

Bayes Factors can only be calculated for pairwise comparisons. Yet, here we are interested in selecting the best out of multiple models. We therefore used the marginal likelihoods directly and chose the model that maximizes the marginal likelihood. For simplicity, we will refer to any of the models that exclude one or more stimuli from the determination of the neuron's parameters as the ‘Selection model’.

The first model is the full probabilistic model described above, assuming a data set consisting of *n* different experimental conditions, e.g. ramped stimuli, where for all responses the first spikes have been triggered by the stimulus. More specifically, the first model assumes that the corresponding delays $\Delta_i = t_{lat}^i - t_{threshold}^i$ , ( $i = 1,2,3$ number of stimuli) have a probability distribution with free parameters $\theta_1 = \{\gamma, T_{threshold}\}$. Here, the unknown skin parameters and other nuisance factors could go into $\theta_1$ as well.

In the ‘Selection models’ only for the first $m < n$ responses the first spikes have been triggered by the stimulus and would therefore contribute meaningfully to the estimate of

depth and threshold. For the remaining responses the first spikes are the result of a stationary background process, e.g. spontaneous discharges or in any other way not triggered by the stimulus. Thus the second model assumes that only the first delays $\Delta_i$, $i = 1, \dots, m,\ m < n$ have the same probability distribution with parameters $\theta_1$ and the remaining delays are based on processes with different distribution functions. This second model has a parameter vector $\theta_2 = \theta_1 \cup \{\tilde{\Delta}_{m+1}, \dots, \tilde{\Delta}_n\}$ that contains the parameters from the first model and some additional parameters to capture the times of the non-stimulus-triggered first spikes.

In the case of our data the delays of three ramped stimuli in first model $M_1$ have the same probability distribution with the parameter space $\theta_1 = \{\gamma, T_{threshold}\}$. In instances of the selection models $M_2$ only two delays out of three have the same distribution with the parameter space $\theta_2 = \theta_1$ and the third delay has a density function $\mathrm{P}(t, \tilde{\lambda})$ with parameter $\tilde{\lambda}$.

To compare the models, we use the marginal likelihood,

$$\mathcal{L}_k = \int \mathrm{P}(\Delta|\theta_k, M_k)\mathrm{P}(\theta_k|M_k)d\theta_k \qquad (2.4)$$

In equation (2.4), $\mathrm{P}(\Delta|\theta_k, M_k)$ is the likelihood of observing the delays given the parameters $\theta_k$ under model $k$. Making the dependence of the likelihood on the model explicit here illustrates that in addition to the parameters of the model, the likelihood of the data depends on the formulated model itself as well. The term $\mathrm{P}(\theta_k|M_k)$ is the prior density of the parameters of model $M_k$. This term provides a way to include other information about plausible values of parameters. Our first concern is thus how to choose prior densities to represent the available information.

The prior densities offer an appropriate way of adding biologically meaningful constraints from the literature into a statistical model. In Table 1 we show a summary of reported parameters and the prior density functions we employed here (for more details of choice of prior densities see section methods).

We applied the 'Selection models' on the 24 neurons. To demonstrate the performance of the selection models, we chose the model $M_{2,i}$ (*i*-th stimulus was omitted) with the highest evidence and compared the estimates with the results of full probabilistic model $M_1$ and with the classical model. Figure 4 shows the $T_{threshold}$, depth and normalized depth $\gamma$. The selection model shows for the 'Group II' a mean threshold of $T_{threshold} = 36.7$ °C and a mean depth $D = 0.8$ mm. In contrast to the full probabilistic model, the selection model

approached successfully to a mean threshold temperature, which is consistent with the previous studies.

We supposed that the main reason why the classical model failed was its inability to account for neural noise and for statistical outliers in the responses. Thus, one might expect that a working stimulus selection model would mainly detect outliers, and thus exclude the response to one stimulus from the parameter determination for those neurons for which the classical model failed. To test this idea, we normalized the sum of the marginal likelihoods for each neuron across all candidate models to 1. We then plotted the normalized marginal likelihood for the full model that does not exclude any stimuli (see Figure 5). Clearly, the marginal likelihood $\mathcal{L}_{full}$ was larger for the 'Group I' for which the classical model had been successful than it was for the 'Group II' for which the classical model had failed to find a consistent parameter estimate. Put another way, this indicates that for many neurons in 'Group II', one of the selection models provided a better description than the full model. As the selection models accounted for outliers, while the full model did not, we conclude that statistical outliers might have contributed to the failure of the classical method on the neurons in 'Group II'.

Thus, the results from our method suggested that for 'Group II', selection models that accounted for statistical outliers were more successful at describing the data, suggesting that outliers had indeed contributed to the failures of the classical method in these neurons.

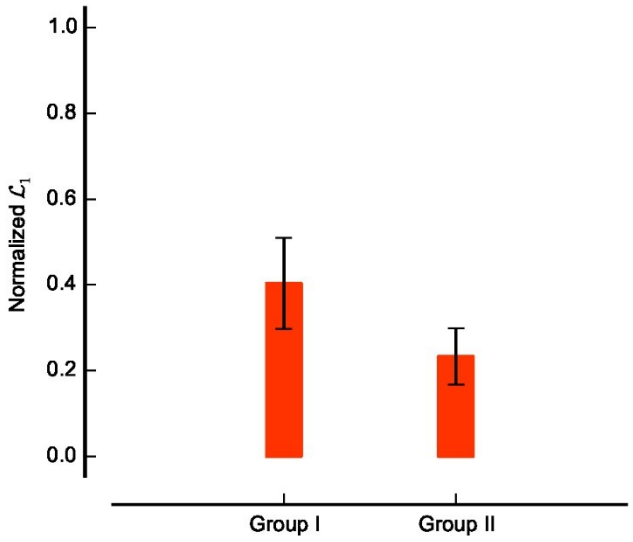


**Figure 5. Normalized marginal likelihood for the full probabilistic model $M_1$ for two groups of neurons.** The 'Group I' includes 7 neurons that could be estimated successfully by classical model. The 'Group II' includes the remaining 17 neurons. The error bars are the standard error of the mean.

**Table 1. Priori distributions for different parameters.** The reported values of $T_{threshold}$ were estimated at either first spike time or first time if reporting pain or any sensations. The priori density functions are: Normal distribution N, Beta distribution B, and Uniform distribution U.

| Parameters | Reported value | Subject | Reference | Prior density | Remark |
|---|---|---|---|---|---|
| Threshold | 36 °C | Human | (Lele, 1954) | N(38,2) | First sensation |
| | 39-41 °C | Monkey | (Tillman, et al., 1995) | N(38,2) | First spike |
| | 43.2 °C | Human | (Stoll & Greene, 1959) | N(38,2) | First pain |
| | 43 °C | Human | (Bromm, et al., 1984) | N(38,2) | - |
| | 45 °C | Human | (Hardy & Stolwijk, 1966) | N(38,2) | - |
| | 47 °C | Rat | (Lynn & Carpenter, 1982) | N(38,2) | - |
| Depth ***D*** | 20-570 µm | Monkey | (Tillman, et al., 1995) | B(4.75,2.25) | C fibers |
| | 180-240 µm | Human | (Stoll & Greene, 1959) | B(4.75,2.25) | C fibers |
| | 100 µm | Human | (Bromm, et al., 1984) | B(4.75,2.25) | C fibers |
| Thermal conductivity $\kappa$ | .05-.14 W/mk | Pig, Human, Monkey, rat | (Xu, et al., 2008) (Tillman, et al., 1995) (Henriques & Moritz, 1947) (Duck, 2013) | U(0.05,0.14) | Dermal & Epidermal |
| Density $\rho$ | 1116-1200 Kg/m$^3$ | Pig, Human, Monkey, rat | | U(1116,1200) | Dermal & Epidermal |
| Specific heat $c$ | 700-950 J/Kg K | Pig, Human, Monkey, rat | | U(700,950) | Dermal & Epidermal |

## 2.3 Discussion

In this study we have shown that considering variability, noise and stochastic processes in study of primary afferent pain receptors improved the classical deterministic models to estimate the depth and threshold of C-fiber nociceptors. We have shown that allowing for a small delay in the first response of C-MH nociceptors modified the localization of the receptor neurons. Moreover, assuming some stochastic activities which were not triggered by stimulus and discarding the outlier responses caused by these stochastic activities further improved the estimation of activation threshold of C-MH neurons. We demonstrated the reliability of our general framework on a challenging data set, in which the stimulus electrode was placed on the corium and dermal side of the skin, the thickness of measured skin was unknown and each stimulus condition was applied only once. Our approach provides a unique insight into how temperature impinges on heat transducers in their native, complex environment. Most studies have hitherto focused on activation of channels by membrane heating in an in vitro context where skin is absent (Cesare & McNaughton, 1996). Our study provides a framework to understand where and with what temperatures native heat transducers are activated in vivo.

Introducing delay in response time allows us to weaken the assumption that latency and the threshold time should be the same. However, a delay is justified only if the probabilistic model converges to the classical model in boundary condition. Because in classical model all delays are neglected it describes an ideal, noise-free case and thus represents the boundary condition for the probabilistic model when delays are zero. Hence in the boundary condition the classically estimated model parameters should maximize the log-likelihood function of delays. Our results confirmed that for negligibly small delays, the probabilistically estimated parameters converge towards the classically estimated results. Hence, the probabilistic model improves the results in cases where the classical model failed and converges to the classical model in boundary condition.

An alternative way to account for noise in the system might be to add white noise into equation (2.1) and treat it as suggested in the classical method. However, this approach would require to either predetermine the amount of the noise, or to assume that noise is generated by a random process and systematically vary the parameter governing that process. Because of the unknown sources and amount of noise, the first method might add more uncertainties to the system and the latter method might result in a biological meaningless source of noise.

In fact, while the probabilistic model improved the estimation of depth, it did not improve the estimate of the mean threshold temperature. The low average threshold temperature around the baseline temperature for some results estimated by probabilistic model suggests that for some responses, a small delay in threshold time might not be sufficient to deal with the noise. Indeed, the estimation of depth and threshold temperature was improved by discarding these outlier responses in the 'Selection models'. In addition, the marginal likelihood ratios suggested that the 'Selection models' described the observed latency better than the initial probabilistic model that used all stimuli to estimate the neuron's parameters. Using marginal likelihoods also offered a way of adding prior information about model parameters from the literature by choosing an *a priori* density function. For some parameters, there were multiple possibilities for choosing the prior density. This could have influenced our computation of model evidence (Kass & Raftery, 1995). Yet, when we repeated our analysis with slightly different priors, the estimated model evidence consistently favored the same model (for more details see section methods; choice of prior density functions). We therefore believe that our outlier-detection method is relatively insensitive to the choice of the exact parametric form of the prior distribution, as long as the range of values from the literature is captured.

Localization of sensory endings is particularly interesting for quantitative models that describe the responses of a neuron to stimulation and for attempts to uncover the neurons encoding strategy. For instance, in mathematical modeling of touch sensitive A-fibers several investigators have used the histologically measured depth to model the somatosensory responses (Sripati, et al., 2006) (Gerling & Thomas, 2008) (Edin, 2004). However, the thickness of epidermis and dermis is variable over a population of animals and depends on the gender, age, area and hair cycle, and anatomical location (Wang, et al., 2013). In many experimental setups the thickness of skin layers and location of neuron have not been measured. Even in such cases our method can be freely adapted to estimate the depth and threshold of neurons by replacing the heat stimulation with mechanical stimulation and the heat transfer function with the stress/strain functions. Whereas other investigators required complex and detailed skin models, we presented a simple probabilistic model of skin. This way, our method can provide results for cases in which the data do not warrant the formulation of a very detailed skin model, or where insufficient information about the thermodynamic properties of the studied tissue is available.

## 2.4 Methods

Experiments were performed in strict accordance with the recommendations in the Guide for the Care and Use of Laboratory Animals of the Max Delbrück Centre for Molecular Medicine. The protocol was approved by the Committee on the Ethics of Animal Experiments of Animal Welfare German authorities (LaGeSo; Permit Number: T (00383/12).

### 2.4.1 Skin nerve preparation and identification of single C-fibers

The skin-nerve preparation was used to record from single primary afferents (Milenkovic, et al., 2007) (Milenkovic, et al., 2008) (Wetzel, et al., 2007) (Martinez-Salgado, et al., 2007). Mice were killed by $CO_2$ inhalation for 2–4 min followed by cervical dislocation. The saphenous nerve and the shaved skin of the hind limb of the mouse were dissected free and placed in an organ bath at 32 °C. The chamber was perfused with a synthetic interstitial fluid (SIF buffer) the composition of which was (in mM): NaCl, 123; KCl, 3.5; MgSO4, 0.7; NaH2PO4, 1.7; CaCl2, 2.0; sodium gluconate, 9.5; glucose, 5.5; sucrose, 7.5; and HEPES, 10 at a pH of 7.4. The skin was placed with the corium side up in the organ bath. The saphenous nerve was placed in an adjacent chamber on a mirror to aid and under microscopy fine filaments were teased from the nerve and placed on the recording electrode. Electrical isolation was achieved with mineral oil.

Single mechanically sensitive units were characterized by probing the skin with a glass rod for mechanically responsive receptive fields. Figure 6 shows the anatomical location of all 24 neurons relative to the saphenous nerve trunk. Using an electrical stimulating electrode, we measured the conduction velocity (calculated by dividing conduction distance over electrical latency for the spike) to select C-fibers whose conduction velocity was in the C-fiber range <1 m/s.

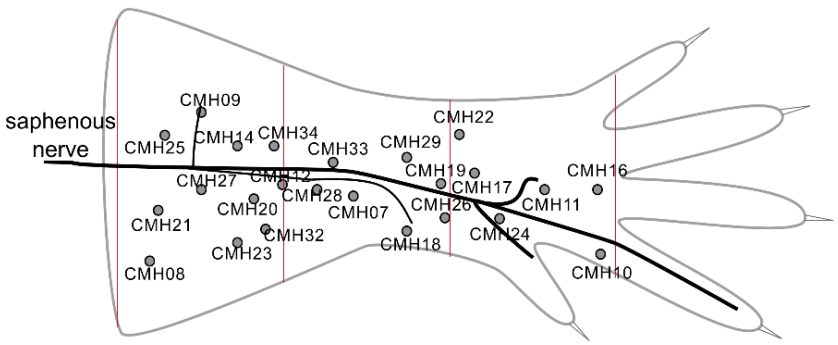


**Figure 6. Schematic of hind-limb skin of mouse and anatomical locations of receptive field.** For all 24 neurons the locations of the receptive fields are illustrated in respect to the saphenous nerve trunk.

### 2.4.2 Thermal stimulation protocol

For heat stimulation, a Peltier element–based contact probe (4x3 mm surface) applied thermal stimuli (custom device built by the Yale School of Medicine Instrumentation Repair and Design) to the receptive field of identified C fibers.

The stimulation protocol sent as a pre-programmed series of commands to the Peltier element were applied to all C-fibers. The thermal stimulation protocol consisted of 3 stimuli (32–48 °C) with different ramp durations (16 s, 4 s, 2 s) and the hold phase of 10 seconds. The interstimulation interval was 60 seconds. The order of stimulation was first heat and then mechanical from the slowest to fastest ramps. After the thermal stimulation we carried out a mechanical stimulation protocol, the results of which are not part of this manuscript. Data were obtained from 11 C57Bl6/N wildtype mice.

### 2.4.3 Heat transfer model of skin

Heat energy flows through the skin to the nociceptive terminals due to the temperature gradients. According to the second law of thermodynamics, heat flows from warmer location to colder location. With no heat source, these thermodynamical effects will let the skin relax to one homogeneous temperature. In an experimental set using a Peltier device, the stimulus acts as a heat source, inducing heat at one location which then flows through the skin and eventually results in a temperature increase at the receptor site of neuron. Because the stimulus temperature varies over time, the resulting heat flow will vary over time as well. In addition, it varies in space because skin is not an ideal conductor and locations further from the stimulus receive lower heat energy and at a later time. Directly measuring the exact temperature profile in the skin at the depth of nociceptor is difficult. Therefore, heat transfer in the skin is typically modeled using thermodynamical laws (Xu, et al., 2008) (Henriques & Moritz, 1947). The general equation describes heat flow in the skin by a diffusion equation,

$$\frac{\partial T}{\partial t} = a^2 \frac{\partial^2 T}{\partial x^2} \tag{2.5}$$

Here, $T = T(x,t)$ is the temperature at time $t$ and distance $x$ from the stimulus contact, such that $T(0,t)$ is the experimentally applied heat stimulus and the temperature at other locations needs to be determined by solving equation (2.5). Furthermore, $a = \sqrt{\kappa/\rho\, c}$ is called the thermal diffusivity. Thermal diffusivity is square root of the ratio between thermal conductivity $\kappa$ and the product of density $\rho$ and specific heat $c$ of the skin.

When solving equation (2.5) analytically, one has to assume that the skin is a solid with uniform thermal properties. Given the complex structure of the skin, this assumption is

likely to be violated. More realistic approaches therefore treat the skin as consisting of multiple layers, where each layer has uniform thermal properties but layers are allowed to differ in their thermal diffusivity. Typical models use separate layers for epidermis, dermis and subcutaneous tissue (Tillman, et al., 1995) (Xu, et al., 2008). Other models have used four layers (Henriques & Moritz, 1947) or up to eight layers (Hardy & Stolwijk, 1966) in live animal models. In all these multi-layer approaches, the stimulus is assumed to be applied at the epidermal side of the skin and the thickness of each layer has to be specified in advance. Then, a system of equations describing the flow of heat into and out of each of the layers can be derived. (Tillman, et al., 1995) (Marchandise, et al., 2014) used a modified finite difference schemes to numerically solve these equations, while (Stoll & Greene, 1959) (Henriques & Moritz, 1947) derived a first order approximation of the time-temperature relationship in every layer and at any distance from the skin surface according to the equation (2.1). This approximation was originally derived for experiments in which the stimulus is abruptly switched on and is then kept fixed until the threshold is reached. However, these approximations have also been successfully applied to conditions where the surface temperature is not constant but is known at every instant in time (Stoll & Greene, 1959). This perspective can be justified if we assume that heat conductance in the skin is sufficiently fast. Then the temperature at any distance can be computed quite accurately until the steady state temperature is reached.

### 2.4.4 Estimation of depth from $\gamma$ using a Monte-Carlo method

Several investigators measured the epidermal and dermal thickness and their thermal properties. In Table 1 we summarized some measurements. So far the experiments don't differ, we would start usually with epidermis as superficial layer and estimate $D$ for a determined diffusivity of epidermis according to,

$$\gamma = \frac{D_e}{2\sqrt{\kappa_e/\rho_e c_e}} \tag{2.6}$$

If the estimated $D$ does not exceed the histological measured epidermal thickness, we would accept it as the depth of nerve endings, otherwise $\gamma$ would compose of epidermis and dermis layers

$$\gamma = \frac{D_e}{2\sqrt{\kappa_e/\rho_e c_e}} + \frac{D_d}{2\sqrt{\kappa_d/\rho_d c_d}}$$

Where, $D_e$ is the depth of the epidermis, and $D_d$ is the depth of dermis. To estimate $D$ in equation (2.6) we would then determine $D_e$ and thermal diffusivities and solve the equation for $D_d$.

In our data set, however, the heat electrode was placed on the dermal and subcutaneous site of the skin and the thickness of the skin wasn't measured. This experimental redundancy prevent using a direct multilayer model of the skin. Therefore we reduced a two layer model with separate layers for epidermis, and dermis to a one layer model, which accords properties of both epidermis and dermis. Next step is to set the skin of a one layer model. To this end, we took the maximum and minimum reported values of thermal conductivity, density, and specific heat of epidermis and dermis from literature (see Table 1). We then sampled three sets for $\kappa, \rho$ and $c$ from respective uniform distributions. The sampling range of the distributions were the maximum and minimum values for epidermis and dermis. For the estimated normalized depth, $\gamma$ we drew every single parameter from the corresponding sampling distribution and computed the depth. We then repeated this procedures for the whole sampling sets with size of $10^8$ and in the end averaged over the computed $D$.

### 2.4.5 Choice of prior density functions

In order to express the prior assumptions about the value of $\gamma = \frac{D}{2\sqrt{\kappa/\rho\, c}}$, we need an *a priori* density function of the depth and all parameters of the thermal diffusivity. According to histological studies most C-MH fibers end in the epidermal to dermal layers of the skin (Breathnach, 1977). Therefore, the probability of finding the nerve endings decreases with increasing depth, but it is unlikely to find nerve endings directly beneath the skin surface. Furthermore, depth cannot be larger than the skin's thickness, which is in our experiments approximately 500 µm to 1 mm. Note that in our experimental set up the position zero refers to some distances deep into dermis and subcutaneous tissue. The shape of this distribution seems to have a probability density function with asymmetric tails but a heavier tail toward zero. A distribution with this property is offered by Beta distribution. Beta distribution has two shape parameters α and β. These shape parameters are determined if two properties of the distribution are known, for example the mode and a given percentile. In previous studies the locations of C-MH fibers were estimated in the depths ranging from 20 to 570 µm (see Table 1 for references). Therefore, we scaled the Beta distribution in an interval of $0 \leq D \leq 600$ µm and assumed that the depth of a receptor neuron had a Beta distribution with 75-80 percent of the distribution's mass in an interval around median of an approximate width of 400µm and model $\frac{\alpha-1}{\alpha+\beta-2} = [0.75, 0.8]$. We arbitrary chose two

shape parameters α = 4.75 and β = 2.25 which satisfied these assumptions. In addition and to verify that this choice of prior did not influence our analysis, we also ran the same analysis with other shape parameters and a uniform and Weibull distribution.

We chose uniform distribution U(a,b) (with a and b being the minimum and maximum values of distribution) for the thermal diffusivity parameters. To this end $\gamma$ composes of four distribution functions in form of $\frac{D_i}{2\sqrt{\frac{\kappa_i}{\rho c_i}}}$ and $D_i \sim \mathcal{B}(4.75,2.25)$ , $\kappa_i \sim \mathcal{U}(0.3,1.3)$ , $c_i \sim \mathcal{U}(700,950)$, and $\rho_i \sim \mathcal{U}(1116,1200)$ , (for the *i*-th draw from sampling population).To define an explicit density function $\mathrm{P}(\gamma)$ we firstly drew samples $D_i, \kappa_i, c_i$ , $i = 1, \dots, 10^8$ from the respective distributions and calculated $\gamma_i$. It is very difficult to derive an analytical form for the distribution of $\gamma$ from these assumptions. Therefore, we approximated the distribution of the sampled $\gamma$ by a mixture of 3 Gaussian distributions with unknown parameters (estimated using expectation-maximization (EM) algorithm for fitting mixture-of-Gaussian models implemented in scikit-learn, the number of components was determined by minimizing Bayesian Information Criterion (BIC).).

A more complicated case is the prior $\mathrm{P}(t, \tilde{\lambda})$ for the outliers $\widetilde{\Delta_1}$ in 'Selection models' $M_2$. In order to create a meaningful marginal likelihood, the prior should be a proper probability density function (Kass & Raftery, 1995). In addition, the priors should be random statistical process that generate the first spikes independently of the stimulus. An example density that satisfies this property assumes that the first spike times are spontaneous events, which are generated by a Poisson process. Under these conditions the first spike time is a random event of an exponential distribution with a rate parameter $\tilde{\lambda} \sim 10$. To estimate the total evidence for a model, we took the expectation with respect to $\tilde{\lambda}$. This expectation was implemented as a numerical integration.In Table 1 we summarized all priori distribution functions for parameters from literature including the references.

### 2.4.6 Calculating the marginal likelihood

Typical strategies to estimate the marginal likelihood (4) are sampling (i.e. Monte-Carlo integration) or analytical approximations like the Laplace approximation, Variational Inference, or Expectation Propagation. For low dimensional parameter spaces (2-4 dimensions), numerical integration may work as well. In equation (2.3), the delays are only given implicitly, which makes analytical approximations quite difficult. Furthermore, numerical integration techniques would be computationally very intensive due to the cost of solving equation (2.3). We therefore used a combination of analytical and numerical integration to determine the marginal likelihood. We interpreted the integral (4) as the

expected value of the likelihood function $\mathrm{P}(\Delta|\theta_k; M_k)$ , under the prior density $\mathrm{P}(\theta_k|M_k)$ for model $M_k$ ,

$$\mathbb{E}[\,\mathrm{P}(\Delta|M_k)]_{\mathrm{P}(\theta_\mathrm{k}|M_k)} = \int \mathrm{P}(\Delta|M_k)\mathrm{P}(\theta_\mathrm{k})d\theta_k$$

and used numerical integration according to trapezoidal rule to compute the expected value. The prior densities are for model $M_1$:$\{\mathrm{P}(T_{threshold}), \mathrm{P}(\gamma)\}$and for model $M_2$: $\mathrm{P}(\theta_k) = \{\mathrm{P}(T_{threshold}), \mathrm{P}(\gamma), \mathrm{P}(t, \tilde{\lambda})\}$ For 'Selection models', $M_2$, however, we assumed the outlier first spike has a fixed value, so that we can formally write the likelihood for the outlier components as a dirac function $\delta(\mathrm{t_{lat}} - t)$, which allowed us to solve for the corresponding components of the marginal likelihood (4) analytically. All other parameters of model $M_2$ were treated in the same way as in $M_1$.

For every potentially excluded stimulus in selection model $M_2$, we estimated the ratio of the marginal likelihood for the full model $M_1$ over the marginal likelihood for the model $M_2$ without the excluded stimuli.

# Chapter 3

# 3 Decoding of Polymodal C-fiber Nociceptor Responses with a Generalized Linear Model and L1 norm Regularization

Understanding how the expression of ion channels affects the responses of polymodal C-fiber nociceptors to different modalities of stimulation is fundamental for understanding the encoding strategy of primary afferent neurons. Yet, less is known about the mechanism of mechanically and thermally activated ion channels accounting for pain sensation. A commonly used method in system neuroscience for understanding the computation carried out by a neural population is to predict the neural responses to the given stimulus using a generative model. A method that has often been neglected in studying nociceptors. In this study we focused on applying advanced statistical methods to give qualitative insights into the encoding strategy of transduction mechanisms at receptor sites. We computed a large dimensional space of stimulus features – strain components (force-induced deformation of skin) and thermal components from the represented mechanical and heat stimuli. We then used a Generalized Linear Model (GLM) with a L1 norm regularization to model the neural responses while selecting the most predictive candidate features. Our results show that in a data set of 24 C-fibers, derivative of vertical compressive strain, maximum compressive and tensile strains are promising candidates to describe the mechanical transduction of C-fibers.

## 3.1 Introduction

Nociceptors are primary afferent neurons responding to tissue injury caused by thermal, mechanical or chemical noxious (painful) stimuli. Activation of specific receptors and ion channels in nerve endings of the nociceptors results in the initiation of action potentials that propagate along the axon of primary fibers, through a synaptic site in the dorsal horn in the spinal cord, to higher brain centers, where they are thought to be perceived as pain. The electrical activity of primary afferent neurons is primarily governed by the expression and function of ion channels. These include voltage-gated sodium, potassium and calcium channels, leak channels, and ligand-gated channels such as acid-sensing ion channels

and transient receptor potential (TRP) channels (see (Julius & Basbaum, 2001) (Waxman, Stephen G & Zamponi, 2014) (Caterina, et al., 1997) (Cho, et al., 2012) (Vriens, et al., 2014) for review on molecular mechanism of pain).

Many investigations of the neural mechanism underlying the responses of nociceptors to noxious stimuli are confronted with a similar challenge, namely identifying the mechanism which shapes the spatial and temporal dynamics of response discharges to different modalities of stimuli. In general, the underlying mechanism can be divided into two steps: (1) the transduction of external stimuli into electrical signals (proximal stimulus) by ion channels, and (2) the generation of action potentials. Remarkable advances have been made towards understanding ion channels expressed in innocuous mechanoreceptors (Delmas, et al., 2011) (Bensmaia, 2008) (Poole, et al., 2015) (Lewin & Moshourab, 2004). However, less is known about the ion channels that are responsible for transducing painful mechanical and heat stimulation in polymodal C-fiber nociceptors (Ranade, et al., 2014). Experimental approaches towards elucidating the functions of polymodal C-fibers are limited mainly because of the small diameter and free nerve endings of C-fibers that make them hard to localize, isolate, and consequently to access for standard patch clamp and electrophysiological recordings.

Alternatively, descriptive or neural spiking models offer a promising framework for understanding how information about different stimulus modalities is encoded in sequences of action potentials of primary afferent neurons. In this regard mathematical models have been developed to study pain pathway at different levels; at molecular and cellular level (Britton, et al., 1995) (Britton & Skevington, 1989), at the central level of the spinal cord (Rho & Prescott, 2012), and in the brain (Cecchi, et al., 2012). Yet, the primary afferent nociceptors innervating the skin disperse their receptor sites over epidermal and dermal layers of skin (Breathnach, 1977). Each layer attenuates or amplifies the energy of thermal stimuli or produces complex mechanical deformations of skin tissue depending on its physical properties, histological structure, and thickness (Wang, et al., 2013). Hence, an adequate model of mechano-heat-sensitive receptor neurons requires to consider both the bio-thermo-mechanical responses of skin tissue and combination of different stimulus modalities by peripheral transduction mechanisms. So far some mathematical approaches have been developed to model the responses of heat-sensitive receptor neurons to attenuated thermal stimuli (Henriques & Moritz, 1947) (Tillman, et al., 1995) (Xu, et al., 2008) and responses of mechano-sensitive receptor neurons to skin deformations caused by mechanical stimuli (strains) (Phillips & Johnson, 1981b) (Sripati, et al., 2006) (Srinivasan & Dandekar, 1996) (Lesniak & Gerling, 2009) . The central assumption of these models is that the frequency of the neuronal firing emitted by the neurons depends

on the intensity of a particular combination of strains (e.g., compressive, tensile, vertical or horizontal and shear strain) in the local neighborhood of the receptor terminals or on the attenuated heat energy at the depth of receptor. However, none of these models suggested a combinatorial approach to model the responses of polymodal C-fibers to both attenuated thermal stimuli and mechanical strains. Further, these models have typically assumed the noise levels to be negligibly small and thus were limited to apply the classical statistical approaches.

Advanced statistical models of signal transduction have been successful at inferring mechanisms of signal transduction in other domains of systems neuroscience such as vision (e.g. (Gerwinn, et al., 2010) (Pillow, et al., 2005)). However, in contrast to visual neurons, primary afferent nociceptors are unique because single primary sensory neurons have the ability to detect a wide range of stimulus modalities, including those of a physical and chemical nature (Basbaum, et al., 2009). Therefore, nociceptors must be equipped with a repertoire of diverse transduction devices. At the same time compared to experimental setups for recording from other sensory neurons, recording from C-fiber nociceptors has been proven as difficult and the data sets are typically small with few repetitions. Overall, statistical modeling of the response discharges in common data sets of recordings from C-fibers is challenging.

In this study we seek to explore the potential uses of a Bayesian model to study the responses of primary afferent C-fiber nociceptors. With this framework we can not only focus on either mechanical or heat receptors but also infer the sensitivity of C-fiber nociceptors to both strain and heat components of stimuli. This study is organized as follow. In section “3.2.2.1 Force profile” we first obtained the stress and strain profiles arising from a mechanical force electrode applied to the dermal side of mouse hind-limb skin according to the continuum mechanics model suggested by Phillips and Johnson (Phillips & Johnson, 1981b). Furthermore, in section “3.2.2.2 Temperature profile” we used the estimated depth of all neurons reported in a previous study (Dezhdar, et al., 2015, in press) and estimated the temperature curves at the depth of receptor site. In section “Methods: Generalized linear Model (GLM) for receptors”, we used these stress-strain patterns and estimated temperature curves to provide a link between the stimulus components and the discharge patterns of C-fiber nociceptors in terms of a generalized linear model (GLM) (Nelder & Wedderburn, 1972). Finally, because experimental data sets are often too small to fully identify the complete strain pattern, we regularized the GLM by the L1 norm of the regression coefficients (least absolute shrinkage and selection operator, LASSO) (Tibshirani, 1996), giving preference to sparse solutions for which only few strain and heat components are used to predict a neuron’s response.

Our results showed that applying a GLM with LASSO penalty provides a novel method of determining the stimulus sensitivity of C-fiber nociceptors and predicting the responses of these neurons. In other words, by choosing an appropriate statistical model and stimulus features one is able to model the responses of even a challenging data set of primary afferent nociceptors with a Bayesian method.

## 3.2 Methods

The continuum mechanics model used to compute the stress and resultant strain profiles in this study has been described in detail by Phillips and Johnson (Phillips & Johnson, 1981b). Modeling the skin as a continuum assumes the multilayer skin tissue to be a homogenous, isotropic, and elastic medium whose mechanical properties can be approximated by those of an ideal medium and obey Hook's law. Given the nonhomogeneous and non-isotropic structure of epidermis, dermis and subcutaneous tissue this assumption is unlikely to hold exactly. However, it has been shown that for skin deflections of 1 mm or less, violations of the assumption of homogeneity and isotropy have minor effects (Phillips & Johnson, 1981b). Therefore, we decided to use these assumptions to simplify modeling of the mechanical properties of skin tissue.

Briefly, we assumed that the receptor site of a neuron is just underneath the center of the stimulus electrode and at an estimated depth that was determined using the method described in chapter 2 (Dezhdar, et al., 2015, in press). We then determined the strain profiles according to Phillips and Johnson (Phillips & Johnson, 1981b). In their study the strain profiles were determined in three steps. A complex spatial force profile at the surface was decomposed into the subcutaneous stresses by; (i) specifying stresses arising from single line loads, (ii) summing these to produce a composite stress pattern, and (iii) the stresses were used to compute subcutaneous strain profiles. For small deflections, the superposition principle holds approximately. Thus, a surface force pattern can be divided and treated as independent, individual subunits of line loads. By superposition, the stresses produced by these single line loads can be combined to produce any possible stress profile beneath the electrode. The combined stress profiles were used to compute the strain profiles in 14 locations at the estimated depth of the receptor site. In case of thermal stimuli we assumed that the whole area underneath the heat electrode and at the previously estimated depths (Dezhdar, et al., 2015, in press) homogenously underwent the same temperature changes.

### 3.2.1 Experimental data

Experiments were performed in strict accordance with the Guide for the Care and Use of Laboratory Animals of the Max Delbrück Centre for Molecular Medicine. The protocol was approved by the Committee on the Ethics of Animal Experiments of Animal Welfare German authorities (LaGeSo; Permit Number: T (00383/12). The C-fiber responses of neurons used here were reported in a previous study where the responses to thermal stimuli were used to estimate the depth and threshold temperature of neurons (Dezhdar, et al., 2015, in press).

#### *3.2.1.1 Skin nerve preparation and identification of single C-fibers*

The skin-nerve preparation was used to record from single primary afferents (Milenkovic, et al., 2008) (Milenkovic, et al., 2007) . Mice were killed by $CO_2$ inhalation for 2–4 min followed by cervical dislocation. The saphenous nerve and the shaved skin of the hind limb of the mouse were dissected free and placed in an organ bath at 32 °C. The chamber was perfused with a synthetic interstitial fluid (SIF buffer) the composition of which was (in mM): NaCl, 123; KCl, 3.5; MgSO4, 0.7; NaH2PO4, 1.7; CaCl2, 2.0; sodium gluconate, 9.5; glucose, 5.5; sucrose, 7.5; and HEPES, 10 at a pH of 7.4. The skin was placed with the corium side up in the organ bath. The saphenous nerve was placed in an adjacent chamber on a mirror to aid and under microscopy fine filaments were teased from the nerve and placed on the recording electrode. Electrical isolation was achieved with mineral oil.

Single mechanically sensitive units were characterized by probing the skin with a glass rod for mechanically responsive receptive fields. Using an electrical stimulating electrode, we measured the conduction velocity (calculated by dividing conduction distance over electrical latency for the spike) to select C-fibers whose conduction velocity was in the C-fiber range <1 m/s.

#### *3.2.1.2 Mechanical and thermal stimulation devices*

The mechanical stimulating probe is driven by a nanomotor (Kleindiek, Reutlingen, Germany) and is also equipped with a force transducer (Kleindiek, Reutlingen, Germany). The probe was a stainless steel rod and the diameter of the flat circular contact area was 0.8 mm. The probe was placed onto a spot within the receptive field where the most reliable responses could be obtained. Mechanical thresholds for nociceptors were measured by reading off the force (obtained from the attached force transducer) at which the first spike was obtained. The signal driving the movement of the linear motor and raw electrophysiological data were collected with a Powerlab 4.0 system (ADInstruments) and spikes were discriminated off-line with the spike histogram extension of the software.

For heat stimulation, a Peltier element–based contact probe (4x3 mm surface) applied thermal stimuli (custom device built by the Yale School of Medicine Instrumentation Repair and Design) to the receptive field of identified C fibers.

#### *3.2.1.3 Mechanical and heat stimulation protocol*

Two stimulation protocols – for mechanical stimuli- sent as a pre-programmed series of commands to the nanomotor (Kleindiek, Reutlingen, Germany) were applied to all C-fibers. The mechanical stimulation protocol consisted of 3 ramp and hold stimuli of 400 µm indentation. The ramp durations was 8 s, 4 s, and 1 s, while the hold phase had a constant duration of 10 s. The interstimulation interval was 60 seconds. The order of stimulation was first heat and then mechanical from the slowest to fastest ramps. Data were obtained from 11 C57Bl6/N wildtype mice.

### 3.2.2 Strain and thermal components

#### *3.2.2.1 Force profile*

The surface force was applied by an electrode with a diameter of 0.8 mm on the corium side of the skin. We divided the spatial area underneath the electrode into 14 line loads. We assumed the center of the electrode is the origin of a Cartesian coordinate system with three orthogonal normal directions of *x* equivalent to the depth, *y* parallel to the surface and at right angles of line load and *z* parallel to the surface and along to the line load (see Figure 1).

The effect of stress (force per area) and strains (fractional changes in length) in a continuum volume can usually be approximated by analyzing a small, isolated cube (see Figure 1). For a cube in static equilibrium (without acceleration or rotation) this results in three stress components along three orthogonal axes and three shear stress components along three planes spanned by a pair of three orthogonal axes. If the cube doesn't change its volume, the stress components cause compression and expansion of the tissue, which is defined as strain. The relationship between stress and strain is governed by Hook's law, from which follows that (i) the stress in any direction produces a strain in the same direction which is proportional to the stress, (ii) the shear strain can be observed when the sides of the cube are tangentially displaced, which is very likely in a complex structure such as skin, (iii) regardless of the stresses, compressive strain is always accompanied by tensile strain and vice versa, which means that it is not possible to infer from a compressive (or tensile) surface stimulus that the effective stimulus at the receptor site is compression (or tension) (Phillips & Johnson, 1981b) (Timoshenko & Goodier, 1970), (iv) the components of strain depend strongly on the orientation of the coordinate frame.

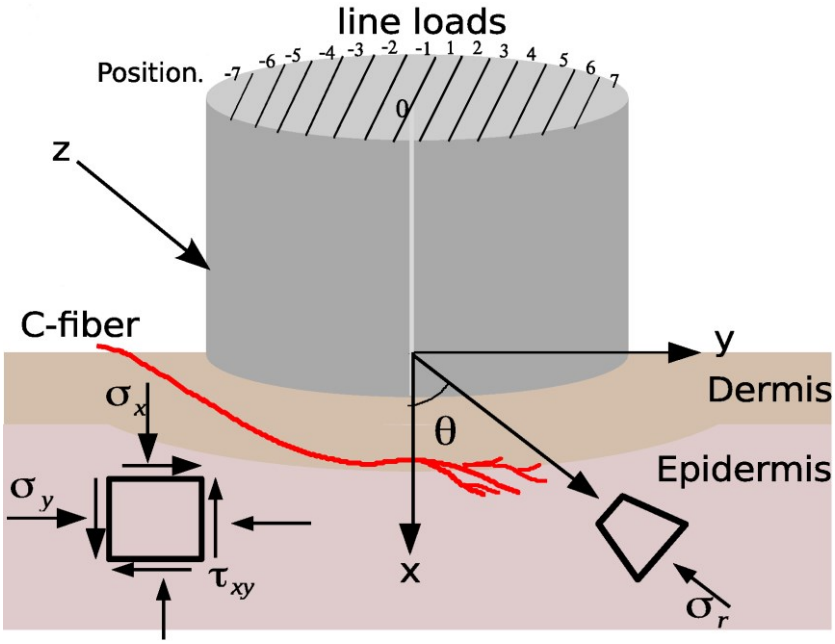


**Figure 1. Schematic of force electrode applied on the surface of the skin.** We divided the area underneath of the electrode into 14 line loads and computed 5 strain components for each line load and 3 thermal components for the whole area. The principal components of stress $\sigma_x, \sigma_y$ and shear stress $\tau_{xy}$ are defined for a small cube of skin underneath one line load. We assumed that the main escape of displaced tissue was along the *z*-axis of the line load and the strain along *x*-, *y*-axis were predominantly compressive. The terminal endings of the C-fibers were at given depths (Dezhdar, et al., 2015, in press) and undefined horizontal positions. We transformed then the principal axes to polar coordinates (Timoshenko & Goodier, 1970). Note that in our experimental condition, the electrode was applied on the dermal site of skin.

To avoid a dependency of the strain components on the orientation of the coordinate frame the best strategy has been to transfer the strain components from Cartesian coordinates to a spherical or cylindrical system. In this way any formal strain in any direction is the fractional reduction in diameter in that direction. In the following we explain briefly the method suggested by Phillips and Johnson. For more details we refer the reader to ref. (Phillips & Johnson, 1981b).

To compute the stress profiles independent to the orientation we first divided the area underneath the electrode into line loads. For the area underneath every line load we specified the complete stress field including 3 normal stress components $\sigma_x, \sigma_y, \sigma_z$ , and 3 shear stress components $\tau_{xy}, \tau_{yz}, \tau_{xz}$ in a Cartesian coordinate system (see Figure 1). Then, by rotation of axes, the stresses in any other coordinate frame and, in particular, the cylindrical coordinate frame can be found. Thus, according to Boussinesq and Wilson (11) for a line load *P* the principal stress-strain axes at any point beneath the surface are aligned with the cylindrical coordinates surrounding the line load. The normal stress components of one line load, transformed in cylindrical coordinates, are then the radial stress $\sigma_r$, which is always compressive, the tangential stress perpendicular to the line load $\sigma_\Theta$, and the longitudinal stress $\sigma_z$, aligned with the line load. After deformation, a small

sphere approximates an ellipsoid. If the coordinate system is aligned with the major and minor axes of the ellipsoid, these axes are called the principle axes and the normal stresses and strains are called the principle stresses and strains. The stress and strain along the minor axis of the ellipsoid are the maximum compressive stress and strain regardless of orientation. The stress and strain along the major axis are the maximum tensile stress and strain regardless of orientation. The shear strain cannot be specified without specifying a rectangular coordinate system. In this case we specified additionally the shear strain in a reference coordinate frame and manifested as a misalignment between the principle axes of ellipsoid and coordinate axes.

In cases where every line load is a subunit of a more complex surface profile, all line loads' individual cylindrical coordinates and the related single radial stress must be expressed in a single coordinate frame. To define a general coordinate frame for all line loads we first transformed the stress components aligned to the cylindrical coordinate of one line load into any arbitrary coordinate frame and rotated the principal axes. In this way transformed stress components of all line loads are independent of the orientation of the coordinate frame.

The components of principal stresses $\sigma_x, \sigma_y$, and shear stress $\tau_{xy}$, at point $(x, y)$ beneath the surface, implied by all line loads $p_j$, $(j = -7, \dots 7)$ located at previously estimated depth (Dezhdar, et al., 2015, in press) and distance $y_j$ of the *j*-th line load (Phillips & Johnson, 1981b),

$$\sigma_x(x,y) = \frac{2x^3}{\pi} \sum_{j=-7}^{7} \frac{p_j}{r_j^4}, \tag{3.1}$$

$$\sigma_y(x,y) = \frac{2x}{\pi} \sum_{j=-7}^{7} \frac{\left(y - y_j\right)^2 p_j}{r_j^4}, \tag{3.2}$$

$$\tau_{xy}(x,y) = 2x^2 \sum_{j=-7}^{7} \frac{\left(y - y_j\right) p_j}{\pi r_j^4}, \tag{3.3}$$

where $r_j = \left(x^2 + \left(y - y_j\right)^2\right)^{1/2}$. The maximum shear stress related to an arbitrary *x*, *y* frame is then

$$\tau_{max} = \left( \left( \frac{\sigma_x - \sigma_y}{2} \right)^2 + {\tau_{xy}}^2 \right)^{1/2} \tag{3.4}$$

The stresses along a coordinate frame independent to the orientation are then,

$$\sigma_1 = \left(\frac{\sigma_x + \sigma_y}{2}\right) + \tau_{max} \tag{3.5}$$

$$\sigma_2 = \left(\frac{\sigma_x + \sigma_y}{2}\right) - \tau_{max}, \tag{3.6}$$

where $\sigma_1$ and $\sigma_2$ are maximum and minimum compressive stresses in the *x*, *y* plane regardless of orientation.

There are various possibilities for computing the strain components from stress components. The transduction process at receptor sites might be activated by tensile deformation, compressive deformation, or shear deformation. It might be sensitive to only horizontal direction, only vertical direction or in any direction. Additionally, there are two possibilities in continuum mechanics termed as 1) plane stress and 2) plane strain, and each of two can occur in conjunction with the other possibilities. Briefly, in the state of plane strain, it is assumed that the tissue cannot expand in *z* direction which implies that strain in this direction is zero, $\epsilon_z = 0$. In the state of plane stress, the main escape of tissue is an elongation along the *z* axis. In this condition $\epsilon_z$, is always negative and $\sigma_z = 0$ (Timoshenko & Goodier, 1970).

To compute the strain components from stress components we supposed that the skin tissue can be elongated along the line load and assumed the state of plane stress.

The computed strain components are then (Phillips & Johnson, 1981b),

Vertical compressive strain, $\epsilon_x = \frac{1}{E}\left(\sigma_x - \frac{\sigma_y}{2}\right)$

Maximum horizontal strain , $\epsilon_h = max\left(|\epsilon_y|, |\epsilon_z|\right)$

Maximum compressive strain regardless of orientation, $\epsilon_c = \frac{1}{E}\left(\sigma_1 - \frac{\sigma_2}{2}\right)$

Maximum tensile strain regardless of orientation, $\epsilon_t = max(-\epsilon_z, -\epsilon_2)$

Maximum strain regardless of orientation weather tensile or compressive, $\epsilon_m = max(\epsilon_c, \epsilon_t)$

With $\epsilon_y = \frac{1}{E}(\sigma_y, \sigma_x/2)$ and $\epsilon_z = \frac{1}{E}\left(\frac{\sigma_y + \sigma_y}{2}\right)$.

Young's modulus of elasticity, *E*, is a measure of skin's resistance to deformation. Assuming an ideal medium, a given surface deformation produces the same subcutaneous distortion patterns independent of the property of the material. Thus, for a fixed displacement the effect of this proportionality factor cancels in the chain of

calculations following from surface displacement to subcutaneous strain (Phillips & Johnson, 1981b). Accordingly, we set *E*=1.

As a brief summary, we first approximated the area underneath the electrode by line loads that would produce approximately the same force as the original stimuli. The stress profile produced by a single line load was computed and then these stress profiles were summed to produce the composite stress pattern. Finally, the composite stresses were used to specify the 5 strain components.

As a 6th strain component we chose the derivative of vertical compressive strain $\frac{\partial \epsilon_x}{\partial t} = \frac{\Delta \epsilon_x}{\Delta t}$ to describe the sensitivity of receptor neurons to the changes of vertical compression in every time bin.

Due to the elasticity of the skin, it acts like a spatial low-pass filter for pressure stimuli. Thus, fine details of mechanical information about the spatial variation of the surface stimulus become weaker as the receptor is located at greater depth (Sripati, et al., 2006). Therefore, an accurate estimation of the depth is important. We determined the depth of receptor terminals using the method from the study in previous chapter 2 (Dezhdar, et al., 2015, in press) resulting in depth estimates between 0.1 mm and 1.5 mm from the surface. We calculated strain profiles for all 24 neurons at these depths.

#### *3.2.2.2 Temperature profile*

According to the laws of Thermodynamics, during conduction of heat through a physical medium thermal energy is exchanged until a thermal equilibrium is reached. The transfer of heat depends on the thermal properties of the mediums. Because skin in not a perfect heat conductor, the energy of a stimulus is attenuated by the skin's different layers. This implies that first, the temperature at the location of receptor differs from the applied temperature at the surface and second the skin tissue changes its volume in response to changes in temperature, a process which is called *thermal tension*.

In previous study (Dezhdar, et al., 2015, in press) we studied the transfer of thermal stimuli in skin and used the heat transfer function to estimate the depth and threshold temperatures of receptor neurons and time to threshold. In this study we used these values to estimate the attenuated temperature profiles at receptor depth. The central equation to estimate the temperature at receptor depth is given by Henriques (Henriques & Moritz, 1947),

$$T_{threshold} = T_{surface} + \left(T_0 - T_{surface}\right)\frac{2}{\sqrt{\pi}}\int_0^{\gamma/\sqrt{\tau}} e^{-x^2}\,dx,$$

where $T_{threshodl}, T_{surface}$ refer to temperature at the receptors' depth and at the surface of skin, $\gamma$ refers to normalized depth and $\tau$ is the estimated time to threshold. Tracing this equation for all temperatures of thermal stimuli we were able to reconstruct the thermal stimuli $T$ at the depth of receptors.

The thermal tension is provided by the equation $\epsilon_T = \alpha \Delta T$, where $\alpha \frac{10^{-4}}{^\circ C}$ is thermal expansion coefficient. We assumed $\alpha = 1$ (Xu, et al., 2008).

Finally, we selected the derivative of temperature profile $\frac{\partial T}{\partial t}$ as the 3rd thermal component. Note that all thermal profiles were estimated at each neurons estimated depth but over the whole area underneath of the heat electrode.

### 3.2.3 Generalized Linear Model (GLM) for receptors

Generalized linear models are a commonly used statistical method for modeling the relationship between neural responses and stimuli. To predict the spike counts from the strain and thermal features we assumed that the number of spikes $Y_i$ in bin *i* was a random variable with Poisson distribution $(r_i)$, where the rate $r_i$ was dependent on the vector of features $X_i$ in bin *i*:

$$r_i = \exp(\sum_{j=1}^{k} \beta_j X_{ij}), \tag{3.7}$$

where $X_{ij}$ denotes the average value of the *j*-th feature in the *i*-th bin. Here the term feature refers either to the properties of the heat stimulus or the strain components as described in the previous section.

Estimates of the regression weights $\beta_j$ can be obtained through maximum likelihood estimation (McCullagh & Nelder, 1989) (Paninski, 2004). However, the number of regression weights *k* that we obtained using this approach was relatively large. In cases where the dimension of parameter space was large but the data was limited, maximum likelihood estimation was impaired and regularization was necessary to avoid overfitting. Therefore, we used the LASSO algorithm (Tibshirani, 1996) (Friedman, et al., 2010) to drive unneeded parameters to zero. Briefly, this was done by maximizing a penalized log-likelihood function with a penalty that was proportional to the L1 norm of the parameter vector. Thus, the vector $\hat{\beta}$ of estimated regression weights was the one that minimized the loss function,

$$L(\beta) = nr_i - \sum_{i=1}^{n} Y_i \log(r_i) + \lambda \sum_{j=1}^{k} |\beta_j|, \tag{3.8}$$

where $\lambda > 0$ is the strength of the regularization and was chosen to maximize cross-validated likelihood (100-fold cross validation). The idea is to minimize the negative log-likelihood function (the first two terms in the equation), while penalizing constellations for which the number of non-zero $\beta_j$ is large.

The LASSO penalty (L1 norm) prefers the solution with fewer nonzero parameter values. It has thus a tendency to select one feature from a group of highly correlated features and deselect the others. This property is advantageous in our sparse data set of 24 neurons in which the features (strain and thermal components) are highly correlated and all stimuli were applied once without any repetitions.

To increase the computational power of GLM and simplify the log-likelihood we binned the feature vector and spike counts into equidistant discretization points. The choice of time bin size is a difficult problem that may critically affect the outcome of the model. A fine time bin that retains precise spike times might result in a large number of discretization points, and increase the number of features for the likelihood function drastically. On the other hand, a large time bin may impair the convergence of the optimization process. Adding discretization points in an adaptive fashion when required could be a compromise. However, in our sparse data set without repetition, an adaptive bin width did not improve the optimization of log-likelihood, but rather had a negative impact.

Further, estimating the bin width for all neurons individually resulted in different optimal bin widths for different neurons, which renders a summary analysis difficult. Hence, we attempt to find a joint bin width for all neurons. To this end we estimated the mean firing rate of all neurons' responses to mechanical and thermal stimuli using a Nadaraya-Watson kernel estimator (Nadaraya, 1964) (Watson , 1964) while we optimized the bandwidth of the kernel with leave-one-out cross-validation. Accordingly the optimal bandwidth is the one which minimizes the cross-validation score or minimizes the risk function.

The 10-fold Cross-Validation of kernel optimization resulted in an optimal bandwidth of 270 ms in our data set. We then chose the bandwidth of the estimated bandwidth of Nadaraya-Watson kernel estimation as the 'optimal' bin width of discretization points.

## 3.3 Results

It is assumed that polymodal C-fiber nociceptors are activated by specific components of deformation (i.e., *strain*) of the tissue at the site of the receptor. In this study we considered 6 strain components and 3 thermal components (all candidate variables and their effect on receptor are summarized in Table 1). However, it is unclear which components account for the activation of a given receptor neuron. To select the components that exhibit the strongest effects on the observed spike trains of single neurons we applied a GLM to predict the responses while shrinking the components and setting the components with a low weight to zero using LASSO penalty (Friedman, et al., 2010). The goal of this analysis is mainly to find out whether we could use this probabilistic approach to select and identify components of mechanical strain that would generally account well for receptor activation.

**Table 1. Summary of stimuli components.**

| Stimuli component | Effect on the receptor |
|---|---|
| vertical compressive strain, $\epsilon_x$ | Elongation along the axis perpendicular to the skin surface |
| Maximum horizontal strain, $\epsilon_h$ | Maximum elongation parallel to the skin surface |
| Maximum compressive strain regardless of orientation, $\epsilon_c$ | Maximum compression in any direction |
| Maximum tensile strain regardless of orientation, $\epsilon_t$ | Maximum elongation in any direction |
| Maximum strain regardless of orientation weather tensile or compressive, $\epsilon_m$ | Maximum deformation in any direction, compressive or tensile |
| Derivative of vertical compressive strain, $\frac{\partial \epsilon_x}{\partial t}$ | Temporal changes of elongation along the axis perpendicular to the skin surface |
| Temperature $T$ | Temperature in a horizontal plane parallel to the surface at the estimated depth of receptors |
| Derivative of temperature, $\frac{\partial T}{\partial t}$ | Temporal changes of temperature in a horizontal plane parallel to the surface at the estimated depth of receptors |
| Thermal tension, $\epsilon_T$ | Deformation in any direction proportional to temperature changes |

We analyzed a data set of responses from 24 neurons to a series of ramp and hold force and heat stimuli with ramp phases of three different velocities. The vector of responses $Y$ consisted of concatenated binned spike trains of three mechanical stimuli and three thermal stimuli (see Methods for more details). By choosing the origin at the center of the heat and mechanical electrode we took advantage of the symmetry of the components and considered only one half of the area underneath the mechanical electrode, from line load at position 1 to the line load at position 7, respectively (see Figure 1). To fit the GLM to the data and estimate the weights β, we maximized the log-likelihood function of the

Poisson distribution, while regularizing the weights using the L1 norm. The strength of regularization was chosen to maximize cross-validated log-likelihood. As we described in section Methods we binned the feature vectors and the vectors of spike trains to increase the prediction power of the GLM. Accordingly, we chose 5 arbitrary bin widths of {100 ms, 250 ms, 500 ms, 750 ms, 1000 ms} and one optimized bin width of 270 ms (see Methods for choice of bin widths) and estimated and regularized weights $\beta_i$ of 9 stimulus components.

The analysis addressed the following questions: Which strain components are mostly involved in activation of single neurons and to what extent do the neurons respond to these components? How are the weight values of responding neurons distributed? What is the spatial distribution of the receptor sites with respect to different positions of line loads relative to the center of the electrode? And the final goal was to demonstrate the applicability of a sparse regularized GLM methods to studying primary afferent C-fibers.

Further, we were interested in how the choice of bin width affected the results. Our experience showed that for the finest bin width of 100 ms the GLM model often failed to converge. To study the stability of the GLM model to predict the responses for different discretization widths we first estimated the regularized weights of all 9 stimulus components for five models M1 to M5 with bin widths M1=100 ms, M2=250 ms, M3=500 ms, M4=750 ms, and M5=1000 ms. We then computed for each model the mean of estimated weights for single components underneath of each line load. Finally we obtained the Euclidian distance of the mean values between different models; d(M2-M1), d(M3-M2), d(M4-M3), and d(M5-M4). The Euclidian distances of mean weights between two models with adjacent bin widths revealed that the largest distance was observed mainly between models M1 with discretization width 100 ms and M2 with a discretization width of 250 ms for all positions (see Figure 2). For the models with a discretization width equal to or above 250 ms, d(M3-M2), d(M4-M3), and d(M5-M4) the Euclidian distances of mean weights remained small and almost constant. The small variance of mean values suggested that the estimated weights of all models with bin widths equal to or above 250 ms converge a stable regime in terms of the choice of bin width. The estimated weights reported for the 'optimal' bin width of 270 ms were in this regime of stable results, while the weights reported for a bin width of 100 ms were not and were likely to be biased. To visualize this variances we showed all results for both bin widths of 100 ms and 270 ms.

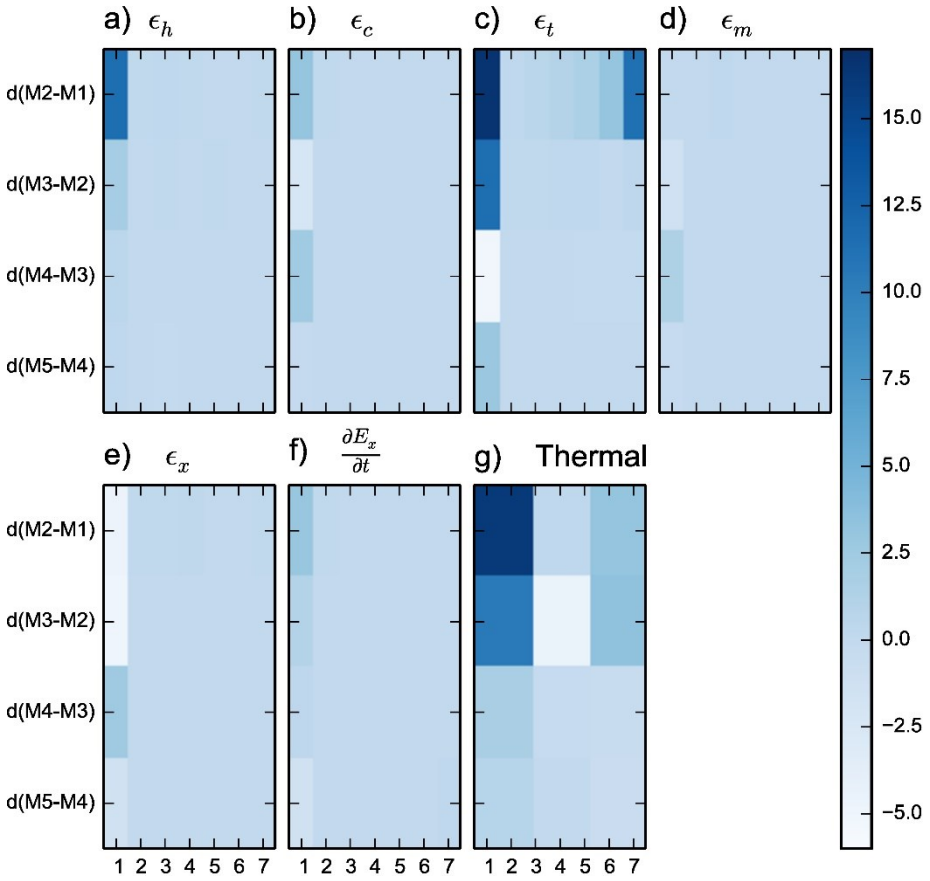


**Figure 2. Euclidian distances of mean weights of stimuli components between two adjacent models of bin widths; M1:100ms, M2: 250ms, M3:500ms, M4:750ms, M5:1000ms.** (**a**) Maximum horizontal strain regardless of orientation at different locations. (**b**) Maximum compressive strain regardless of orientation. (**c**) Maximum tensile strain regardless of orientation. (**d**) Maximum strain regardless of orientation whether tensile or compressive. (**e**) Vertical compressive strain. (**f**) Derivative of vertical compressive strain. (**g**) Thermal components.

Figure 3 shows how many neurons were sensitive to any of the thermal- and strain components over all 14 positions underneath of line loads. Each bar in Figure 3 refers to a line load at a location relative to center and shows the number of neurons that responded to every single stimulus component at this location. The neurons that responded to the stimulus showed non-zero weights $\beta_j$.

According to Figure 3 maximum compressive strain regardless of orientation, $\epsilon_c$ and maximum strain regardless of orientation whether tensile or compressive, $\epsilon_m$ showed the lowest activation ability. The number of responding neurons decreases for locations farther from the center. This observation held for all other strain components, which indicated that the receptor sites of neurons were mostly located directly under the center of the electrode or slightly lateral to the center.

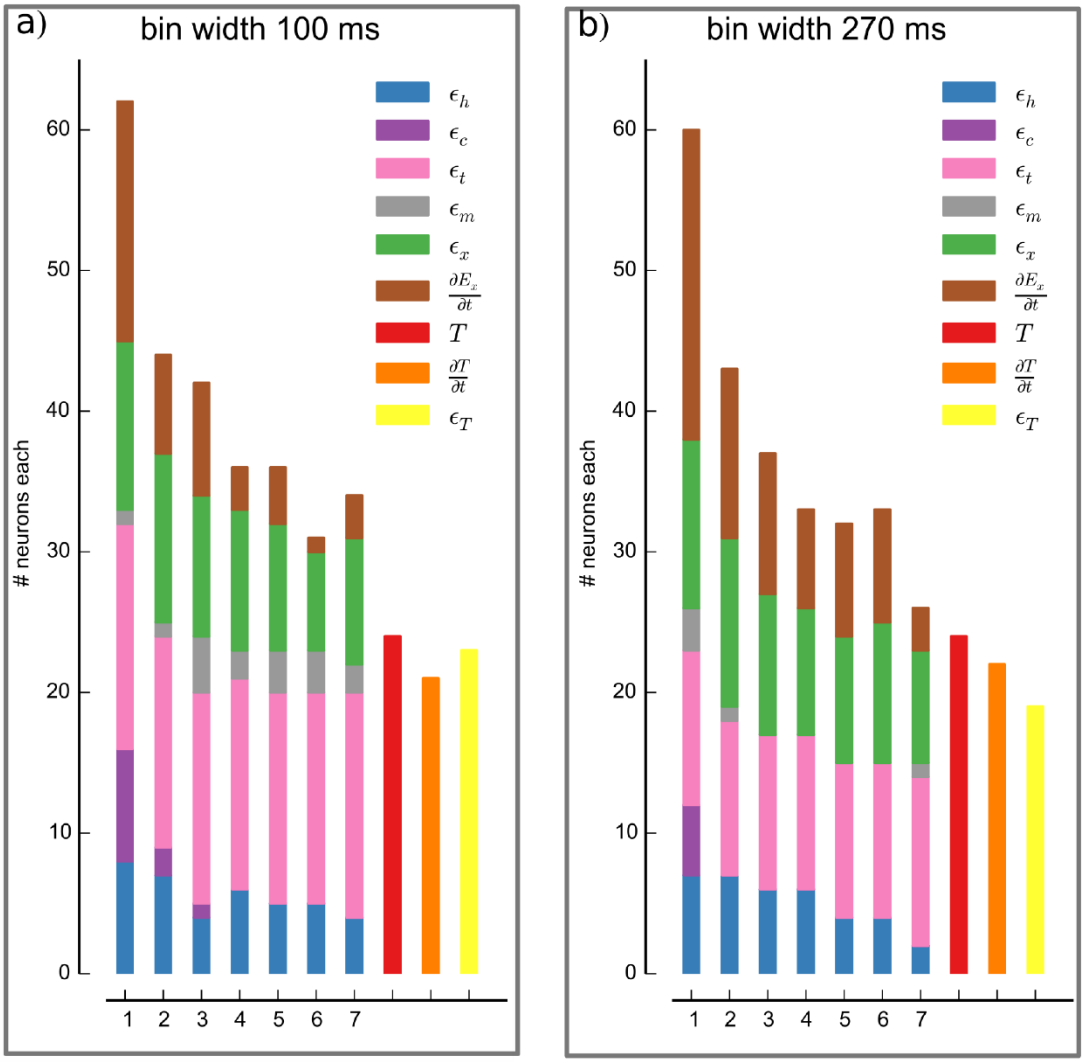


**Figure 3. The number of neurons with non-zero weights obtained by a Lasso regularization and GLM for two different bin widths.** For every neuron the responses were estimated using 6 strain components $\epsilon_x, \epsilon_h, \epsilon_c, \epsilon_t, \epsilon_m$, and $\frac{\partial \epsilon_x}{\partial t}$ in 7 different positions underneath the force electrode and 3 thermal components. If the neurons did not respond to the stimuli component the corresponding weight set to zero according to the Lasso method. (**a**) Results for a temporal resolution of 100 ms binning. (**b**) Results for a temporal resolution of 270 ms binning.

For the location directly under the center (position 1 in Figure 3) we counted the number of responding neurons for both, fine and optimal bin widths. For bin width 270 ms (100 ms), 12(12) out of 24 responded to vertical compressive strain$\epsilon_x$, 22(17) to derivative of vertical strain $\frac{\partial \epsilon_x}{\partial t}$, 7(8) to maximum horizontal strain $\epsilon_h$, 11(16) to maximum tensile strain regardless of orientation $\epsilon_t$, and 5(8) to maximum compressive strain regardless of orientation$\epsilon_c$. The lowest number of responding neurons 3(1) related to the maximum strain regardless of orientation, whether tensile or compressive, $\epsilon_m$. According to the definition of $\epsilon_m = max(\epsilon_c, \epsilon_t)$, this strain component is highly correlated with the maximum tensile strains and consequently the weights for $\epsilon_m$ set to zero in the LASSO regularization

for many neurons. The highest sensitivity were obtained for the derivative of the vertical compressive strain. The results showed non-zero weights for all 24 neurons to attenuated thermal stimuli $T$. 22(21) neurons showed sensitivity to derivative of thermal stimuli and 19(23) to the thermal tension, $\epsilon_T$.

To determine the stability of the results in terms of the variance of the estimated weights for each component in a population of 24 neurons we computed the standard error of weights over all locations. Figures 4 shows the standard errors of the weights of single strain components for all horizontal positions underneath the line loads (positions 1,…,7) and the area underneath of the heat electrode both at previously estimated depths (Dezhdar, et al., 2015, in press).

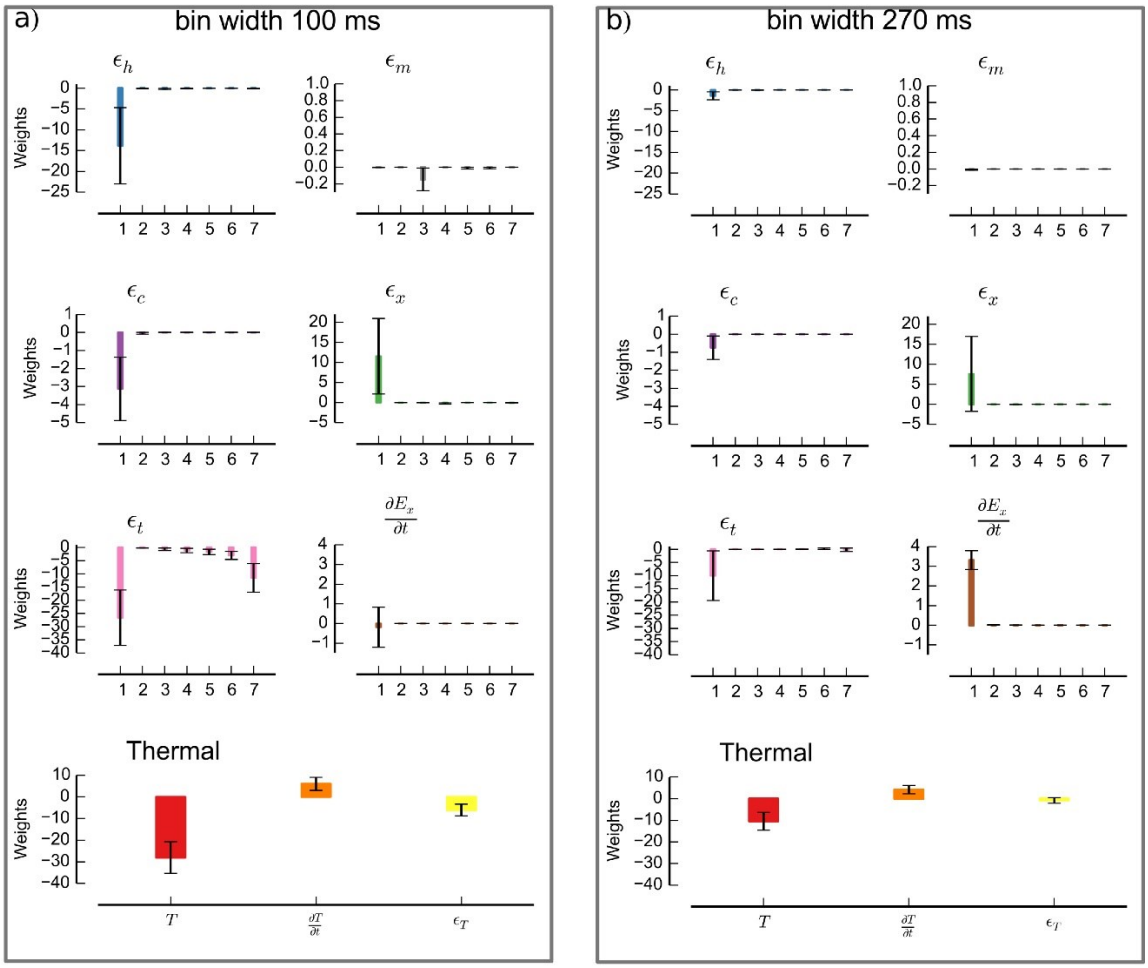


**Figure 4 . Standard errors of weights. Data for 24 neurons and 6 single strain components over 7 horizontal positions.** Thermal components refer to the whole area underneath of thermal electrode. The strain and thermal components were obtained at the estimated depth of receptors. The strain components are as follow; Maximum horizontal strain, $\epsilon_h$. Maximum compressive strain regardless of orientation, $\epsilon_c$. Maximum tensile strain regardless of orientation, $\epsilon_t$. Maximum strain regardless of orientation, whether tensile or compressive, $\epsilon_m$. Vertical compressive strain, $\epsilon_x$. Derivative of vertical compressive strain $\frac{\partial \epsilon_x}{\partial t}$. Attenuated heat stimuli,$T$, derivative of heat, $\frac{\partial T}{\partial t}$, thermal expansion, $\epsilon_T$ for the whole area beneath the heat electrode at the depth of receptor. (**a**) Results of discretization width of 100 ms. (**b**) Results of discretization width of 270 ms.

Figure 4a shows the results for the fine bin width of 100 ms and Fig. 4b for the optimized bin width of 270 ms. For all stimulus components the neurons responded mainly to locations at the center of the electrode (position 1). According to Figure 4 in general, for finer bin width (100 ms) the estimated weights showed a higher variance and larger error bars. This result is consistent with the results of Euclidian distance analysis.

## 3.4 Discussion

The mechanism with which primary afferent C-fibers perform the transduction of mechanical force and thermal changes into action potentials is still poorly understood at the molecular level. In part because it is difficult to isolate the free nerve endings and consequently measure the transducer currents. Several models have been developed to characterize the stimulus components that evoke transformation from static mechanical stimuli into proximal signals for mechanosensitive slowly adapting A-fiber (SA1) and rapidly adapting A-fibers (RA). The candidate variables that have been proposed to drive transduction are mainly the maximum compressive strain (Phillips & Johnson, 1981b), strain energy density (Dandekar & Srinivasan, 1997) (Srinivasan & Dandekar, 1996), stress (Del Prete, et al., 2003) (Khalsa, et al., 1996), tensile strain and changes in receptor area (Sripati, et al., 2006). In general these variables are physical quantities that are closely correlated and related to local membrane stretch (Sripati, et al., 2006) and may be distinguished using a wide variety of not only static but dynamical stimuli. In this study we focused in selecting from the highly correlated candidate variable those strain components that are most predictive of the neural responses of C-fiber nociceptors. One result of the present study was to provide a probabilistic model for studying the primary afferent responses.

The computation of strain components in this study was based on continuum mechanics model suggested by Phillips and Johnson (Phillips & Johnson, 1981b). We divided the area underneath the electrode into 14 line loads to provide a finer spatial profile for the spatial distribution of receptors sites. The candidate variable were computed for a given receptor location $(x, y_i)$, in which *x* refers to depth of receptor and $y_i$, *i*=-7,…,7, refers to the location of line loads. The depth of receptor was estimated in a previous study (Dezhdar, et al., 2015, in press). Previous studies showed that stress and strain components are strongly affected by receptor depth (Sripati, et al., 2006) (Srinivasan & Dandekar, 1996), our model therefore provides a more accurate estimate of the candidate

variables, whereas, the predecessor models assumed either a constant depth or have estimated depth as a model parameter.

According to our results, neuronal responses of C-fibers were explained most effectively by the following stimulus properties: In 22 out of 24 neurons, the “derivative of vertical compressive strain $\frac{\Delta\epsilon_x}{\Delta t}$ “ (based on a bin width of 270 ms) was important to predict the neuronal response. The second components were “maximum tensile strain regardless of orientation, $\epsilon_t$ “ (11 out of 24 neurons based on bin width of 270 ms) and “vertical compressive strain, $\epsilon_x$ “ (12 out of 24 neurons based on bin width of 270 ms). These results suggest that the receptor neurons are most sensitive to temporary compression of receptor surface area and relative stretch of surface area. However, the vertical compressive strain and maximum horizontal tensile strain are highly correlated. The maximum horizontal strain is large when the electrode is above the receptor and the receptor is compressed in the vertical direction but elongated along the horizontal. An alternative way to distinguish tensile and compressive components more efficaciously might be to realize experiments in which a force electrode is applied independently in both vertical and tangential direction.

In our modeling framework we assumed that each line load delivered equal force normal to the surface of the skin. Consequently, all line loads induce an equal skin tissue displacement even for the line loads along the edges of the electrode. This simplification was a trade-off between a uniform feature space and flexibility of the model to describe the edge enhancement. Therefore, our framework cannot provide a model to predict the edge enhancement of receptor neurons. However, whether individual mechanoreceptors of C-fibers are edge enhancement sensitive or orientation sensitive is unknown. Our results and previously reported results of slowly adapting (SA1) and rapidly adapting (RA) mechanoreceptors responses suggests that these receptor neurons are not orientation sensitive (Sripati, et al., 2006).

Our results showed that assuming the recordings of 24 neurons as the realization of 24 repetitions of one neuron resulted in more stable GLM convergence and parameter estimation. The experimental design used in this study sacrificed the repeatability to obtain wide-ranging thermal and mechanical responses. This shortcoming calls for an experimental design with repeated observation of each stimulus. The other source of error (between the observed data and model) might be raised by the simple skin model. We assumed skin as a homogenous and isotropic model. In our experimental set up of single neurons the shaved skin was dissected from the dermal side and the electrode was applied at the corium side of skin. This experimental contingency provided a better access to the nerve endings but caused the thickness of the dissected layer and the skin model to remain

unknown and variying among neurons. Therefore, we assumed skin as a one layer, homogenous and isotropic model and didn't consider a more complex and multilayer model.

This study suggested a model for describing the sensitivity of C-fibers to heat and strain features and provided a first approximation of the transduction dynamics of these nociceptors. To capture the temporal dynamics of the firing rates of C-fibers, we suggest to extend this model with the biophysical properties of the afferent neurons, such as the mechanisms of action potential generation, relative and absolute refractoriness, and rate of adaptation. To this end we suggest to incorporate the outcome of our sparse GLM into a spiking neuron model or a descriptive model of firing rate and adaptation. Such a general framework offers a characterization of spatiotemporal dynamics of neural representation of different stimulus modalities conveyed through the same polymodal sensory channel.

# Chapter 4

# 4 A Parametric Model of Firing Rates and Adaptation: a Study of Discharge Responses of Primary Afferent Neurons and Nociceptors

Nociceptors are primary afferent neurons responding to tissue injury caused by noxious mechanical, chemical, or thermal stimuli. Spikes evoked from these neurons are transmitted to the central nervous system and are thought to be perceived as pain. In this study, we assess the processing taking place in peripheral pathway of primary afferents using probabilistic models. We introduce parametric models of stimulus-driven instantaneous firing rate. Each model consisted of two coupled ordinary differential equations (ODEs) describing the rate of an inhomogeneous point process; either a Poisson process or a Gamma process. These models describe how the neuron's temporal dynamics depend on stimulation. We fitted the models on response discharges of polymodal, unmyelinated C-fibers, and thinly myelinated A-fibers recorded in an *in vitro* mouse skin preparation. Our models characterize the responses of single neurons to different stimulus modalities and provide a parametric framework to study the potential differences in temporal dynamics of responses.

## 4.1 Introduction

Nociceptors are primary afferent neurons responding to noxious (painful) stimuli. The functionality of these neurons is crucial for a living organism to interact with the environment and avoid harmful stimuli. The key role of these neurons has subjected them to intensive investigations in several research areas, using pharmacological and electrophysiological to psychophysical methods, and, at the molecular and cellular levels, to more abstract mathematical and computational neurosciences. In recent years and in the light of improving advanced statistical models to describe the coding strategies of single neurons as well as heterogeneous populations of neurons, research in nociception received more attention from neuroscientists. In this regard pain studies can benefit from the mathematical and computational methods. However, the relatively dynamical experimental set ups of recordings from nociceptors often make multiple recordings of the

same stimulus condition infeasible. A typical data set of nociceptor recordings thus often consists only of single recordings of different stimulus conditions and are limited to small numbers of neurons. The limitations in number of recorded neurons and number of trials often make data sets of nociceptors inappropriate for standard statistical inference and machine learning methods. In this study we introduced methods to validate the models based on single neuron statistics. Thus the models provide a framework to study the temporal dynamics of responses even with different modalities of stimuli and amount different data sets.

Main class of nociceptors, called C-fibers, have small diameter unmyelinated axons (Woolf & Ma, 2007) bundled in fascicles surrounded by Schwann cells and support conduction velocities of 0.25–1.25 m/s (Julius & Basbaum, 2001). Initial fast-onset pain is mediated by A$\delta$-fiber nociceptors whose axons are myelinated and support conduction velocities of approximately 5–30 m/s (Kumazawa , et al., 1996). The majority of C-fibers are polymodal. They respond to mechanical pressure, chemical irritants and have been referred to as the main population responding to thermal stimuli (Patapoutian, et al., 2003). Although different modalities of stimuli can trigger spikes in the same C-fiber neuron, these modalities thought to be perceived as distinct qualities at the end of the processing pathway. One of the main questions of pain studies has been to explain how, and at which level of processing, discrimination of different stimulus modalities takes place. Addressing this question will give valuable insights into the encoding strategy of these neurons, their transduction mechanism and the constituting ion channels.

Recent studies strengthen the hypothesis that different noxious stimulus modalities can be distinguished from the earliest stages of processing (Cavanaugh, et al., 2009) and spatiotemporal dynamics of responses might code the differences between the distinct modalities (Milenkovic, et al., 2014). Yet, the histological structure, geometry and small diameters of C-fibers make them hard to isolate and access for standard electrophysiological measurements of transducer currents. On the other hand, different stimulus modalities such as heat and mechanical pressure impart different physical effects on the skin and hence their impacts may not be directly comparable. Consequently, a direct comparison of their discharge patterns might be fundamentally inappropriate. To overcome these limitations, in this study, we suggested to characterize the responses of single neurons to stimulus modalities by sets of model parameters and to compare each neuron's best fitting parameters instead of a direct comparison of their spike trains. To this end we introduced a parametric model of coupled ordinary differential equations of instantaneous firing rate and adaptation. We assumed that the neurons' spikes were generated by a point process and estimated the model parameters. We investigated two

types of ordinary differential equations (ODEs); one describing a linear adaptation process and another describing a nonlinear, divisive adaptation. We examined the models in data sets of measurements from C-fiber and A $\delta$ -fiber nociceptors and A-fiber mechanoreceptors. The data sets were collected from previous studies. Thus, to record from these neurons different stimulation protocols were employed. However, our modeling approach provides model validation based on single neuron statistics. Thus, although different nociceptors and different modalities were employed, we were able to compare the estimated parameters of each neuron as a result of the modeling process.

## 4.2 Methods

The model we introduced to describe the instantaneous firing rate of responses consisted of two coupled ordinary differential equations (ODEs) of firing rate and adaptation. The main idea behind using a system of ODEs was to describe the changes in firing rate at each instant of time $t$ for the next instant of time $t + \Delta t$, which lies infinitesimally in the future, and to describe these changes as a function of all model parameters at time $t$. The parametric model consisted of four parameters describing the coupling of firing rate and adaptation, the neuron's sensitivity to the input stimulation, and two parameters that describes firing rate and adaptation. In addition the models included a parameter to estimate the spontaneous activity of neurons. To estimate the parameters we fitted the model to the firing rate of a single neuron using maximum likelihood estimation.

### 4.2.1 Experimental data

The main focus of this study was to develop a parametric model of single neurons and identify their response characteristics by the model parameters rather than by a direct comparison of their spike trains. We therefore were able to use spike trains recorded with different stimulation protocols. All data sets have been reported in previous studies (Wetzel, et al., 2007) (Moshourab, et al., 2013). The *in vitro* skin-nerve preparation to record from primary neurons, characterization of single units and mechanical and thermal devices were used as previously reported (Wetzel, et al., 2007) (Moshourab, et al., 2013) (Milenkovic, et al., 2008) and described in chapters 2 and 3.

The mechanical stimulation protocol consisted of an ascending series of ramp and hold stimuli, sent as a pre-programmed series of commands to the nanomotor that controlled the steel rod for mechanical stimulation. The magnitude of the displacements of the rod was between 10 and 800 $\mu m$ . The standard ramp speed used in the ascending series had a constant velocity of 1435 $\mu m s^{-1}$. This protocol was employed on C-fibers, slowly

adapting mechanoreceptors (SA), and Aδ-mechano-nociceptors (AMs), all fibers with predominantly static responses. Only for a group of 10 mechano-heat sensitive C-fibers (C-MH) a controlled ramp and hold heat stimulation was applied and the responses were recorded. During the ramp duration of 10 s, the base temperature of these neurons were increased from 15 °C to 52°C and held for 5 s. The remaining C-fibers were tested for their heat responsiveness with an uncontrolled heat stimulation. A preheated synthetic interstitial fluid (SIF buffer) was applied on the receptive field isolated with a small metal ring (see (Moshourab, et al., 2013) (Milenkovic, et al., 2008) for more details of SIF buffer compositions).

Mechanical stimulation protocols were quite heterogeneous and most notably, the magnitude of force levels was only known up to an unknown scale factor. We therefore decided to only model the neurons' responses to the highest force level. Furthermore, because of the uncontrolled heat stimulation of the SIF buffer, we restricted our modeling efforts to discriminate between heat and mechanical responses to the responses of 10 C-MH neurons.

### 4.2.2 Model

Each neuron was described by two state variables, an instantaneous firing rate $r(t)$ and a latent adaptation $A(t)$ (we will often drop the argument t for notational clarity). The dynamic of these state variables were described by the equations

$$\begin{cases} \frac{dr}{dt} = a(r - E(s, A)) \\ \frac{dA}{dt} = c\, r - d\, A \end{cases} \tag{4.1}$$

with parameters $a, c, d > 0$. Despite its simplicity, the ordinary differential equation offers a strong model of describing the spike rate of a single neuron in response to stimulation, and physiological relevant model parameters (Wilson, 2005). This model has been proven as successful model to describe the firing rates of visual neurons in response to stimuli of varying contrast or intensity in the past (Sclar, et al., 1990) (Albrecht & Hamilton, 1982).

According to equation (4.1) the firing rate converges to a steady state $E(s, A)$, which is determined by stimulation *s* and an abstract adaptation variable *A* that summarizes all possible physiological adaptation mechanisms. To derive a mathematical expression of adaptation we considered two alternatives, linear adaptation $E(s, A) = r_0 - b_{lin}s - A$ and nonlinear adaptation $E(s, A) = r_0 + \frac{b_{nonlin}}{1+A}s$.

The parameterization of the steady states $E(s, A)$ adds two more parameters to the model, namely the level of spontaneous activity $r_0$and the stimulation sensitivity $b_{lin}$ or $b_{nonlin}$.

We estimated the mean firing rate $r$ of responses in time intervals of 1 ms. We assumed that the mean firing rate of each instant of time over the whole trial's duration is the rate function of a point process.

Our first assumption was that the neurons' spikes were generated by an inhomogeneous Poisson process with time-varying rate function r(t). A Poisson process is a stochastic process, for which the number of (spikes) events observed in a given time interval $[t_i, t_{i+1})$ follows a Poisson distribution [1] with rate parameter $\lambda_i = \int_{t_i}^{t_{i+1}} r(t')dt'$ , $i = 1, \dots, n-1$. We obtained the log-likelihood function of observing $k$ spike counts, given sets of parameters $\theta = \{a, b_{lin}, b_{nonlin}, c, d, r_0\}$

$$\ln \ell(\theta|k) = \ln \prod_{i=0}^{n-1} \frac{\lambda_i^{k_i} e^{-\lambda_i}}{k_i!} \tag{4.2}$$

and selected the set of parameters which maximized the log-likelihood function using the Nelder-Mead simplex algorithm (Nelder & Mead, 1965) implemented in the python package scipy.optimize (Jones, et al., 2001 --).

We also considered the alternative assumption that the spikes were generated by an inhomogeneous Gamma process. We assumed that, (1) the process started with an event at time point $t = t_0$ and $t_0 \to -\infty$, and we considered the development of the process from the origin $t = 0$ onwards. (2) If $t_1, \dots, t_n$ were the times of first n events, the first time interval $x_1$ is exponentially distributed and the *n* inter-spike time intervals $\{x_2, x_3, \dots, x_n\}$ were distributed according to a Gamma distribution with a rate function $\lambda_i = \int_{t_i}^{t_{i+1}} r(t')dt'$. The log-likelihood of observing inter-spike intervals given sets of parameters $\theta = \{a, b_{lin}, b_{nonlin}, c, d, r_0\}$ and shape parameter $\{\kappa\}$ is (Berman, 1981),

$$\ell_{exp}(\theta|x_1) = \lambda(t_1)e^{-\lambda(t_1)}$$

$$\ell_{gamma}(\theta, \kappa|x_i) = [\prod_{i=2}^{n} \lambda(t_i)\{\Lambda(t_i) - \Lambda(t_{i-1})\}^{\kappa-1}]e^{-\Lambda(t_n)}/\{\Gamma(\kappa)\}^{n} \tag{4.3}$$

$$\ln \ell(\theta, \kappa|x_i) = \ln \ell_{exp} + \ln \ell_{gamma} \tag{4.4}$$

[1] Note that there are two different mathematical concepts involved here that are both named after Simeon Denis Poisson (1781-1840). The first one is the Poisson *distribution*, which describes a distribution of counts. The second one is the Poisson *process*, which describes a distribution of event sequences.

In this equation $\Lambda(t) = \int_0^t \lambda(x)dx$.

We estimated the model parameters $\theta$ and shape parameter $\kappa$ using maximum likelihood estimation. Note that for the Gamma process, we need to express the likelihood in terms of inter-spike intervals rather than spike counts, which turned out to be considerably less stable numerically.

### 4.2.3 Goodness-of-fit

Typical goodness of fit testing uses the fact that for large data sets, the deviance (derived from the model's log-likelihood) converges in distribution to a Chi-square distribution. Yet, this isn't necessarily true for smaller data sets (Wichmann & Hill, 2001), where "small" data sets can consist of several thousand observations. We therefore evaluated how well the introduced model described the observed spike train using a Monte-Carlo method to simulate the null-hypothesis. The measure for the Monte-Carlo hypothesis testing method is a *p*-value. To test a null-hypothesis $H_0$, we specify a test statistic $T$. If the observed value of the test statistic is $t_{obs}$, then the p-value is:

$$p = P(T \geq t_{obs}|H_0) \tag{4.5}$$

Then large values of $T$ provide evidence against the hypothesis $H_0$. To evaluate this probability we need the distribution of $T$ when $H_0$ is true.

Our null-hypothesis was that the spikes were generated by the point process under consideration (either Poisson, or Gamma). Thus, for the Poisson model, we sampled 1000 spike trains from a Poisson process with the modeled rate function given by equation (4.1). For the Gamma model, we sampled 1000 spike trains from a Gamma process with the modeled rate function given by equation (4.1) and the additional irregularity parameter $\kappa$. Then the test statistic $T$ was the log-likelihood of rate functions of the simulated spike trains under the respective model and $t_{obs}$ was the log-likelihood of the observed spike train. Thus, the probability P was approximated as the fraction of sampled spike trains for which the log-likelihood exceeded the log-likelihood of the observed spike train. The null-hypothesis is rejected if the value of the log-likelihood of simulated spike trains were larger than the log-likelihood of the observed spike train for more than 95% of the simulated spike trains. In other words, we sampled spike trains from the fitted model to approximate the distribution of likelihoods under the null-hypothesis that the fitted model is correct and then used standard null-hypothesis testing to compare the observed spike train to this distribution. We reported the *p*-value of this test.

### 4.2.4 Sampling methods

To sample a large number of spike trains from a Poisson process, we assumed that for every single neuron the spikes in each time bin were Poisson distributed with a rate given by the fitted firing rate model.

In sampling from an inhomogeneous Gamma process we employed the alternative method of deriving the inhomogeneous Gamma process introduced by Berman (Berman, 1981), who pointed out that for a Gamma process, differences in cumulative rate are Gamma distributed. Thus, samples from a Gamma process can be generated by generating a sequence of Gamma random variables $\mathrm{d_i}, i = 1, \dots, n$ and then selecting time points $t_i$ such that

$$\sum_{i=1}^{j} \mathrm{d_i} = \int_{0}^{t_j} \lambda(x)dx$$

Here, $\lambda(x)$ is the firing rate function given by the fitted model.

### 4.2.5 Model selection

To select which models of adaptation describe our data "better" we used the Akaike Information Criterion (AIC) (Akaike, 1974). The AIC is a model selection criterion, which provides a relative measure of goodness of fit while penalizing more complex models. This approach uses the maximum of the likelihood function as the goodness-of-fit measure and the number of parameters $k$ as the complexity of the model. The model selection criterion is a tradeoff between these two measures.

$$AIC = -2\log \ell(\theta|k) + 2k$$

Thus, the preferred model is the one for which the AIC is smaller. In our modeling framework, however, both models; linear and nonlinear adaptation have the same number of parameters. Therefore, the negative maximum of log-likelihood provided the measure for model selection. The preferred model was the model with the higher log-likelihood.

## 4.3 Results

In this study we developed parametric models of temporal changes in firing rates of primary afferent neurons as function of four model parameters and spontaneous firing rate. Given any stimulus, the goal was to predict the neural response, and to estimate the model parameters of single neurons as well as possible, as this can give insights into the computations carried out by the neurons.

### 4.3.1 Descriptive model of firing rate and adaptation

Our first assumption was that the spikes were generated by an inhomogeneous Poisson process. We tested this assumption on 53 thermally and mechanically evoked response discharges of 48 C-fibers including 30 polymodal C-fibers and 18 heat insensitive C-fibers.

For all neurons the neural responses to mechanical stimulation was recorded. But only for 10 out of 48 neurons we applied a controlled heat stimulation and recorded thermally evoked responses. The remaining 38 neurons were tested for their heat responsiveness with uncontrolled heat stimuli. Hence, we did not consider the heat evoked responses of neurons in the second group. In the first group 6 out of 10 neurons responded to controlled heat stimuli. We refer to the heat responses of this group as 'Heat'. 9 out of 10 responded to controlled mechanical stimuli. We refer to mechanically evoked responses of this group as 'Mechanical'. 24 out of 38 neurons of second group were sensitive to heat stimuli. We refer to mechanically evoked responses of this group as 'C-MH' and 14 out of 38 were heat insensitive. We refer to the mechanically evoked responses of this group as 'C-M'.

In Figure 1a-b we reported the *p*-values for all fitted responses as result of the goodness-of-fit test for the firing rate models based on a Poisson process and two types of adaptations; a linear adaptation (Figure 1a) and nonlinear adaptation (Figure 1b). The *p*-value refers to the fraction of sampled spike trains for which the negative log-likelihood exceeded the negative log-likelihood of the observed spike train. The gray bars of Figure 1a-b show the significance levels of the test (see 2.3 for more details). For all responses with a *p*-value above significance level, the hypothesis that the spikes were generated by the corresponding model was rejected. Figure 1a shows that all 53 response discharges were well described by the nonlinear model, while the linear model (Figure 1b) failed to describe the firing rate variations for 3 out of 53 responses ($p<0.05$, Monte-Carlo simulation of expected model responses).

Figure 1c shows the results of model selection analysis (AIC). For responses with positive AIC, the test was in favor of model with nonlinear adaptation and for negative AIC, the test was in favor of model with linear adaptation. The model selection analysis (AIC) shows that in cases where the linear model failed to describe the firing rate the AIC was significantly in favor of nonlinear adaptation $\ell_{nonlinear} - \ell_{linear} \gg 0$ (see Figure 1c).

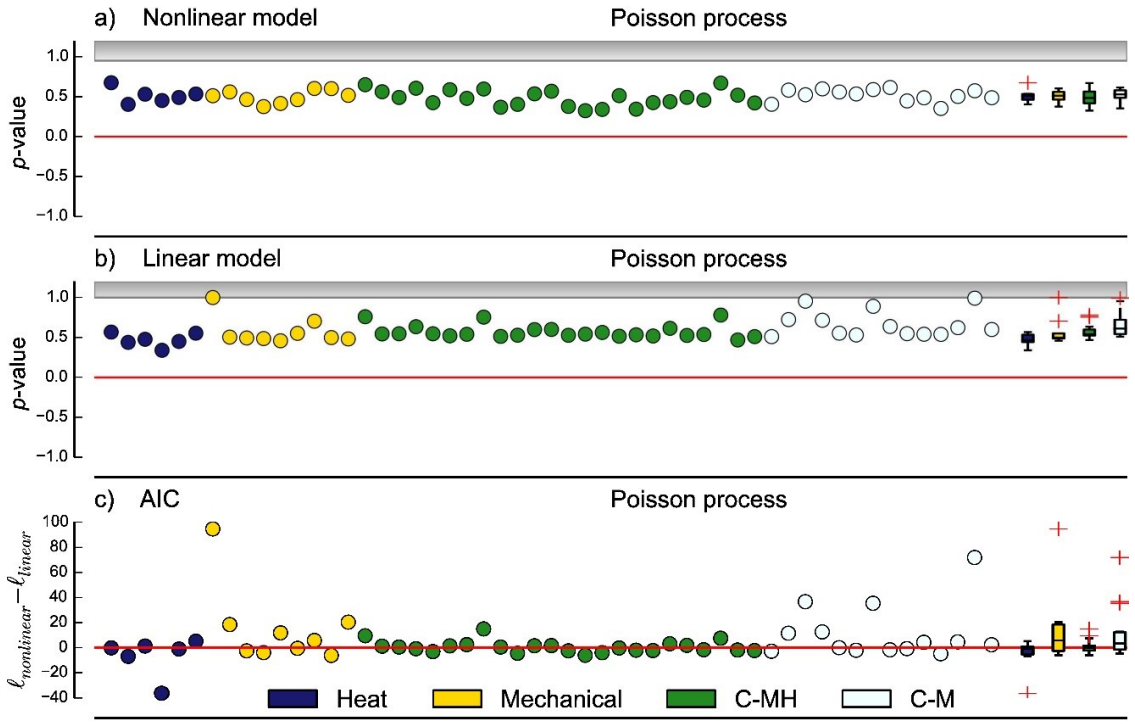


**Figure 1. The results of goodness-of-fit for Poisson-generated spike trains according to Monet-Carlo simulation and model selection test (AIC) for two models; a linear model and a nonlinear model.** Each point represents the results of one spike train of single neuron. The data set included 48 neuron and 53 spikes trains. 'Heat' responses refer to responses of polymodal C-fibers to controlled heat stimulation 'Mechanical' refer to responses of the same neuron to mechanical stimulation. 'C-MH' refer to mechanically evoked responses of second group of polymodal C-fibers. 'C-M' refer to mechanically evoked responses of a group of mechanical sensitive and heat insensitive C-fibers. (**a**) *p*-value of Monte-Carlo test for nonlinear model and Poisson assumption. (**b**) *p*-value of Monte-Carlo test for linear model and Poisson assumption. For a value in the gray bar the null-hypothesis was rejected. (**c**) Model selection according to AIC. For responses with values smaller than zero, the test may be in favor of the linear model and for values above zero the test may be in favor of nonlinear model. In (**a-c)** the box plots represents the distribution of values for each group of neurons. The whiskers show the range of the estimates. Flier points are those past the end of the whiskers.

Figure 2a shows for an example neuron the estimated firing rates of mechanically evoked responses for two adaptation models with the assumption that the spike trains were generated by a Poisson process. Both estimated firing rates have their peaks during the first 2 s after spike onset and within the ramp phase of the stimulation. The linear model shows a fast adaptation of the firing rate while the nonlinear model converges slowly towards the base line. To compare the two models, we simulated spike trains given the firing rate of the selected model and reported *p*-value of Monte-Carlo test as described by equation (4.5) and of the following form: If the fitted model described the observed spike train correctly, then the log-likelihoods of spike trains simulated from the fitted model should not differ significantly from log-likelihood of the observed spike train (see Figure 2c). The *p*-value we report refers to the null-hypothesis that the fitted model is correct.

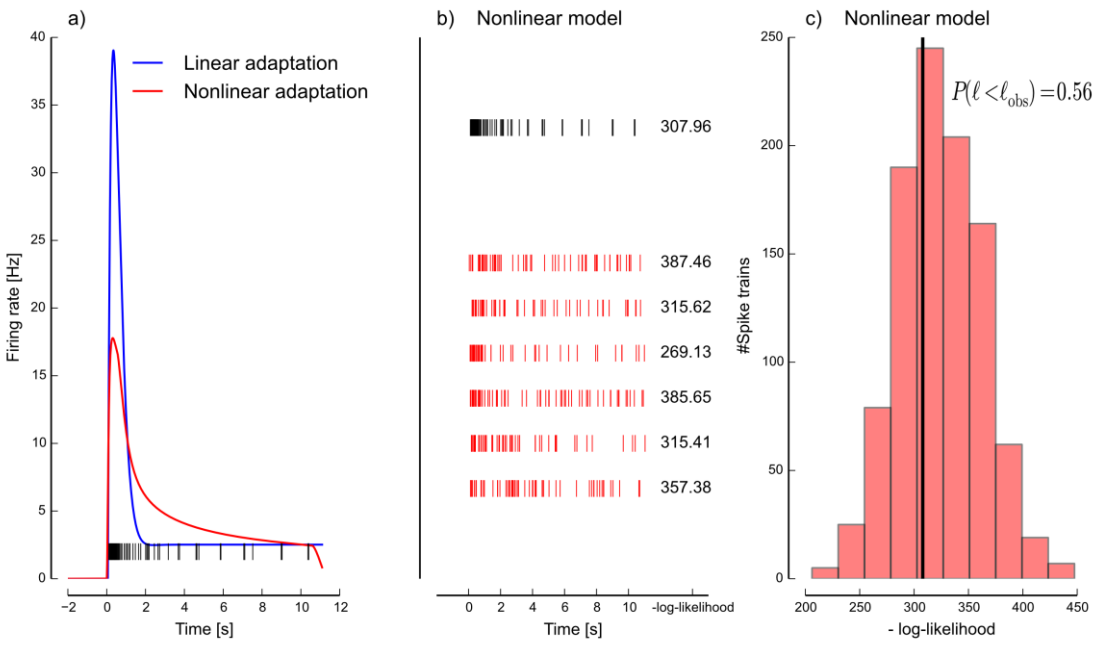


**Figure 2. Estimated firing rates and histogram of the simulated p-values of Monte-Carlo test for an example neuron and two adaptation models. The hypothesis was that the spikes were generated by a Poisson process.** (**a**) The estimated firing rates for two adaptation models for an example neuron. The spike train shows the observed spike train. (**b**) The observed spike train of the example neuron and the simulated spike trains from the model with nonlinear adaptation. For each spike train the log-likelihood of observing this spike train given the estimated parameter was calculated. (**c**) Histogram of negative log-likelihood of simulated spike trains. The line shows the negative log-likelihood of the observed spike train. The p-value of Monte-Carlo test indicates that the hypothesis is not rejected.

By observing the simulated and recorded spike trains the recorded spike train seemed to show more regularity in spike-timing in comparison to the simulated spike trains. We supposed that the fully random nature of the Poisson process contributed to the irregularity of the simulated spike trains. To test this observation we asked if a more elaborate point process, a Gamma process, captured the spiking dynamics and regularity of spike trains more accurately. To this end we examined a superset of spike responses of 80 C-fiber nociceptors, including the 38 C-fibers of previous analysis of Poisson assumption. In addition, this data set included slowly adapting SAs mechanoreceptors, and A$\delta$ mechano-nociceptors (AMs). As all neurons in this data set were stimulated by the same mechanical protocol, this dataset provided a uniform initial condition to examine the assumption. However, we emphasize that our models and model validation method (Monte-Carlo test of single neurons) are based on statistical characterization of single neurons and thus provide a framework to compare the temporal dynamics of responses even with different modalities and intensity of stimulations.

Modeling the spike trains using an inhomogeneous Gamma process required estimation of an additional parameter $\kappa$ to assess the regularity of the observed spike trains. Figure 3a illustrates schematically how the shape parameter $\kappa$ affects the regularity of simulated

spike trains. Note that for $\kappa = 1$, the Gamma process turns into a Poisson process. Figure 3b shows the distribution of the estimated $\kappa$ values. The estimated shape parameter $\kappa$ for 64 out of 80 neurons were larger than 1 (see Fig 3b). This results might explain the irregularity observed by the Poisson-generated spike trains compared with the observed spike train. However, an analysis of the distribution of shape parameters in each group (boxplots in Fig 3b) indicated that the shape parameters are not very far from 1. Although there seems to be evidence that the inter-spike intervals are less dispersed than expected for a Poisson process, there are too few data to reject the Poisson hypothesis.

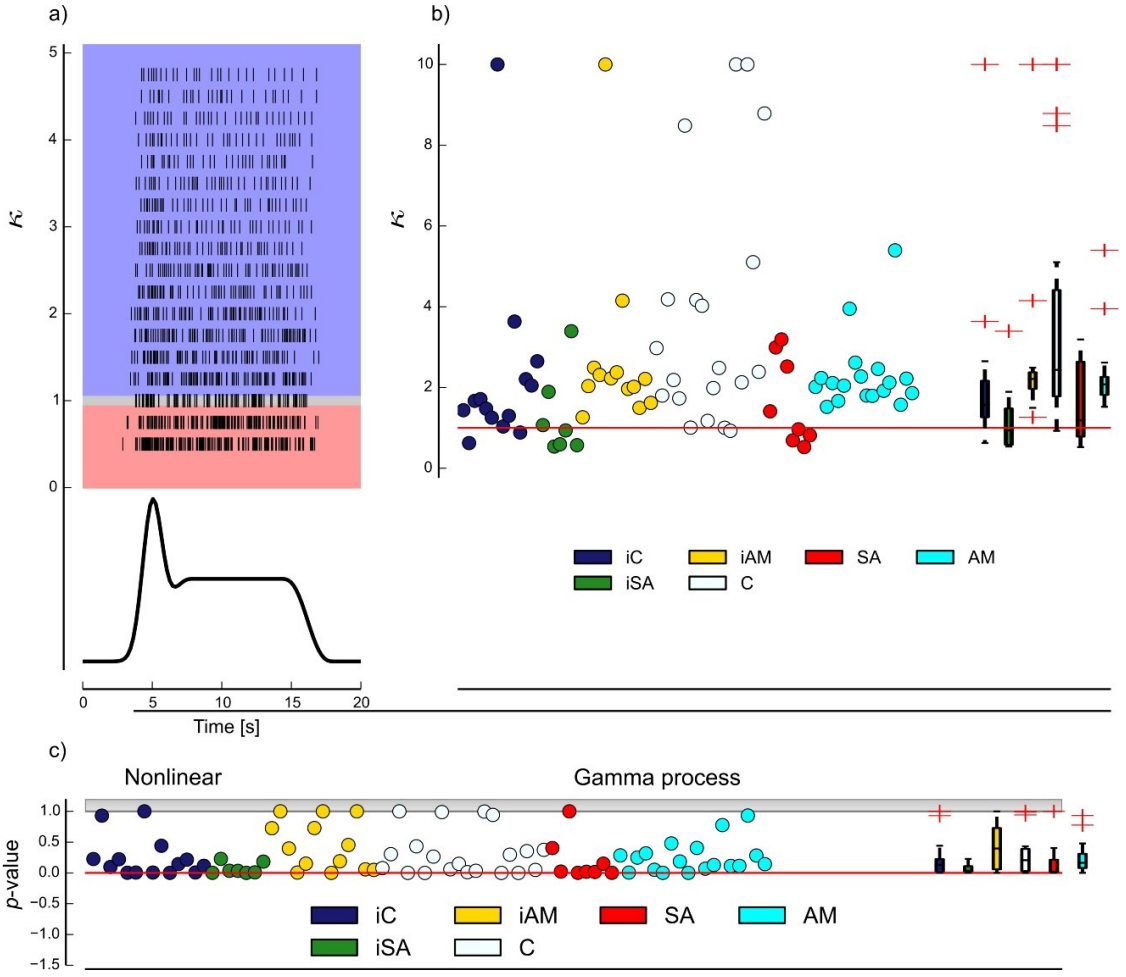


**Figure 3. A schematic of how shape parameter $\kappa$ affects the spiking patterns of simulated spike trains and variation of $\kappa$ for all observed spike trains.** (**a**) Each spike train is a realization of a Gamma process with varying shape parameter. The black curve illustrates the rate function of Gamma distribution. (**b**) Estimated shape parameter $\kappa$ of Gamma process as a measure for the regularity of the spike trains. The data set included C-fibers (C, iC). Slowly adaptation A-fibers mechanoreceptors (SA, iSA). A$\delta$-fiber mechano-nociceptors (AM, iAM). (**c**) *p*-value of Monte-Carlo test for nonlinear model and Gamma assumption. (**b-c**)The box plots represents the distribution of values for each group of neurons. The whiskers show the range of the estimates. Flier points are those past the end of the whiskers.

To test the goodness-of-fit for a Gamma process we test the hypothesis that the spikes were generated by a Gamma process and reported the p-value of Monte-Carlo simulation as described in section 2.3. As Figure 3c shows the Gamma process failed to describe 8 out of 80 neurons for the selected nonlinear model ($p<0.05$, Monte-Carlo simulation of expected model responses).

### 4.3.2 Discriminant analysis of estimated parameters

The main idea of developing a parametric model of responses was to compare the model parameters instead of comparing the spike trains directly, as the temporal dynamics of responses to different stimulus modalities might give insights into the encoding mechanisms of distinct modalities. In this way we were able to span a parametric space in which the neural responses were represented by their parameters and to be potentially classified into distinct stimulus responses such as thermal or mechanical. To this end we characterized the responses of 10 C-MH polymodal C-fibers of first group including both heat evoked and mechanically evoked responses. We then applied a discriminant analysis test to classify the estimated parameters $\theta = \{a, b, c, d\}$. Only this data set provided neural responses to controlled heat stimuli. Our results showed no classification of responses to thermal and mechanical stimuli. Yet, the small number of neurons which responded to thermal stimuli (6 neurons), may explain this observation.

To summarize the results, we developed a probabilistic framework to characterize the temporal dynamics of responses as a function of stimulation. We proposed a method to validate the models based on single neuron statistics. This framework allowed us to compare the responses of single neurons to different stimulus modalities and conditions. Both linear and nonlinear models described the Poisson-generated and Gamma-generated spikes reasonably well.

## 4.4 Discussion

In this study we introduced a parametric model of single neurons to characterize the temporal dynamics of their responses to different stimulus-modalities. Each neuron was described by two variables, instantaneous firing rate and adaptation. We chose two types of adaptation, linear and nonlinear divisive adaptation. We assumed that the spikes were generated by one of two inhomogeneous point process: A Poisson process that assumed the inter-spike intervals were independent and a Gamma process that assumed that successive inter-spike intervals were dependent, the first spike occurred at time point in infinity, and the origin is at time point zero.

We suggested that the estimated parameters can span a parameter space. In such a parameter space the response discharges evoked by different stimulus modalities and/or conditions can be represented as a point. This characterization of responses allowed us to compare the specific and defined properties of the neural responses even in cases where the stimulation itself was not directly comparable, such as heat stimulus and mechanical pressure applied on the same polymodal C-fiber.

To test the goodness-of-fit we applied a null-hypothesis test. Here, we used likelihood as a test statistic, and simulated the null-distribution of the test statistic. In a classical setting, one might have used deviance instead of likelihood (deviance is a monotonic transformation of likelihood) and use an asymptotic chi-square distribution for the deviance. We decided to deviate from this classical approach, mostly because our dataset was very small. Strictly speaking, the chi-square distribution is a good approximation of the null distribution of deviance only in the limit of infinite data. It has been shown (Wichmann & Hill, 2001) that for small data sets, this approximation can be very bad and that deviations from the chi-square distribution are quite unsystematic. This motivated us to explicitly simulate the null-distribution to achieve the results that are still valid for the small data sets used in this study. Yet, approximating the null-hypothesis by samples implies that the reported *p*-values are subject to a small amount of sampling error. Yet, the sampling error is much easier to characterize than the inaccuracies of the chi-square approximation.

Our results showed that both adaptation models and both assumed point process described the neurons reasonably well. However, our model provides some evidence in favor of a Poisson process and nonlinear adaptation for mechanical responses. This observation can be supported by the previous studies. Previous studies have shown that the transduction mechanism of mechanoreceptors are a more nonlinear process (Johnson, 2001) (Phillips & Johnson, 1981a) (Phillips & Johnson, 1981b) (Sripati, et al., 2006). Transduction mechanism of noxious cold seems to be a more linear process (Dubin & Patapoutian, 2010) (Vriens, et al., 2014). Preliminary data show a higher spontaneous activity of primary afferent neurons during conditions of inflammatory and persistent pain. Thus, we see modeling of spontaneous activity as an important long term goal of our models. Yet, modeling spike trains as realizations of an inhomogeneous Gamma process has to assume that spontaneous activity is close to zero. Furthermore, the additional shape parameter $\kappa$ increases the complexity of the Gamma process compared to a Poisson process. Thus, parsimony implies that based on our data, the Poisson process should be the preferred model. Yet, we acknowledge that reliably fitting the spikes as a realization of a Gamma process requires more and more reliable data. Current results

suggest that the Poisson assumption overestimates the irregularity of peripheral neurons (Farkhooi, et al., 2009), so that with a larger data set the Gamma process might indeed prove a good model. Therefore, we believe that a nonlinear adaptation under an inhomogeneous Poisson assumption offers a good framework for modeling the responses to thermal and mechanical stimulation in our rather limited data set.

Yet, analyzing the estimated parameters revealed that the parameter spaces of thermal and mechanical responses of a small data set overlapped. This result might be due to the small number of neurons but it also might be due to the single stimulus recordings which resulted in lack of fit (the difference between observed and predicted firing rates).

The parametric model developed in our study served a direct link between the stimulus signal and discharge rate and is entirely descriptive. Modifying this model by a mechanistic model that specifies the transduction mechanism or a spike generation mechanism may improve the prediction power of our model. An alternative approach to improve this model might be by adding two additional stages to the model. First it might be expanded to include the propagation of the stimulus within the skin from surface to the receptor terminal endings. In this way we could include information about histological properties of receptors terminals and skin (i.e. depth of receptor neuron, branching of terminals). Moreover, a stimulus propagation model might offer a generalization to make different modalities comparable. Second our model might be improved by including a transducer stage to describe the dynamics of underlying transduction at receptor terminals.

We suppose that such a three stage model provide a framework to capture different features of stimulus and transduction mechanism. The realization of a more complex model, however, increases the risk of overfitting and requires a reliable data set of recordings from polymodal C-fibers to guarantee an effective characterization of both, average responses and stochasticity. The different stochastic processes studied here mainly differ in the variability they expect for a given neuron. Characterizing a neuron's variability requires multiple repetitions of the same stimulus to be recorded. Clearly, as more repetitions are recorded, this characterization will become more accurate. We therefore suggest a controlled experimental protocol of only one condition for which the thermal and mechanical stimulation start just above their threshold to provide for a comparable initial condition of neurons and to increase the number of repetitions. Furthermore, an equal ramp velocity of thermal and mechanical stimulus might retain neurons in some similar dynamical conditions. Different levels of ramp velocities might offer studying different dynamical systems of neurons.

The descriptive model developed in this study allows for a quantitative characterization of nociceptors and thus provides a basis from which these more detailed mechanistic models can start.

# Chapter 5

# 5 General Discussion

## 5.1 Summary

The basic circuitry of the “pain pathway” is well known – it consists of specialized sensory fibers known as nociceptors projecting to specific spinal cord neurons, which in turn project on to the thalamus and cerebral cortex (Woolf & Ma, 2007). However, it is still far from understood how the activity in nociceptor populations individually and collectively is related to the perception of pain. Some undefined properties of this circuity, such as dissociation between the nociceptor activities and behavioral responses indicating pain (Prescott, et al., 2014), and central and peripheral sensitization illustrate the need for more quantitative approaches to the nociceptive system, specifically at the peripheral level and for the main class of nociceptors, the polymodal C-fibers. Although, different stimulus modalities, like noxious heat and mechanical stimuli, are conveyed through the same multimodal C-fibers, these stimuli are perceived as distinct qualities. Yet it is difficult to address how and at which level in the pain circuity the discrimination of different modalities occurs (Mendell, 2011). Addressing these questions requires an adequate identification of expression and functionality of the constituted ion channels and transduction mechanism. The early attempts to record transduction currents for nociceptors were partially unsuccessful because of the difficulties in isolating and recording single neurons. Thus, despite remarkable advances in identifying the ion channels expressed in transduction of different stimulus modalities, less in known about their mechanism. Hence, computational and modeling approaches might offer strong tools to fill the gap of knowledge and to give insights into the neural representation of different stimulus modalities and underlying encoding mechanism. Nevertheless, small data sets of recordings, lack of repetition in recordings of single stimulus from one side and difficulties in choosing the right statistical model and prior distributions from the other side make using advanced statistical models less feasible. In the present study, I introduced methods to circumvent these difficulties and to develop novel statistical framework to characterize the responses of polymodal C-fibers to different stimulus modalities.

In general, detecting and encoding noxious stimuli involves three main processes: transfer of a stimulus in the skin to the receptor site(s), generation of a receptor potential to trigger action potentials and generation of spike trains. Similarly, a general modeling framework may consider these three steps.

In chapter 2, I studied the interaction of heat energy and skin. Transfer of heat energy in the material is a well-studied theory and an established model in pain studies to estimate the location (e.g depth) and activation threshold temperature of C-fiber nociceptors from temporal dynamics of their responses to heat ramped stimuli (Henriques & Moritz, 1947) (Tillman, et al., 1995) (Stoll & Greene, 1959) (Hardy & Stolwijk, 1966). To summarize, in classical approaches, it is assumed that the first spike after stimulus onset is the exact time of reaching the threshold temperature (threshold time) and the corresponding stimulus temperature on surface at this time is called the surface threshold temperature. Knowing these two parameters for two or more experimental conditions provides a system of equations to estimate the threshold temperature and the depth of receptor terminals. In classical approaches an accurate estimation of threshold time is therefore crucial. Small inaccuracies in spike time measurement, internal random processes which could result in a delay between reaching the threshold and generation of first spike, and trial-to-trial variability of neural responses, would result in misinterpretation of depth and threshold temperatures and sometimes make depth estimation impossible. To improve the estimation of depth and threshold temperature and to make this approach more flexible for challenging data sets, I modified the classical model by taking noise into account in the system, and by solving the heat equation as a part of a Bayesian model. The Bayesian framework allows one to add additional information as prior knowledge to improve the estimation. Two challenges emerged: First, to find the appropriate probability density functions of prior distributions, when such information does not exist or has not been reported in an appropriate statistical format in the literature; second, to overcome computational difficulties that one may face using sampling methods.

Another new aspect of the probabilistic approach presented here, was a statistical model of the skin. In this model I used Monte-Carlo sampling to estimate physical properties of dermal and epidermal layers of a two layer skin model. The results showed that the probabilistic model is capable of providing estimates of threshold and depth for cases where the classical method is failing. The highlight of this approach was adding noise in a way that represent the randomness but is still biophysically meaningful and offering a method to solve the probabilistic formulation of heat equation and noise.

In chapter 3, I studied different strain profiles of skin at the location of receptor terminals, using the depth estimates from chapter 2. Strain or deformation of skin tissue caused by a force-induced stress is the way how a mechanical stimulus affects the skin. The obtained strain and thermal components were used to define a large dimensional space of input components that I used to predict the neural responses and to model the transduction of single neurons.

To model the neural responses as point processes I used a Generalized Linear Model (GLM) with a L1 norm regularization (Tibshirani, 1996). To summarize, I assumed that the spikes were generated by a Poisson process with a rate function that was estimated by maximizing a penalized log-likelihood function. The penalty was proportional to the L1 norm of the parameter vector. The idea behind using a sparse regularization was to select those stimulus components that strongly affect the discharge of single neurons, and deselect the dependent and correlating components. The results indicated that the receptor neurons showed most sensitivity to the temporal changes of vertical strain and compressive as well as tensile strains regardless of orientation. I concluded that these components might be interpreted as the stimulus aspects to which the receptor membrane respond. Using a L1 norm regularization is mostly efficient in setups with a large number of candidate features of which only a few are likely to be useful in the end. In this case, the L1 regularization allows an automatic identification of those dimensions of this high dimensional feature space that drive the neural responses. Hence, finding a large dimensional space of strain and heat parameters and reducing it to only the most relevant features through the application of a probabilistic model resolves previous inconclusive reports about the relevant feature that drive C-fibers (Sripati, et al., 2006) (Johnson, 2001). In this way using a LASSO regularization could potentially be used to characterize individual ion channels rather than complete neurons.

In chapter 4, I introduced parametric models of stimulus-driven instantaneous firing rates of single neurons to characterize the temporal dynamics of firing rates. These models described how the neuron's temporal dynamics depend on stimulation modality. To estimate the parameters, I assumed that the spike trains were generated by a point process. These models are of descriptive nature – they illustrate the temporal dynamics of the firing rate, while estimating stimulus relevant parameter. Four model parameters were estimated; one parameter to capture the stimulus sensitivity, two parameters to represent the firing rate and adaptation, and a coupling parameter that links the firing rate to the adaptation. Particularly, these parameters can be used to characterize each neurons' responses to different stimulus modalities as a point in a four dimensional parameter space. A representation of neural responses in a parametric space offers a

platform to discriminate the thermal and mechanical responses at peripheral level in a substantial data set.

## 5.2 Moving Towards a General Model

So far the models describe separately the main processes of responding to noxious stimuli: the effect of stimuli at the receptor site, the dynamics of transducer, and the dynamics of firing rate and adaptation. I asked how one can realize a general framework, which includes all three steps. This general framework would offer a completely Bayesian approach to give a parametric characterization of the transduction and temporal dynamics of firing rate to different stimulus modalities in primary C-fibers and hence, might provide a basic for discrimination of stimulus modalities.

To this end I sought to extend the differential equation (4.1) with the regularized strain and thermal components obtained by sparse GLM model (equation (3.7)). In other words, I replaced a direct stimulus signal *s* and used the selected vector of non-zero strain and thermal components $\beta_i X_{ij}$ as an input layer of the differential equation model,

$$\begin{cases} \frac{dr}{dt} = a(r - E(X, A)) \\ \frac{dA}{dt} = c\, r - d\, A \end{cases} \tag{5.1}$$

where $E(X, A) = r_0 + \frac{b_{nonlin}}{1+A}\, \beta_i X_{ij}$ .

However, the attempts to fit the combined differential equation model (equation 5.1) of spike trains as realization of both Poisson and Gamma processes faced technical difficulties in the convergence process. It seemed that a naïve attempt to combine these models might fail, mainly because of either the differential equation model, or design of the main data set, or a combination of both together. The differential equation model (4.1) converged successfully for a preliminary data set of responses evoked by a different mechanical protocol as showed in chapter 4. For most neurons, the response showed an initial peak of the firing rate, followed by a relatively stable plateau of firing activity. Direct comparison of the mean firing rate of the preliminary data set and main data set of 24 C-fibers, indicated a more pronounced activity peak at the onset of firing and a higher mean firing rate during the response plateau in the preliminary data set. The higher activity of neurons in the preliminary data set referred to the stronger mechanical stimulus used to evoke the responses of these neurons compared to the applied stimulus level of main data set. Whereas, the neurons of the main data set showed a peak firing rate at the ramp-

phase and a sparse spiking in the hold-phase. Therefore, I speculate the sparser response discharges in the main data set might be the reason why the ODE model cannot fit this data. The other reason for a failure compared to the preliminary data set might be a failure of optimization because of the number of likelihood functions that were to be maximized simultaneously. In chapter 4 the ODE models were fitted to the single spike trains of either one mechanical or one heat stimulus while for the main data set the model was supposed to be fitted on three mechanical and/or three heat stimuli.

Therefore, this results suggest that the differential equations developed in chapter 4 are intended to model the response to a single stimulus. Future work will have to extend this model to be able to handle multiple different stimuli simultaneously.

## 5.3 Outlook of Future Investigations

For further investigations I suggest to modify the GLM model of transduction equation (3.7) to capture the temporal dynamics of the firing rate, for example by directly incorporating the rate of adaptation into the GLM model. Analogous to the strain and thermal components one can convolve the recent history of spike train with a feedback filter and estimate the superimposed space of stimulus components and spike history filter outputs with a GLM model as described in chapter 3. The additional regularization of the parameter space with L1 norm penalty offers a method to not only select the stimulus components but to estimate the weights of spike history filter outcomes. This combined model offers a framework to connect the temporal dynamics of action potential generation to the temporal dynamics of proximal stimulus of transduction mechanism. The difficulty of this method is to find an appropriate feedback filter which improves the estimation power of GLM while avoiding the overfitting of data.

Fründ et al. (Fründ, et al., 2014) used geometrically decaying history weights and applied an orthogonalization procedure to reduce interdependencies between the different features. An alternative model was suggested by Gerwinn et al. (Gerwinn, et al., 2010). In their work, the authors studied the stimulus selectivity of a population of retinal ganglion cells by fitting GLM with history terms and cross-neuron terms. For the features describing the spiking history, they used the density function of a Gamma distribution. In a similar way I suggest to use a density function of an Exponential distribution. Exponential filters have long been used successfully in spiking neuron models (see for example the many applications in the book by Dayan & Abbot (Dayan & Abbott, 2001)). However, finding the right filter requires a systematic analysis of filter parameters such as mean and variance

for the density function of either Exponential, or Normal, or Gamma distribution, or bin width and number of bins for a box filter.

C-fibers are recorded in a relatively dynamical setting and the number of repeated recordings in response to the same stimulus is often very limited. Therefore, an effective stimulus protocol is usually a tradeoff between multiple recordings of one stimulus or single recordings of different experimental conditions. In this study the experimental protocol was in favor of different experimental conditions (e.g. different ramp velocities). For further investigations I suggest an experimental protocol of repeated recordings of one intermediate ramp velocity of suprathreshold mechanical and heat stimuli separately and simultaneously. This would require finely localized application of both, heat and mechanical force. Laser technology allows for such localized generation of heat (Marchandise, et al., 2014) (Mouraux, et al., 2012) (Olausson, 1998) and could in conjunction with a regular mechanical stimulation protocol potentially achieve such combined stimulation of the receptor. In this way evoked spike trains comprehend information of both mechanical and thermal transducer. Thus, a sparse GLM analyzing of single modality responses versus the multimodality responses might give valuable insights into how and to what extent the mechanical and thermal sensitive ion channels share and/or compete their broad dynamic range.

As a last word, a common characteristic of a research project is to raise more questions and this study in not an exception. Nevertheless, the main contribution of this work was to introduce a basic for applying advanced statistical models to study nociceptors and pain circuity at the earliest stage of processing. I have demonstrated the utility of probabilistic approaches in the research field related to peripheral encoding of pain. Progresses in recording techniques to obtain larger data sets from one side and application of modern tools from statistics and machine learning that allow for identification of pain pathway from the other side offer a promising future for the study of pain systems.

# 6 References


Akaike, H., 1974. A new look at the statistical model identification. *IEEE Transactions on Automatic Control,* 19(6), pp. 716-23.

Albrecht, D. G. & Hamilton, D. B., 1982. Striate cortex of monkey and cat: contrast response function. *J. Neurophysiol.,* 48(1), pp. 217-37.

Apkarian, A. V., Bushnell, M. C., Treede, R. D. & Zubieta, J. K., 2005. Human brain mechanisms of pain perception and regulation in health and disease. *Eur. J. Pain,* 9(4), pp. 463-84.

Basbaum, A. I., Bautista, D. M., Scherrer, G. & Julius, D., 2009. Cellular and molecular mechanisms of pain. *Cell,* 139(2), pp. 267-84.

Bensmaia, S. J., 2008. Tactile intensity and population codes. *Behav. Brain Res.,* 190(2), pp. 165-173.

Berman, M., 1981. Inhomogeneous and Modulated Gamma Processes. In: *Biometrika.* s.l.:Oxford University Press, pp. 143-52.

Bessou, P. & Perl, E. R., 1969. Response of cutaneous sensory units with unmyelinated fibers to noxious. *J. Neurophysiol.,* Volume 32, pp. 1025-43.

Braz, J. M., Nassar, M. A., Wood , J. N. & Basbaum , A. I., 2005. Parallel ‘‘pain’’ pathways arise from subpopulations of primary afferent nociceptor. *Neuron,* 47(4), pp. 787-93.

Breathnach, A. S., 1977. Electron microscopy of cutaneous nerves and receptors. *J. Invest. Dermatol.,* 69(1), pp. 8-26.

Britton, N. F. & Skevington, S. M., 1989. A mathematical model of Gate Control Theory of pain. *J. Theor. Biol.,* Volume 137, pp. 91-105.

Britton, N. F., Skevington, S. M. & Chaplain, M. A. J., 1995. Mathematical modeling of acute pain. *J. Biol. Syst,* 3(4), pp. 1119-24.

Bromm, B., Jahnke, M. & Treede, R. D., 1984. Responses of human cutaneous afferents to CO2 laser stimuli causing pain. *Exp. Brain Res.,* 55(1), pp. 158-66.

Burgess, P. R. & Perl, E. R., 1967. Myelinated afferent fibres responding specifically to noxious stimulation of the skin. *J. Physiol.,* 190(3), pp. 541-62.

Caterina, M. J., Schumacher, M. A., Tominaga, M., Rosen, T. A., Levine, J. D. & Julius. D., 1997. The capsaicin receptor : a heat-activated ion channel in the pain pathway. *Nature,* October, 389(6653), pp. 815-24.

Cavanaugh, D. J., Lee, H., Lo, L., Shields, S. D., Zylka, M. J., Basbaum, A.I. & Anderson D.J., 2009. Distinct subsets of unmyelinated primary sensory fibers mediate behavioral responses to noxious thermal and mechanical stimuli. *PNAS,* 106(22), pp. 9075-80.

Cecchi, G. A., Huang, L., Hashmi, J. A., Baliki, M., Centeno, M. V., Rish, I. & Apkarian, A.V., 2012. Predictive Dynamics of Human Pain Perception. *PLoS Comput. Biol.,* 8(10), p. e1002719.

Cesare, P. & McNaughton, P., 1996. A novel heat-activated current in nociceptive neurons and its sensitization by bradykinin. *Proc. Natl. Acad. Sci. USA,* December, 93(26), pp. 15435-39.

Cho, H., Yang, Y.D., Lee, J., Lee, B., Kim, T., Jang, Y., Back, S.K., Na, H.S., Harfe, B.D., Wang, F., Raouf, R., Wood, J.N. & Oh, U., 2012. The calcium-activated chloride channel anoctamin 1 acts as a heat sensor in nociceptive neurons. *Nat. Neurosci.,* 15(7), pp. 1015-21.

Dandekar, K. & Srinivasan, M. A., 1997. *Role of Mechanics in Tactile Sensing of Shape..* Cambridge, MA: MIT Press..

Dayan, P. & Abbott, L. F., 2001. *Theoretical Neuroscience: Computational and Mathematical Modeling of Neural Systems.* Massachusetts: MIT Press.

Del Prete, Z., Baker, S. P. & Grigg, P., 2003. Stretch responses of cutaneous RA afferent neurons in mouse hairy skin. *J. Neurophysiol.,* 89(3), pp. 1649-59.

Delmas, P., Hao, J. & Rodat-Despoix, L., 2011. Molecular mechanisms of mechanotransduction in mammalian sensory neurons. *Nat. Rev. Neurosci.,* 12(3), pp. 139-53.

Dezhdar, T., Moshourab, R. A., Fründ, I., Lewin, G. R. & Schmuker, M., 2015, in press. A probabilistic model for estimating the depth and threshold temperature of C-fiber nociceptors. *Scientific Reports.*

Dhaka, A., Viswanath, V. & Patapoutian, A., 2006. Trp ion channels and temperature sensation. *Annu. Rev. Neurosci.,* Volume 29, pp. 135-61.

Dubin, A. E. & Patapoutian, A., 2010. Nociceptors: the sensors of the pain pathway. *Journal of Clinical Investigation,* November, 120(11), pp. 3760-72.

Duck, F. A., 2013. *Physical Properties of Tissues: A Comprehensive Reference Book.* London: Elsevier Science.

Edin, B. B., 2004. Quantitative Analyses of Dynamic Strain Sensitivity in Human Skin Mechanoreceptors. *J. Neurophysiol.,* 92(6), pp. 3233-43.

Farkhooi, F., Strube-Bloss, M. & Nawrot, M. P., 2009. Serial correlation in neural spike trains: Experimental evidence, stochastic modeling, and single neuron variability. *Phys. Rev. E,* 79(2), p. 021905.

Fleischer, E., Handwerker, H. O. & Joukhadar, S., 1983. Unmyelinated nociceptive units in two skin areas of the rat. *Brain Res.,* 267(1), pp. 81-92.

Freeman, A. W. & Johnson, K. O., 1982. Cutaneous mechnoreceptors in Macaque monkey: Temporal discharge patterns evoked by vibration, and a receptor model. *J. Physiol.,* Volume 323, pp. 21-41.

Friedman, J., Hastie, T. & Tibshirani, R., 2010. Regularization paths for Generalized Linear Models via coordinate descent. *Journal of Statistical Software,* 33(1), pp. 1-22.

Fründ, I., Wichmann, F. A. & Macke, J. H., 2014. Quantifying the effect of intertrial dependence on perceptual decisions. *J. Vis.,* 14(7), pp. 1-16.

Gerling, G. J. & Thomas, G. W., 2008. Fingerprint lines may not directly affect SA-I mechanoreceptor response. *Somatosensory and Motor Research,* March, 25(1), pp. 61-67.

Gerwinn, S., Macke, J. H. & Bethge, M., 2010. Bayesian inference for generalized linear models for spiking neurons. *Front. Comput. Neurosci.,* May, 4(May), p. 12.

Global Industry Analysts, I., 2011. *The American academy of pain medicine.* [Online] Available at: http://www.prweb.com/pdfdownload/8052240.pdf

Goldscheider, A., 1894. *Uber den Schmerz in Physiologischer und Klinischer Hinsicht.* Berlin: Hirschwald.

Haeri, M., Asemani, D. & Gharibzadeh, S., 2003. Modeling of pain using artificial neural networks. *J. Theor. Biol.,* 220(3), pp. 277-84.

Handwerker, H. O., Anton, F. & Reeh, P. W., 1987. Discharge patterns of afferent cutaneous nerve fibers from the rat's tail during prolonged noxious mechanical stimulation. *Exp. Brain Res.,* 65(3), pp. 493-504.

Hao, J. & Delmas, P., 2010. Multiple desensitization mechanisms of mechanotransducer channels shape firing of mechanosensory neurons. *J. Neurosci.,* 30(40), pp. 13384-95.

Hardy, J. D. & Stolwijk, J. A. J., 1966. Tissue Temperature and Thermal Pain. In: *Touch, heat and pain.* s.l.:John Wiley & Sons, Ltd., pp. 27-56.

Henriques, F. C. & Moritz, A. R., 1947. I. The conduction of heat to and through skin and the temperatures attained therein. A theoretical and an experimental investigation. *Am J Pathol. ,* 23(4), pp. 531-49.

Hu, J., Milenkovic, N. & Lewin, G. R., 2006. The high threshold mechanotransducer: a status report. *Pain,* 120(1-2), pp. 3-7.

Jeffreys, H. B., 1935. Some tests of significance, threatened by the theory of probability. *Proc. Camb. Phil. Soc.,* Volume 29, pp. 83-7.

Johnson, K. O., 1974. Reconstruction of population response to a vibratory stimulus in quickly adapting mechanoreceptive afferent fibre population innervating glabrous skin of the monkey. *J. Neurophysiol.,* Feb., 37(1), pp. 48-72.

Johnson, K. O., 2001. The roles and functions of cutaneous mechanoreceptors. *Curr. Opin. Neurobiol.,* 11(4), pp. 455-61.

Jones, E., Oliphant , T., Peterson, P. & and others, 2001 --. *SciPy: Open source scientific tools for Python.* s.l.:s.n.

Julius, D., 2013. TRP channels and pain. *Annu. Rev. Cell Dev. Biol.,* Volume 29, pp. 355-84.

Julius, D. & Basbaum, A. I., 2001. Molecular mechanisms of nociception. *Nautre,* September, 413(6852), pp. 203-10.

Kass, R. E. & Raftery, A. E., 1995. Bayes Factors. *Journal of American Statistical Association,* 90(430), pp. 773-95.

Kass, R. E. & Wassermann, L., 1995. A reference Bayesian test for nested hypotheses and its relationship to the Schwarz Criterion. *Journal of American Statistical Association,* 90(431), pp. 928-34.

Khalsa, P. S., Hoffman, A. H. & Grigg, P., 1996. Mechanical states encoded by stretch-sensitive neurons in feline joint capsule. *J. Neurophysiol.,* 76(1), pp. 175-87.

Kress, M., Koltzenburg , M., Reeh , P. W. & Handwerker, H. O., 1992. Responsiveness and functional attributes of electrically localized terminals of cutaneous C-fibers in vivo and in vitro. *J. Neurophysiol.,* 68(2), pp. 581-95.

Kumazawa , T., Mizumura , K. & Kruger, L., 1996. *The Polymodal Receptor-- A Gateway to Pathological Pain.* New York(New York): ELSEVIER.

Lele, P. P., 1954. Relationship between cutaneous thermal threshold, skin temperature and cross-sectional area of the stimulus. *J. Physiol.,* 126(2), pp. 191-205.

Lesniak, D. R. & Gerling, G. J., 2009. Predicting SA-I mechanoreceptor spike times with a skin-neuron model. *Math. Biosci.,* 220(1), pp. 15-23.

Lewin, G. R. & Mendell, L. M., 1994. Regulation of cutaneous C-fiber heat nociceptors by nerve growth factor in the developing rat. *J.Neurophysiol.,* 71(3), pp. 941-49.

Lewin, G. R. & Moshourab, R. A., 2004. Mechanosensation and pain.. *J. Neurobiol.,* 61(1), pp. 30-44.

Lynn, B. & Carpenter, S. E., 1982. Primary afferent units from the hairy skin of the rat hind limb. *Brain Res.,* 238(1), pp. 29-43.

Ma, Q., 2010. Labeled lines meet and talk: population coding of somatic sensations. *J. Clin. Invest.,* 120(11), pp. 3773-78.

Ma, Q., 2012. Population coding of somatic sensations. *Neurosci. Bull.,* 28(2), pp. 91-9.

Marchandise, E., Mouraux, A., Plaghki, L. & Henrotte, F., 2014. Finite element analysis of thermal laser skin stimulation for a finer characterization of the nociceptive system. *J.Neurosci Methods,* Volume 223, pp. 1-10.

Martinez-Salgado, C., Benckendorff, A. G., Chiang , L-Y, Wang, R, Milenkovic, N., Wetzel, C., Hu, J., Stucky, C. L., Parra, M. G., Mohandas, N. & Lewin, G. R., 2007. Stomatin and sensory neuron mechanotransduction. *J Neurophysiol 98, 3802–3808,* Volume 98, pp. 3802-3808.

McCullagh, P. & Nelder, J. A., 1989. *Generalized Linear Models.* New York: Chapman and Hall/CRC.

Melzack , R. & Wall, P. D., 1965. Pain mechanisms: a new theory. *Science,* 150(3699), pp. 971-9.

Melzack, R. & Wall, P. D., 1962. On the nature of cutaneous sensory mechanism. *Brain,* Volume 85, pp. 331-56.

Melzack, R. & Wall, P. D., 1982. *The Challenge of Pain.* Harmondsworth, Middlesex: Penguin Books.

Mendell, L. M., 2011. Computational functions of neurons and circuits signaling injury: Relationship to pain behavior. *PNAS,* Volume 108 Suppl, pp. 15596-601.

Milenkovic, N., Frahm, C., Gassmann, M., Griffel, C., Erdmann, B., Birchmeier, C., Lewin, G. R. & Garratt , A. N., 2007. Nociceptive tuning by stem cell factor/c-Kit signalling. *Neuron,* 56(5), pp. 893-906.

Milenkovic, N., Wetzel , C., Moshourab, R. & Lewin, G. R., 2008. Speed and temperature dependences of mechanotransduction in afferent fibers recorded from the mouse saphenous nerve. *J. Neurophysiol.,* 100(5), pp. 2771-83.

Milenkovic, N., Zhao, W. J., Walcher, J., Albert, T., Siemens, J., Lewin, G. R. & Poulet, J. F.A., 2014. A somatosensory circuit for cooling perception in mice. *Nat. Neurosci.,* 17(11), pp. 1560-66.

Minamitani, H. & Hagita, N., 1981. A neural network model of pain mechanisms: computer simulation of the central neural activities essential for the pain and touch sensations. *Systems, Man and Cybernetics,* 11(7), pp. 481-93.

Moshourab, R. A., Wetzel, C., Martinez-Salgado, C. & Lewin, G. R., 2013. Stomatin-domain protein interactions with acid-sensing ion channels modulate nociceptor mechanosensitivity. *J. Physiol.,* 591(22), pp. 5555-74.

Mouraux, A., Ragé, M., Bragard, D. & Plaghki, L., 2012. Estimation of intraepidermal fiber density by the detection rate of nociceptive laser stimuli in normal and pathological conditions. *Neurophysiol Clin.,* 42(5), pp. 281-91.

Nadaraya, E. A., 1964. On Estimating Regression. *Theory Probab. Appl.,* 9(1), pp. 141-2.

Nathan, P. W., 1976. The gate-control theory of pain: a critical review. *Brain,* 99(1), pp. 123-58.

Nelder, J. A. & Mead, R., 1965. A simplex method for function minimization. *The Computer Journal,* 7(4), pp. 308-13.

Nelder, J. A. & Wedderburn, R. W. M., 1972. Generalized Linear Models. *Journal of the Royal Statistical Society. Series A (General),* Jan..135(3).

Olausson, B., 1998. Recordings of human polymodal single C-fiber afferents following mechanical and argon-laser heat stimulation of inflamed skin. *Exp Brain Res.,* 122(1), pp. 55-61.

Paninski, L., 2004. Maximum likelihood estimation of cascade point-process neural encoding models. *Network: Comput. Neural. Syst.,* 15(4), pp. 243-62.

Patapoutian, A., Peier, A. M., Story, G. M. & Viswanath, V., 2003. ThermoTRP channels and beyond: mechanisms of temperature sensation. *Nat. Rev. Neurosci.,* 4(7), pp. 529-39.

Perl, E., 2011. Pain mechanisms: a commentary on concepts and issues. *Prog. Neurobiol.,* 94(1), pp. 20-38.

Perl, E. R., 1996. Cutaneous polymodal receptors: Characteristics and plasticity. *Prog. Brain Res.,* Volume 113, p. 21–37.

Perl, E. R., 2007. Ideas about pain, a historical view. *Nat. Rev. Neurosci.,* 8(1), pp. 71-80.

Phillips , J. R. & Johnson, K. O., 1981a. Tactile spatial resolution. II. Neural representation of bars, edges, and gratings in monkey primary afferents. *J. Neurophysiol.,* 46(6), p. 1192–203.

Phillips , J. R. & Johnson, K. O., 1981b. Tactile spatial resolution. III. A continuum mechanics model of skin predicting mechanoreceptor responses to bars, edges, and gratings. *J Neurophysiol.,* 46(6), pp. 1204-25.

Pillow, J. W., Paninski, M., Uzzell, V. J., Simoncelli, E. P. & Chichilnisky, E. J., 2005. Prediction and decoding of retinal ganglion cell responses with a probabilistic spiking model. *J. Neurosci.,* 25(47), pp. 11003-13.

Poole, K., Moroni, M. & Lewin, G. R., 2015. Sensory mechanotransduction at membrane-matrix interfaces. *Pflugers Arch.,* 467(1), pp. 121-32.

Pouget, A., Beck, J. M., Ma, W. J. & Latham, P. E., 2013. Probabilistic brains: knowns and unknowns. *Nat. Neurosci.,* 16(9), p. 1170–8.

Prescott, S. A., Ma, Q. & De Koninck, Y., 2014. Normal and abnormal coding of somatosensory stimuli causing pain. *Nat. Neurosci.,* 17(2), pp. 183-91.

Price, D. D., 1988. *Psychological and neural mechanisms of pain.* New York: Raven Press.

Raja, S. N., Meyer, R. A., Ringkamp, M. & Campbell, J. N., 1999. *in Textbook of Pain.* Churchill Livingstone, Edinburgh: Elsevier.

Ranade, S. S., Woo, S. H., Dubin, A. E., Moshourab, R. A., Wetzel, C., Petrus, M., Mathur, J., Bégay, V., Coste, B., Mainquist, J., Wilson, A. J., Francisco, A. G., Reddy, K., Qiu, Z., Wood, J. N., Lewin, G. R. & Patapoutian, A., 2014. Piezo2 is the major transducer of mechanical forces for touch sensation in mice. *Nature,* Dez., 516(7529), pp. 121-5.

Ratté, S., Zhu, Y., Lee, k. Y. & Prescott, S. A., 2014. Criticality and degeneracy in injury-induced changes in primary afferent excitability and the implications for neuropathic pain. *eLIFE,* Volume 3, p. e02370.

Rho, Y.-A. & Prescott, S. A., 2012. Identification of Molecular Pathologies Sufficient to Cause Neuropathic Excitability in Primary Afferents Using Dynamical Systems Theory. *PLoS Comput. Biol.,* 8(5), p. e1002524.

Rugiero, F., Drew, L. J. & Wood, J. N., 2010. Kinetic properties of mechanically activated currents in spinal sensory neurons. *J. Physiol.,* 588(Pt. 2), pp. 301-14.

Schepers, R. J. & Ringkamp, M., 2009. Thermoreceptors and thermosensitive afferents. *Neurosci. Biobehav. Rev,* 33(3), pp. 177-84.

Sclar, G., Maunsell, J. H. & Lennie, P., 1990. Coding of image contrast in central visual pathways of the macaque monkey. *Vision Res.,* 30(1), pp. 1-10.

Sherrington, C. S., 1906. The Integrative Action of the Nervous System.

Smith, E. S. J. & Lewin, G. R., 2009. Nociceptors: a phylogenetic view.. *J Comp Physiol A Neuroethol Sens Neural Behav Physiol.,* 195(12), pp. 1089-106.

Spray, D. C., 1986. Cutaneous temperature receptors. *Ann. Rev. Physiol.,* Volume 48, pp. 625-38.

Srinivasan, M. A. & Dandekar, K., 1992. Role of fingertip geometry in the transmission of tactile mechanical signals. *Advances in Bioengineering,* Volume 22, pp. 569-72.

Srinivasan, M. A. & Dandekar, K., 1996. An investigation of the mechanics of tactile sense using two-dimensional models of the primate fingertip. *J Biomech Eng,* 118(1), pp. 48-55.

Sripati, A. P., Bensmaia, S. J. & Johnson, K. O., 2006. A Continuum Mechanical Model of Mechanoreceptive Afferent Responses to Indented Spatial Patterns. *J. Neurophysiol.,* 95(6), pp. 3852-64.

Stoll, A. M. & Greene, L. C., 1959. Relationship between pain and tissue damage due to thermal radiation. *J. Appl. Physiol,* 14(3), pp. 373-82.

Tibshirani, R., 1996. Regression shrinkage and selection via the Lasso. *Journal of the Royal Statistical Society. Series B (Methodological),* 58(1), pp. 267-288.

Tigerholm, J. et al., 2014. Modeling activity-dependent changes of axonal spike conduction in primary afferent C-nociceptors. *J Neurophysiol.,* 111(9), pp. 1721-35.

Tillman, D. B., Treede, R. D., Meyer, R. A. & Campbell, J. N., 1995a. Response of C fibre nociceptors in the anaesthetized monkey to heat stimuli: correlation with pain threshold in humans. *J. Physiol.,* 485(Pt. 3), pp. 753-65.

Tillman, D. B., Treede, R. D., Meyer, R. A. & Campbell, J. N., 1995. Response of C fibre nociceptors in the anaesthetized monkey to heat stimuli: estimates of receptor depth and threshold. *J. Physiol.,* 485(Pt. 3), pp. 753-65.

Timoshenko, S. & Goodier, J. N., 1970. *Theory of Elasticity.* New York: McGRAW-Hill.

von Frey, M., 1894. *Bet. Kgl. Siichs. Ges. Wiss.*

Vriens, J., Nilius, B. & Voets, T., 2014. Peripheral thermosensation in mammals. *Nat. Rev. Neurosci.,* 15(9), pp. 573-89.

Vriens, J., Owsianik, G., Hofmann, T., Philipp, S. E., Stab, J., Chen, X., Benoit, M., Xue, F., Janssens, A., Kerselaers, S., Oberwinkler, J., Vennekens, R., Gudermann, T., Nilius; B. & Voets, T., 2011. TRPM3 is a nociceptor channel involved in the detection of noxious heat. *Neuron,* 70(3), pp. 482-92.

Wang, Y., Marshall, K. L., Baba, Y. & Gerling, G. J., 2013. Hyperelastic Material Properties of Mouse Skin under Compression. *PLoS One,* 8(6), p. e67439.

Wasserman, L., 2004. *All of Statistics-- A Concise Course in Statistical Inference.* New York: Springer-Verlag New York.

Watson , G. S., 1964. Smooth Regression Analysis. *Sankhyā: The Indian Journal of Statistics,* 26(4), pp. 359-72.

Waxman, Stephen G, S. G. & Zamponi, G. W., 2014. Regulating excitability of peripheral afferents: emerging ion channel targets. *Nat. Neurosci.,* 17(2), pp. 153-63.

Weddell, G., 1955. Somesthesis and chemical senses. *A. Rev. Psychol.,* Volume 6, pp. 119-136.

Wetzel, C., Hu, J., Riethmacher, D., Benckendorff , A., Harder , L., Eilers, A., Moshourab, R. A., Kozlenkov, A., Labuz , D., Caspani, O., Erdmann, B., Machelska, H., Heppenstall, P. A. & Lewin, G. A., 2007. A stomatin-domain protein essential for touch sensation in the mouse. *Nature,* 445(7124), pp. 206-9.

Wichmann, F. A. & Hill, N. J., 2001. The psychometric function: I. Fitting, sampling, and goodness of fit. *Percept Psychophys.,* 63(8), pp. 1293-313.

Wilson, H. R., 2005. *Spikes, decisions and actions.* New York: Oxford University Press Inc..

Woolf, C. J. & Ma, Q., 2007. Nociceptors—noxious stimulus detectors. *Neuron,* 55(3), pp. 353-64.

Wooten, M., Weng, HJ, Hartke, T. V., Borzan, J., Klein, A. H., Turnquist, B., Dong, X., Meyer, R. A. & Ringkamp, M., 2014. Three functionally distinct classes of C-fibre nociceptors in primates.. *Nature communications,* 5(4122).

Xu, F., Lu, T. J. & Seffen, K. A., 2008. Skin thermal pain modeling—A holistic method. *Journal of Thermal Biology,* 33(4), pp. 223-37.

Xu, F., Wen, T., Seffen, K. & Lu, T., 2008. Modeling of skin thermal pain: A preliminary study. *Appl. Math. Comput.,* 205(1), pp. 37-46.

Zimmermann, K., Hein, A., Hager, U., Kaczmarek, J. S., Turnquist, B. P., Clapham, D. E. & Reeh, P. W., 2009. Phenotyping sensory nerve endings in vitro in the mouse. *Nat Protoc,* 4(2), pp. 174-96.